Near Infrared Spectroscopy of LINER Galaxies

Thesis by

James E. Larkin

In Partial Fulfillment of the Requirements

for the Degree of

Doctor of Philosophy

California Institute of Technology

Pasadena, California

1996

(Submitted October 9, 1995)

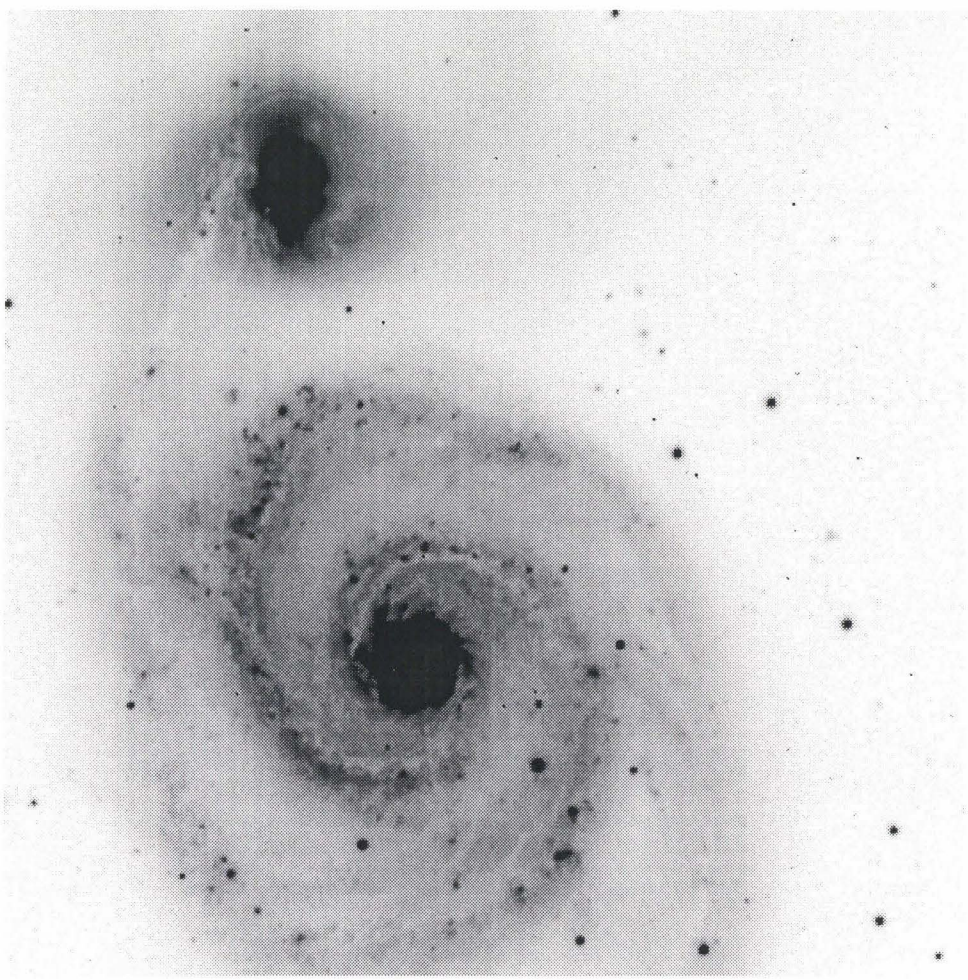

To Debbie

Acknowledgements

I have spent a fifth of my life on this thesis and associated projects, and it is therefore hard to make a truly complete list of everyone who has helped me along the way. The list I give below, unfortunately, must therefore be considered incomplete and I apologize to anyone I left out.

First and foremost, I must thank my advisor Tom Soifer who has given me opportunities beyond any I could have wished for. Not only did he allow me to work on the design and construction of the spectrograph, but he also gave me an important role to play on the early infrared results from the Keck Telescope. Tom has not only been a helpful and supportive advisor, however, he has also been a kind and understanding friend during the difficult periods of my graduate career. I will always be indebted to him and I will greatly miss working so closely with him.

Lee Armus also deserves an infinite number of thank yous for being a great friend and teacher. Much of what I've learned about AGN and many other areas of astronomy come directly from him. I also thank him for his great patience in reading drafts of this thesis and other papers. He's also a pro at frisbie golf.

I also owe a great deal to my office mate for these past five years, Robert Knop. He's co-creator of the spectrograph and plays a good game of Cowboy on cloudy nights at Palomar. Thanks also to Gerry Neugebauer, the founder of the Infrared Army at Caltech and an endless source of enthusiasm and wisdom. He has always been very supportive of me and especially of J.I.P.. Thanks to Keith Matthews, the instrument guru of the group as well as a first rate astrophysicist. He always had an interesting

solution to difficulties with the spectrograph. I am also grateful to David Shupe for his friendship and knowledge of Galactic sources, infrared detectors, UNIX and rental trucks. Thanks also to James Graham who introduced me to infrared astronomy, M82, and sardines. Special thanks to Joe Mazzarella who is a good friend and fellow father, and who introduced me to the wonders of IRAF (Uh, maybe I shouldn't thank him for that last thing). I also want to thank Andrea Ghez for showing me by example how to be a successful graduate student. I am also grateful to Alycia Weinberger for her friendship and many interesting conversations. To the newest IRA graduate student, Tom Murphy, thanks for all the lunches at Ernies and discussions ranging from ant behavior to brain waves. I also want to thank Bruce Pirger, who only stayed at Caltech a short time, but whom I will always consider a good friend and a so-so tennis player (just kidding Bruce). Thanks also to the infrared secretaries: Susan McCurdy, Dheera Sharma, Lydia Suarez, and Mike Rogers, who have helped a naive graduate student with paper work, travel arrangements, publications and many other thankless tasks.

I also want to thank the other two committee members (besides Tom and Gerry) Roger Blandford and Nick Scoville. They not only sat through two oral presentations, and read my thesis, but also were very supportive and made many helpful suggestions and comments.

Sean Lin also deserves a great deal of credit for his work on the spectrograph and his many answers to my sometimes naive questions. Thanks also to Doug Warden who always had a special tool or paint for the job. Don't worry Doug, I won't be borrowing your tools anymore. Thanks to the great machinists Richard Borup and Fernando Lopez who not only machined many pieces for the spectrograph but who also taught me how to machine much of the rest. The Palomar crew and telescope assistants also deserve a great deal of credit and thanks for helping with the spectrograph and observing and for running the best telescope in the world.

A very special thank you goes to Ron Marquardt who has been a great friend for many years. Ron, I still remember when we first met at LLNL 9 years ago. Take care and I'll see you at thanksgiving. Thanks also to Deepto Chakrabarty for many interesting discussions about theses, finding housing, gamma ray pulsars and many other topics. I also want to thank my office mate, Dominic Benford for his enthusiasm in wacky projects, such as mechanical walkers, homemade fireworks, and sword fighting. Thanks also to Todd Hunter, one of the most knowledgable astronomy students I know, and a great collector of dollar bills. Thanks too, to Jason Surace for including me in his wedding and for showing me the steam tunnels.

I dedicate this thesis to my wife and first and only true love, Debbie, and also to our recently created son Ryan. Debbie has had to endure many lonely days and nights while I've been observing or studying or building and yet she has always been supportive and in many ways inspirational. Graduate school has not always been an easy road, yet we are closer now than ever before. This thesis could not have been completed without her infinite love and understanding. I must also thank my son Ryan, who in these final days of my thesis, has brought me more joy than I ever thought possible.

Thanks to my family for their love and support. Mom, thank you for your love, for putting up with my annoying questions as a kid, and for supporting my education. To my brother Brad, thanks for playing war games, bringing home the school computers and teaching me how to build snow men. To my dad, I really wish you could see this moment. I love you. Thanks also to my granny and granddad for spoiling me rotten and letting me drive the tractor. Thanks also to Debbie's family: Art, JoAnne, Laura and Michael Wood, who have all become my family too.

A special thanks to Susan Fox Knowles, who's helped Debbie and I more than she'll ever know. Thanks too to Crystal Mazzarella for her friendship and for showing me where to get beef raviolis. Thanks also to William Mazzarella, the cutist 2 year

old in the world. To Terry Borman and her cats, thanks for being a good friend and babysitter.

Thanks also to God for creating such a marvelous and beautiful Universe for me to study and ponder upon.

Abstract

This thesis reports the design and operation of a new near infrared spectrograph for the 5 m Hale telescope and its use to observe a sample of LINER galaxies. The spectrograph operates between 1 and 5 microns using existing infrared array cameras. It has two long-slit spectroscopy modes yielding resolutions ($\lambda/\Delta\lambda$) of ~850 and ~3300 with a 0.75" wide by 40" long slit. The spectrograph also has a direct imaging mode giving a 10"x40" field of view.

The galaxy sample includes 15 LINERs with spectra covering the [FeII] (1.2567 μm), Paβ (1.2818 μm), H_2 (1-0 S(1), 2.1218 μm) and Brγ (2.1655 μm) near infrared emission lines, and one additional galaxy with only [FeII] and Paβ line coverage. The sample included, twelve low luminosity objects (classical LINERs) selected from surveys of nearby galaxies, and four high luminosity multiple nuclei systems.

All of the classical LINERs with infrared line detections have strong [FeII] and/or H_2 emission, with about half (4 out of 9) having extremely high ratios (>2) of [FeII] to Paβ. The strength of the H_2 and [FeII] lines is well correlated with the optical [OI] line, with many LINERs having higher ratios of [FeII]/Paβ, H_2/Brγ and [OI]/Hα compared to other galaxy types. The LINERs with the highest [FeII]/Paβ ratios (termed "strong" [FeII] LINERs) show evidence for recent star formation. Shocks from compact supernova remnants may enhance the [FeII] emission in these "strong" [FeII] LINERs. The LINERs with lower [FeII]/Paβ ratios (termed "weak" [FeII]

LINERs) are more consistent with Seyfert-like activity, including higher ionization states, some strong x-ray sources and some broad Hα detections. The [FeII] luminosity and the [FeII]/Paβ ratio in these objects is more easily explained by hard x-ray excitation than in the "strong" [FeII] LINERs. These "weak" [FeII] LINERs are considered prime candidates for being low luminosity Seyfert nuclei.

The two multiple nuclei LINERs with line detections, IRAS 17132+5313 and Arp 220, had lower ratios of [FeII]/Paβ and/or H_2/Brγ than the classical LINERs. The spectra of Arp 220 show that the extended emission has higher ratios of [FeII]/Paβ and H_2/Brγ than found on the nuclei. It is suggested that in these merging systems, the low ionization line emission probably results from shocks, either from cloud-cloud collisions or winds in the gas surrounding the nuclei.

Contents

List of Figures

List of Tables

Chapter 1

Introduction

During the past several decades, many galaxies have been found to have unusual activity within their nuclear regions. When first studied, the nuclei of galaxies were thought to contain only a relatively old population of stars. In 1908, however, Edward A. Fath discovered that NGC 1068 had spectral emission lines which had previously been observed in gaseous nebulae within our own Galaxy but which were not present in stellar spectra. Since this early discovery, a small but significant fraction of galactic nuclei have been found to have emission line spectra or other features such as large radio emitting lobes of gas, which cannot easily be explained through the activity of stars or star formation. The most extreme examples of these active galactic nuclei (AGN) are quasars, in which the nuclear luminosity is so high that the surrounding galaxy is lost in the glare. It is interesting that quasars were much more common at earlier times in the Universe, and that many of the local, "normal" galaxies may be the quiescent remnants of these monsters. Understanding the great variety of properties seen in AGN is one of the most important and vigorously studied areas of astrophysical research.

Recent unification models based on massive (10^7 solar masses), central black holes, often referred to as "monsters" or "central engines" have proven very successful at explaining the variation among AGN. Gas falling into such a black hole forms an accretion disk that is heated to extreme temperatures as it loses gravitational energy. Clouds orbiting close to the black hole have extremely high rotational speeds and Doppler broadening of the emission lines can reach several thousand kilometers per second, consistent with the broadest lines observed in AGN. A great deal of the observed variation among AGN is explained by varying the level of activity, which depends both on the size of the black hole and on the rate that material falls in. In the model a torus of dust at the outer edge of the accretion disk is thought to obscure parts of the central region. The viewing angle into the "central engine" then has a great impact on what features are observed since the most extreme environment where the broadest lines are produced is thought to be only a few times 0.1pc in size. If the accretion disk is viewed edge on, the thick torus can heavily obscure it from view while the milder narrow line region which extends to much larger radii, is observed more directly. If the disk is viewed close to face on, however, much more extreme activity is observed (Antonucci 1993). This unification model, although very successful, is not fully accepted, and models based on unusual stellar activity are being investigated to explain at least some AGN activity (Terlevich 1990).

In addition to these true AGN, some galaxies have unusual nuclear activity in the form of rapid star formation. These "starburst" galaxies have line ratios comparable to star forming regions within our Galaxy. The star forming rates, however, are too high to be sustained over the life of the galaxy, and probably result from some transient event such as a tidal interaction with another galaxy or a rapid infall of material into the nuclear region.

LINERs (Low Ionization Nuclear Emission-line Region galaxy) are among the most recently identified groups of galaxies with nuclear activity. They went unnoticed for so long partly because of the extremely low level of activity, often a factor of 100 down from more heavily studied types of active galaxies such as Seyfert's. Heckman (1980) estimates that $\sim \frac{1}{3}$ of all galaxies have LINER type spectra, making them by far the most common form of active galaxy. In spite of their numbers, the source of nuclear excitation is poorly understood, and it is not clear if they are true AGN or are related to starburst galaxies. If LINERs are AGN, then their large numbers may imply that virtually all galaxies harbor central blackholes, and that apparently normal galaxies are the quiescent remains of quasars.

Visible observations of broad line regions in AGN, and perhaps in LINERs if they do have broad line regions, are often plagued by the relatively high dust obscuration towards the galactic nuclei. Dust is more transparent to infrared emission, however, and infrared observations may penetrate into regions with more than 10 magnitudes of visual extinction. Optical observations of LINERs are also plagued by strong absorption lines from stellar atmospheres within the host galaxies and a careful removal of these features is necessary to measure the emission lines. Infrared absorption lines are usually much weaker, but unfortunately, infrared emission lines are also often much weaker than similar optical lines. Infrared observations also suffer from higher backgrounds and smaller detector arrays. All of these factors make infrared spectroscopy a powerful, yet relatively unexplored technique for the study of LINERs.

1.1 What are LINER galaxies

LINERs (Low Ionization Nuclear Emission-line Region galaxies) are the most common and lowest energy examples of active galaxies (Heckman 1980) known. The main

LINER characteristic is unusually strong forbidden line transitions from low ionization states such as [OII](λ=3727 Å) , [NII](λ=6583 Å) and [SII](λ=6717,6731) relative to lines from higher ionization states. The original definition used by Heckman (1980) was [OII](λ=3727 Å) / [OIII](λ=5007 Å) > 1 and [OI](λ=6300 Å) / [OIII](λ=5007 Å) $> 1/3$. Classical LINER galaxies also have much less total energy in the spectral lines as compared to Seyfert galaxies and other types of active galactic nuclei (AGN); often down by a factor of a 100 in comparison to Seyfert's. The weakness of the spectral lines, makes LINERs difficult to study, particularly when the galaxies often have strong stellar absorption features.

In Heckman (1980), shock heating was proposed as the most likely excitation mechanism for LINERs. He found that shock models with shock wave speeds of $\sim$100 km s^{-1} were able to match the observed spectra and shock heated filaments in supernova remnants also had similar line ratios. Recent models have also shown that photoionization from a power-law source (e.g. Ho, Filippenko, & Sargent 1993) or from a cluster of very hot stars (e.g. Terlevich & Melnick 1985; Shields 1992), especially in very dense environments, can also duplicate the observed line ratios. An important new aspect of the star formation models, involves compact supernova remnants which are confined by the high densities within the nuclear region and which produce strong shocks. X-ray heating is particularly attractive for photoionization because hard x-rays are able to penetrate deeply into molecular clouds creating large partially ionized regions where low ionization species will dominate.

An intriguing possible variation on the photoionization models recently proposed by Eracleous, Livio & Binette (1995), is that LINERs have a compact object (probably a black hole) in the nucleus which periodically disrupts a star during a close orbital approach. As the stellar material accretes onto the central source, high energy photons are produced and a Seyfert-like broad line region appears. As the material is

consumed, the ionizing flux drops and the high ionization states weaken quickly. Low ionization lines, however, remain strong for much longer since the decay time is longer and the light crossing time in this region is much larger than that of the broad line region. This "Duty Cycle Hypothesis" was motivated by the observation that about 20% of LINERs had detectable 2300Å emission with HST (Maoz et al. 1995). These UV bright galaxies, have no other obvious difference from the UV dark LINERs. Under this theory, the UV bright galaxies would still have ongoing accretion, while the others are in the quiescent phase. In support of this theory, Eracleous et al. (1995) point to NGC 1097 which was observed to make a sudden transition from a LINER to a Seyfert 1 (Storchi-Bergmann, Baldwin & Wilson 1993).

It is also possible that LINERs represent a heterogeneous class of objects. Some LINERs may have a central "monster" like Seyfert galaxies, while others have one or more dense clusters of hot young stars. Shocks may play a role in enhancing the forbidden lines in either of these two groups. Whatever the case, extending the number of observed spectral diagnostics into the infrared gives greater leverage on the problem.

1.2 Near Infrared Spectroscopy

High resolution near infrared spectroscopy of AGN is still in its infancy, primarily due to technical difficulties as compared to optical studies. The background level in the near infrared is much higher than at optical wavelengths due to atmospheric emission, both from thermal radiation and from discreet molecular transitions, and due to thermal emission from warm objects such as the telescope, dome, and other equipment. An astronomical signal in the infrared is further degraded by atmospheric

absorption which blocks all radiation except within several semi-transparent windows at 1.27 μm (J-Band), 1.65 μm (H-Band), 2.2 μm (K-Band) and at 3.5 μm (L Band).

Detector technology has also been a limiting factor in the near-infrared, since detector arrays have traditionally been very small. Recent advances in array fabrication, however, have allowed the creation of large imaging arrays of up to 256 by 256 elements. New 1024 by 1024 pixel arrays are expected in the very near future. Such large arrays can be used to make long slit spectrometers, such as the one described in this thesis, with significant spatial extent and large spectral coverage.

Although spectroscopy in the infrared is more difficult than in the optical, a significant number of important infrared spectral features exist and provide useful astrophysical insights. Among these are the Brγ (2.1655μm) and Paβ (1.2818μm) hydrogen recombination lines. These lines trace ionizing photons and can be directly related to other recombination lines and to the strength of the UV continuum. Another series of important infrared lines are the H_2 rotation-vibration transitions. The strongest H_2 line is the 1-0 S(1) transition at 2.1218 μm. H_2 emission is ubiquitous in starburst and Seyfert galaxies and is thought to originate in slow shocks, UV fluorescence and X-ray heating. Another set of strong infrared lines, are the forbidden transitions of singly ionized iron ([FeII]). Iron is believed to play an an important role as a coolant in shocked environments (Nussbaumer and Storey 1988) but in the general interstellar medium is often depleted compared to other elements since most iron is locked up in dust grains. The strongest near infrared [FeII] line is the 1.2567μm transition in the J band. This line is often very strong in AGN and in most cases is thought to trace faster shocks ($\sim$100 km sec^{-1}) than the H_2 lines (Graham et al. 1990). [FeII] is also thought to be strong in x-ray heated environments where dust grains have been evaporated.

1.3 Outline of Thesis

The first step in this project was the completion of the cryogenically cooled near-infrared spectrograph in April, 1994. The instrument is a variant of an Ebert-Fastie spectrograph and is used at the Cassegrain focus of the Hale 5 meter Telescope. The instrument was designed by Robert Knop and myself with the assistance of Sean Lin, Keith Matthews and our advisor, Tom Soifer. The spectrograph is detailed in chapter 2 of this thesis.

One of the first LINERs observed was the ultraluminous infrared galaxy Arp 220. Many of the ultraluminous infrared galaxies have spectra consistent with the LINER definition, although they are many times more luminous that classical LINERs. The spectra of Arp 220 are discussed in detail in chapter 3.

The spectrograph was used to examine a sample of 12 classical LINERs from Heckman's original sample and from two more recent samples (Keel 1983, and Ho et al. 1993). Also four multiple nuclei galaxies with LINER-like spectra were observed to investigate the LINER phenomenon as a function of luminosity and galactic environment. These spectra are presented in chapter 4.

1.4 References

Antonucci, R 1993, Annu.Rev.Astron.Astrophys., 31, 473.

Eracleous, M., Livio, M., & Binette, L. 1995, Ap.J., in press.

Graham, J. R., Wright, G. S., & Longmore, A. J. 1990, Ap.J., 352, 172.

Heckman, T. M., 1980, A&A, 87, 152.

Ho, L. C., Filippenko, A. V., & Sargent W. L. W. 1993, Ap.J., 417, 63.

Keel, W. C., 1983, Ap.J., 269, 466.

Maoz, D., Filippenko, A. V., Ho, L. C., Rix, H.W., Bahcall, J. N., Schneider, D. P., & Macchetto, F. D. 1995, Ap.J.., 440, 91.

Nussbaumer, H., & Storey, P. J., 1988, A&A, 193, 327.

Shields, J. C. 1992, 399, L27.

Storchi-Bergmann, T., Baldwin, J. A., & Wilson, A. S., 1993, Ap.J., 410, L11.

Terlevich, R. 1990, *Windows on Galaxies*, p.87, ed. Fabbiano, G., Kluwer Academic Publishers.

Terlevich, R., & Melnick, J. 1985, M.N.R.A.S., 213, 841.

Willner, S. P., Elvis, M., Fabbiano, G., Lawrence, A., & Ward, M. J. 1985, Ap.J., 299, 443.

Chapter 2

Spectrometer Design and Construction

Prologue: This chapter describes the design, construction and performance of a near infrared spectrograph for the 5m Hale Telescope at Palomar Observatory. The instrument is designed to operate between 1 and 5 microns using existing infrared array cameras. The spectrograph has two long-slit spectroscopy modes yielding resolutions ($\lambda/\Delta\lambda$) of $\sim$850 and $\sim$3300 with a 0.75" wide by 40" long slit. The spectrograph also has a direct imaging mode in which a mirror is moved in front of the gratings giving a 10"x40" field of view through the same optical path. All mirror surfaces are cryogenically cooled to liquid nitrogen temperatures to reduce thermal emission after dispersion.

The spectrometer was a joint project with Robert Knop, and we received assistance from Sean Lin, Keith Matthews, and Tom Soifer. I was involved in all phases of the instrument design and construction, including: optical layout and ray tracing, mechanical design and drafting, machining, assembly, and testing. A paper describ-

ing this work has been submitted for publication in *Publications of the Astronomical Society of the Pacific.*

2.1 Introduction

With the advent of large format infrared arrays, infrared spectroscopy has become a powerful and practical endeavor. The infrared atmospheric bands between 1μm and 5μm contain a wealth of atomic and molecular transitions of astrophysical importance. Interstellar dust is also much more transparent to infrared radiation as compared to optical radiation, so obscured regions such as galactic nuclei and star forming regions can be probed more deeply with infrared line diagnostics.

2.2 Instrument Design

The infrared spectrograph was designed to operate at the f/70 Cassegrain focus of the Hale 5 m Telescope at Palomar Observatory. The goal was to construct a medium resolution spectrograph to feed the existing high quality infrared cameras. The spectrograph would be appropriate for observing active galactic nuclei, as well as other astrophysical sources. Two cameras are currently available, one with a 256×256 element InSb detector array operating from 1 to 5 μm, and one with a 256×256 element HgCdTe (NICMOS 3) array operating from 1 to 2.4 μm.

As shown in figure 2.1, the optical design is basically an Ebert-Fastie spectrograph with spherical mirrors used to collimate and refocus the light. With the f/70 infrared secondary, ray tracing predicts that the use of spherical mirrors introduces negligible aberrations, about 1/20th of an arcsecond. All mirrors are glass with gold coatings. The grating is an aluminum blank, with a aluminum coated, epoxy ruling. Since the

spectrograph uses the infrared cameras, it was designed as a reimaging system with both an input and output window which accepts the f/70 beam from the infrared secondary, and produces an f/70 beam for the cameras with the correct focus and pupil locations. As shown in the light path diagram (figure 2.1), one camera can be mounted in the dedicated imaging position while the other can be mounted to the spectrograph. Although they cannot be used simultaneously, the switch over can be made in approximately 5 minutes when both instruments are already mounted. This greatly increases the flexibility of a night's observing.

Although the use of the cameras is economical, such a system does have some drawbacks. The most important of these is a loss in transmission due to the presence of two additional CaF_2 windows with $\sim$ 92% transmission each. The windows also collect dust particles, which are at room temperature, and are an additional source of background in the K band (2.2 μm) due to thermal emission. The problems from thermal emission, have been minimized in the latest observing runs by using a 5% filter to order sort instead of the broad band K filter. Another consideration is that the image scale is completely determined by the cameras (0.167 and 0.125 arcsecond pixel^{-1}) which is somewhat oversampled even for the best conditions. A larger plate scale of 0.25 arcsecond pixel^{-1} would have allowed for a slightly larger image size and greater wavelength coverage in a single exposure. We consider these drawbacks somewhat minor compared to the extra effort of incorporating an array within the device.

Active galaxies typically have narrow line regions with spectral line widths from $\sim$200 to 1,000 km sec^{-1} and broad line regions with widths up to 10,000 km sec^{-1}. For the best sensitivity and the ability to just resolve narrow line components, the main grating's resolution was set at $\sim$ 850 (350 km sec^{-1}) for a 0.75" slit (note: unless otherwise stated, all resolutions within this thesis are for a 0.75" slit). The main

grating has 240 lines mm^{-1} and a blaze angle of 34 degrees. First order diffraction is used in the L band (3.5μm), second order for the K band (2.2μm), third order for the H band (1.65μm), and fourth order for most of the J band (1.27 μm). Broad band filters in the cameras are therefore used for order separation, except in the K band where a 5% filter is used to minimize thermal emission. The spectral line curvature with this grating is ~2 pixels from the center of the array to either edge, and is easily corrected in software.

An echelle grating is also available when higher resolution is desired. Within the J (1.25 μm) and H (1.65 μm) infrared bands, the dominant source of background is from discreet OH atmospheric lines. The echelle's resolution was chosen to well separate these atmospheric lines and thus greatly reduce the background over most of the spectra. Figure 2.2 shows the average fraction of OH contaminated pixels versus spectral resolution in the J, H, and K windows. A good compromise between spectral coverage and number of clear pixels was a resolution of ~3300 for the echelle grating. The echelle grating has 52.67 lines mm^{-1} and a blaze angle of 69 degrees. Several orders are needed to cover each broad band, and order separation is carried out by a 1% circular variable filter within the K band, and narrow band filters within the J and H bands. Both infrared cameras contain grisms with resolutions of ~100 which disperse perpendicularly to the grating dispersion. This arrangement allows for cross dispersed spectra covering a large fraction of each broad band. In long-slit mode, the spectral line curvature with the echelle grating is ~8 pixels across the entire array.

Both gratings are mounted on a spring loaded, rotating grating carriage connected to a stepper motor. By pre-loading the grating carriage, wavelength repeatability is ~1 pixel (~70 km sec^{-1} for the lower resolution grating and 20 km sec^{-1} for the echelle). Using atmospheric lines which are present throughout the infrared, wavelengths can be determined to a fraction of a pixel for all observations (see Oliva

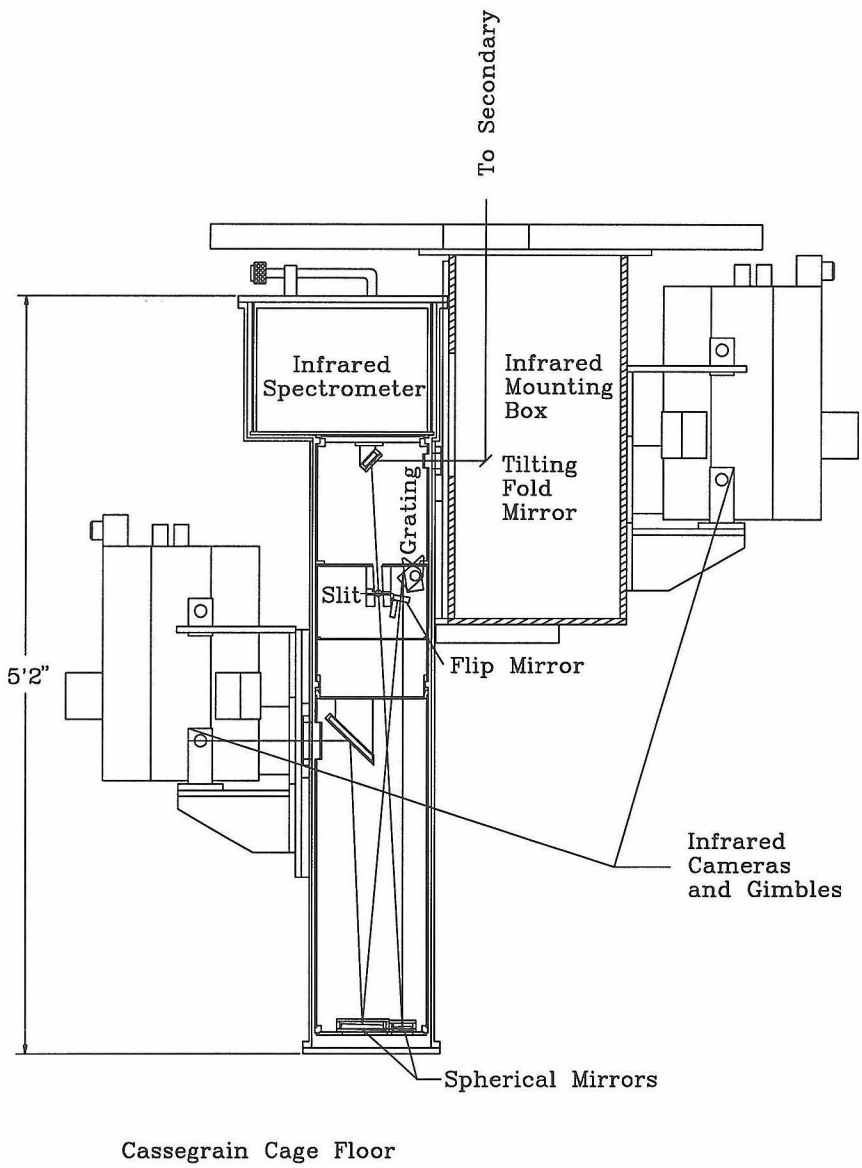

Figure 2.1: Light path of the spectrograph. The two infrared cameras are shown in the imaging station and mounted to the spectrograph.

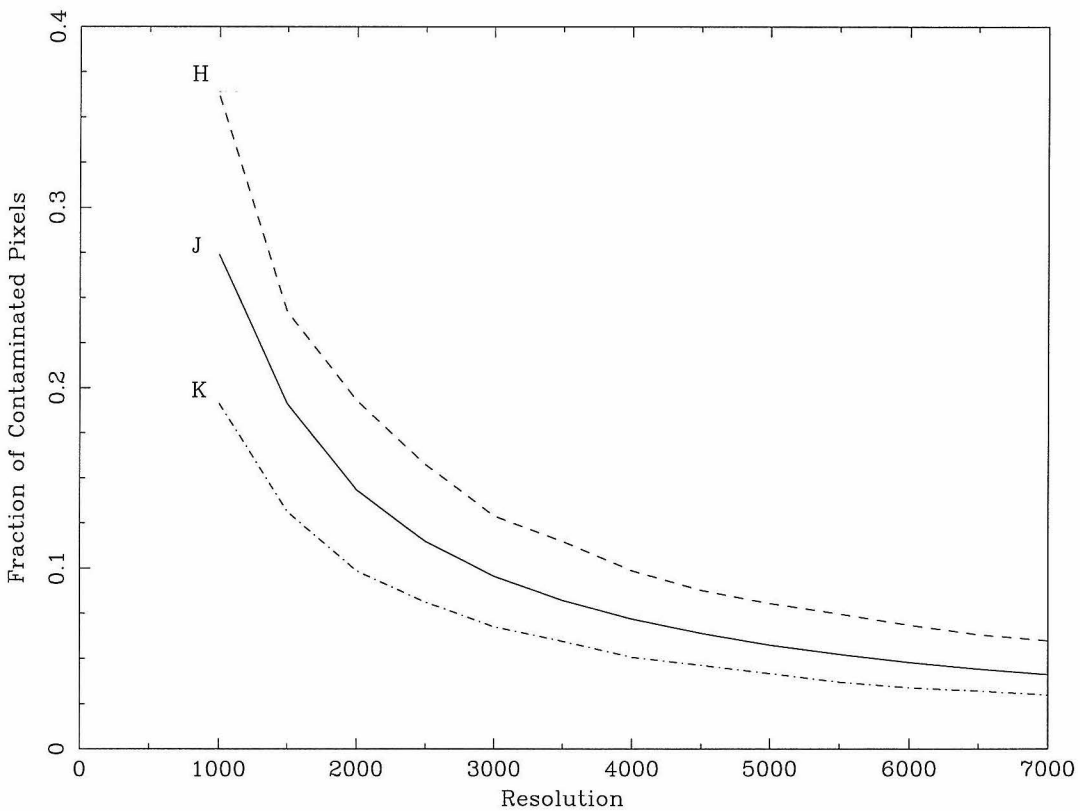

Figure 2.2: The fraction of OH contaminated pixels versus spectral resolution in each of the three broad band filters where OH emission plays a significant role. A pixel is considered contaminated if it contains any part of an OH line listed in Oliva and Origlia (1992).

& Origlia 1992, for a detailed discussion of using OH lines for wavelength calibration). Past 2.3 microns, the number of OH lines begins to drop, and may not be sufficient to calibrate the echelle spectra. In these settings, calibration lamps, discussed below can be used to augment the atmospheric lines. The time required to change wavelength settings or even to change between gratings is less than 5 seconds (including all computer and controller overhead), and observations at different settings can be taken in rapid succession.

A two jawed slit mechanism is placed at the telescope focus. The 40" long slit jaws are coupled to a rack and pinion drive that moves both jaws simultaneously and maintains the center of the field at the same location regardless of slit width. Any slit width can be used from completely closed to 10" wide in 1/150th arcsecond steps.

An important feature of the spectrograph is the direct imaging mode. A mirror can be moved into place just in front of the grating wheel allowing the light to continue undispersed into the camera. Since the mirror is a separate mechanism, it can be moved in and out without changing the grating position, giving greater spectral reproducibility.

For spectral calibration, four lamps (neon, argon, krypton, and xenon) are mounted on the front face of the spectrograph. The lamps are controlled by a stepper motor operating a rotary switch. To take calibration spectra, the mirror within the mounting box, which normally sends the telescope beam into the spectrograph's input window, is moved to its extreme position which causes a small mirror cover to come down. The back surface of the aluminum mirror cover is sandblasted and acts as a diffuser to send the lamp light into the spectrograph. Since the camera pupil is well matched to the telescope secondary, only lamp light which follows the same path as the telescope beam is accepted. The lamp lines, therefore, have the same wavelength solution as astronomical lines and provide a good wavelength calibration source.

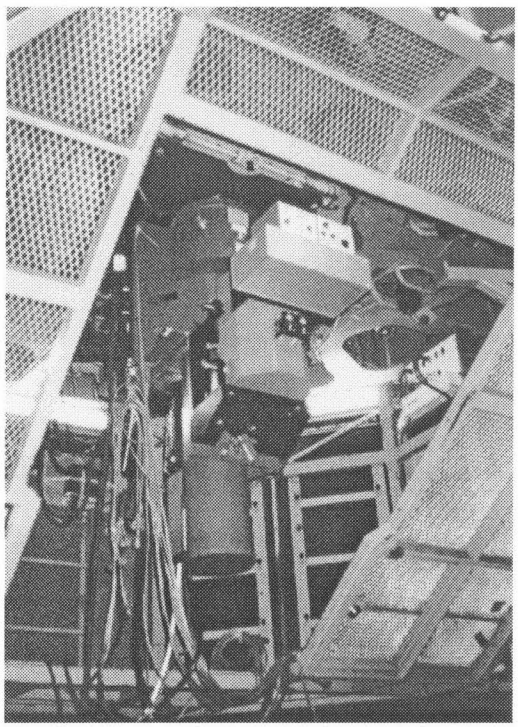

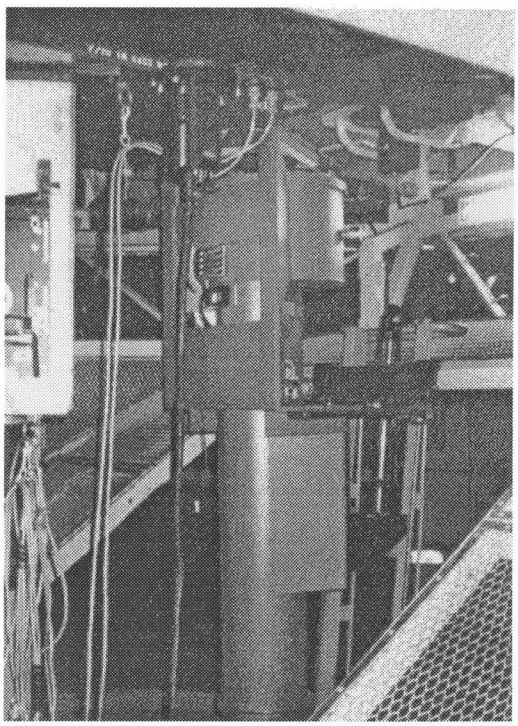

Figure 2.3: The photo on the left shows the spectrograph in its working position within the Cassegrain cage of the 200 Inch Telescope. The spectrograph is the tall thin cylinder with the larger cylindrical top. One of the infrared cameras is also shown mounted to the spectrograph. The camera is the octagonal dewar on the black mount. The photo on the right is of the front face of the spectrograph dewar just prior to mounting on the telescope. The black rectangular opening is the input window for the telescope's beam. Just above the aperture are four calibration lamps each mounted horizontally.

The spectrograph is cooled with liquid nitrogen (T = 77K) in order to reduce thermal emission from the mirrors, mounting surfaces, and baffles. This cooling is particularly important in the last stages of the spectrograph because the signal is greatly reduced after dispersion. The nitrogen dewar is located at the top of spectrograph (see figure 2.1.) and is connected by a fiberglass cylinder to the top plate. The mirrors and mechanisms are mounted on an aluminum cylinder which is cantilevered off the bottom of the nitrogen dewar. The only outside connection is through three fiberglass motor shafts which operate the various mechanisms. The nitrogen dewar contains ~18 liters giving a hold time of >40 hours.

In the near infrared, thermal emission from the telescope, the mounting box and other warm components are a large source of scattered background radiation. To reduce the effects of scattered light, a large set of baffles is included in the spectrograph. The aluminum cylinder which serves as the optical bench has only five openings: the input and output apertures, and three small (1" diameter) holes for motor shafts to enter. The interior surface of the cylinder and all aluminum components within are painted black with Eppley-Parsons Optical Black Lacquer. The path between the input aperture and the first flat mirror is surrounded by a rectangular box with five baffle planes. Between this mirror and the slit is another box with eight more baffle planes. At the slit, the top and bottom parts of the cylinder are separated by a plate whose only aperture is the slit itself. In the lower portion of the spectrograph, 10 baffle plates are evenly spaced with openings made for the criss-crossing beams. The infrared cameras contain similar baffling systems including a cold Lyot stop to further reduce extraneous background emission.

Since the spectrograph uses the f/70 secondary, instrument alignment requires relatively high precision. Within the box that the spectrograph is mounted to, a flat mirror on a sliding mount can be moved to direct the telescope's beam into the

spectrograph or out of the way to allow other instruments to work. This flat mirror can be continuosly tipped and tilted, with a smallest reliable motion of about 0.5 milliradian (~1/30th of the secondary diameter), to allow accurate alignment of the spectrograph and the secondary. The only internal alignment mechanism is the ability to slide the two spherical mirrors. Since they are spherical, a displacement of these mirrors is equivalent to tipping or tilting them. The internal components were aligned once when warm, and since all mounts and the mounting surfaces are aluminum, there is no differential contraction when cooled, so the components have remained in alignment ever since. The camera is mounted on an adjustable gimble with four micrometers (x,y, pitch and yaw) controlling the alignment with the spectrograph. Each camera requires a slightly different alignment, but each is reproducible with the micrometers.

The measured efficiency of the spectrograph was >56% (thin cirrus) at 2.25 microns as of May, 1995. This is the fraction of photons leaving the spectrograph into the camera that originally try to enter the first window. The calculated efficiency is 64%, where the biggest losses are due to the grating (78.5% efficiency on blaze) and the two windows (85% combined transmission). The measurement has significant uncertainties including: fraction of the starlight through the slit (a 0.5" slit was used in good seeing conditions); atmospheric transmission (10% variation during the year); and variability within the camera. It is important to note that only 15% of the predicted losses could be avoided by placing the optics in the same dewar with the detector.

2.3 Performance

The spectrograph was first mounted at the telescope on April 19, 1994. No significant instrument problems developed, but due to bad weather, the spectrograph could not be fully tested and used until July, 1994. The spectrograph has proved reliable and has met all of the design goals. Chapters 3 and 4 feature a number of spectra taken during the past year with the spectrograph. In addition to taking the infrared spectra of LINERs described in this thesis, observations of planetary nebulae, Seyfert and starburst galaxies have also been taken. Several papers on the scientific results are in press or are being prepared (Knop et al., Larkin et al., Shupe et al.).

2.4 Summary

This chapter has described the design and operation of a new infrared spectrograph for the Hale 5m Telescope at Palomar Observatory. The spectograph's capabilities are:

1. Operation from 1.0 μm to 5.0 μm using 256×256 element arrays which are part of pre-existing cameras.

2. Medium resolution ($\lambda/\Delta\lambda$ ~850 for 0.75" slit) long slit spectroscopy (up to 40" long slit). In this mode, broad band filters within the cameras provide order sorting.

3. High resolution ($\lambda/\Delta\lambda$ ~3300 for 0.75" slit) long slit spectroscopy (up to 40" long slit). A circular variable filter is used within the K band for order sorting, and narrow band filters in the J and H band.

4. Adjustable slit widths from closed to ~10" in steps of 1/150th of an arcsecond. The double slit jaws always maintain the same field center regardless of aperture width.

5. Direct imaging through the same optical path and slit mechanism with a field of view up to 10"×40". In this mode, the cameras can be used to take broad band, and narrow band images and even grism spectra at a resolution of 100.

6. Crossed dispersed high resolution spectra using both the high resolution grating described above and grisms within the cameras.

Using the pre-existing cameras has allowed the instrument to be created with relatively low cost, while greatly enhancing the infrared capabilities at Palomar's Hale 5 Meter Telescope.

2.5 References

Knop, R. A., Armus, L., Larkin, J. E., Matthews, K., Soifer, B. T., in preparation.

Larkin., J. E., Armus, L., Knop, R. A., Matthews, K., Soifer, B. T., Ap.J, submitted.

Oliva, E., & Origlia, L., 1992, A&A, 254, 466.

Shupe, D. L., Knop, R.A., Larkin, J. E., Armus, L., Matthews, K., Soifer, B. T., in preparation.

Chapter 3

Arp 220 : Observing the Nuclear Rotation

Prologue: Arp 220, like many of the other Ultraluminous infrared galaxies, has a LINER-like spectral ratio. It was included in the sample of galaxies to investigate this more exotic side of the LINER phenomenon. The infrared spectra were used to examine the nuclear line ratios and possible excitation source, and also revealed a spectral shift, most likely resulting from the rotation of the two merging nuclei about their common center of mass. This work was performed in collaboration with Lee Armus, Robert Knop, Keith Matthews and Tom Soifer, and a paper on these results has been accepted for publication in *The Astrophysical Journal.*

3.1 Summary

This chapter reports spatially resolved near infrared spectroscopy at a resolution $(\lambda/\Delta\lambda) \sim 1000$ of the double nucleus of Arp 220 in the Paβ, Brγ, [FeII] (λ=1.2567μm) and H_2 (1-0 S1) (λ=2.1218μm) emission lines. The Brγ hydrogen recombination line is strongly peaked on the two nuclei, and the Paβ is centered on the western nucleus

with emission across the eastern nucleus. Both lines show a velocity separation of $\sim$200 km s^{-1} between the eastern and western nuclei, the former being redshifted relative to the latter. Both the magnitude and the direction of this velocity shift are consistent with recent CO millimeter measurements of larger scale gas motions over the central two arcseconds. The implied rotation requires a central mass greater than 1.5 x 10^9 $M_\odot$. The extinction determined from the ratio of the Paβ and Brγ lines is found to be $A_V \sim 10$ mag for the western nucleus, and $A_V \sim 13$ mag for the eastern nucleus. The [FeII] and H_2 lines show a different morphology than the hydrogen recombination lines, particularly the H_2 line which shows significant flux between the two nuclei. The [FeII] and H_2 lines also do not show velocity splitting between the two nuclei. The difference in spatial and velocity structure between the [FeII], H_2 and ionized hydrogen lines implies multiple excitation processes are at work within the nucleus. The [FeII] and H_2 lines may have a significant contribution from extranuclear shocks related to either a starburst driven wind, or the ongoing merger process.

3.2 Introduction

Arp 220 (= IC 4553/4 = UGC 9913 = IRAS 15327+2340) is the nearest (cz $\sim$ 5450 km s^{-1}), and therefore most studied example of an ultraluminous infrared galaxy (ULIRG), having a far infrared luminosity of 1.5 x 10^{12} $L_\odot$ (Sanders et al. 1988). ULIRGs, which were defined as a class to have infrared luminosities, L(8-1000 μm), greater than 10^{12} $L_\odot$ by Soifer et al. (1987) and Sanders et al. (1988), are thought to be the result of the recent collision and subsequent merging of two gas rich galaxies (Sanders et al. 1988). In these galaxies, most of the energy emerges in the far infrared.

In the visual, Arp 220 possesses two faint tidal tails (e.g., Joseph and Wright 1985), and two bright knots straddling a thick dust lane which obscures the true nuclei (e.g., Joy et al. 1986). At 2.2μm, a double nucleus was found by Graham et al. (1990), with a spatial separation of 0.95"$\pm$0.01" and a position angle of 92°. This separation agrees very well with the 0.93" separation for the compact, nonthermal, double radio source observed at 6 cm, 2 cm, and 1.3 cm (Becklin and Wynn-Williams 1987; Norris 1988). For $H_o = 75$ km s^{-1} Mpc^{-1} (which we use throughout this thesis), 0.95" corresponds to a projected separation of only 330 pc. Graham et al. (1990) use this extremely small separation to argue that Arp 220 is in the final stages of a merger.

This chapter presents near infrared spectra of Arp 220 which reveal two components of H^+ gas coincident with the two infrared nuclei which are clearly separated in both position and velocity space. Also presented are observations of molecular and forbidden line transitions of H_2 and [FeII] which do not show the same spatial and velocity structures as the hydrogen recombination lines. These spectra have a spectral resolution a factor of 10 greater than any previously published near-infrared emission line spectra over the central most region of Arp 220, and were taken under excellent seeing conditions.

3.3 Observations and Data Reduction

Near infrared spectra of Arp 220 were obtained using the 200inch Hale telescope at Palomar Observatory on 1994 July 26. The spectra were taken with a new near infrared longslit spectrograph, fully described in chapter 2 and in Larkin et al. (in prep.). The spectrometer is cryogenically cooled and can take direct images through the same optical path by placing a flip mirror in front of the grating. The spectrometer

uses a separate near infrared camera containing a 256 x 256 NICMOS 3 HgCdTe detector. At the f/70 Cassegrain focus, the array has a plate scale of 0.167" per pixel along the spatial axis or along both axes in the imaging mode. Two gratings are available with ~1000 and ~4000 resolution for a 0.7" slit width.

During these observations, the seeing, as determined from images of a calibrator star, was ~0.5" at 2 μm, although the observations of Arp 220 may have a slightly worse resolution since we cannot fully resolve the separate K Band nuclei in images taken with the spectra. The sky had very light cirrus clouds, which made for non-photometric conditions. A nearby star was used with an offset guider which controls a tip-tilt secondary. With this guiding system, tracking errors (<0.1") are insignificant compared to the seeing.

For the Arp 220 observations, the lower resolution grating was used with the slit set at 0.75" x 40". The slit was oriented east-west so that the two nuclei, which have a position angle of 92^o (Graham, et al. 1990), could both be included in the same spectrum. Two grating angles were used to give wavelength coverages from 1.240 to 1.295 μm (R~1050, FWHM ~ 280 km sec^{-1}), and 2.090 to 2.200 μm (R~800, FWHM ~ 375 km sec^{-1}). These wavelength ranges were selected to include the redshifted [FeII] ($\lambda = 1.2567\mu$m), and Paβ ($\lambda = 1.2818\mu$m) spectral lines, and the redshifted H_2 ($\lambda = 2.1213\mu$m) and Brγ ($\lambda = 2.1655\mu$m) lines. All wavelengths quoted in this paper are values in air. The J-band spectrum consisted of two 600s exposures in which the nucleus was moved 20" along the slit between the two exposures. The airmass during these exposures was between 1.50 and 1.62. The K band spectrum consisted of four 300s frames, again with the nucleus moved 20" back and forth along the slit between frames. The airmass for the K band frames ranged from 1.66 to 1.81. Thus the total integration time was 1200s for each grating rotation. The Yale Bright Star, BS 5213 (Hoffleit 1964) (spectral type G3V) was observed at air masses ranging from

1.62 to 1.67 in order to remove telluric absorption features of the atmosphere and as a spectral flat field. No emission or absorption lines other than atmospheric lines were observed in the standard star, although our ability to independently flat field our spectral flats is limited.

The spectra were reduced by first subtracting image pairs and then dividing by a sky subtracted standard star frame. Bad pixels were then removed with linear interpolation. Atmospheric OH emission lines in the stellar spectrum were fit with third order polynomials in order to remove a slight curvature in the spectral lines and to wavelength calibrate the spectra. Wavelengths for the OH lines were obtained from Oliva and Origlia (1992). The absolute wavelength calibration is accurate to about 1 pixel (70 km sec^{-1}) and the relative wavelength calibration is accurate to about 1/3rd of a pixel (25 km sec^{-1}). Slight spatial curvature was removed by fitting spectra taken of a calibrator star which was moved in 5" steps along the slit. Continuum subtraction was performed by fitting the continuum with a second order polynomial along every column and subtracting this fit. After continuum subtraction, all unaccounted for features are below three sigma per resolution element.

Broad band 1.25μm (J-band) and 2.2μm (K band) images were also taken in order to flux calibrate the spectra. A 5" synthetic aperture was used to determine the broad band flux calibration from earlier single beam photometry measurements by Neugebauer et al. (1987). A 0.75" x 5" synthetic aperture on the same broad band images was then used to determine the flux within our slit. This was then compared to the spectra which were assumed to be flat across each band (lower resolution grism spectra show that this is a good approximation).

3.4 Results

3.4.1 Hydrogen Recombination Lines

Figure 3.1 shows the position-velocity maps for the [FeII], Paβ, H_2 and Brγ lines over the inner 2.5" x .75". The slit orientation was east-west, across the two nuclei. The central, brightest knot in both the J and K bands, is identified with the western infrared nucleus and was selected as the reference velocity. The absolute velocity of the Paβ line at the western nucleus was 5380$\pm$70 km s^{-1}, and of the Brγ line, 5460$\pm$80 km s^{-1}. The mean heliocentric redshift, as determined from CO(J=1-0) emission, is cz = 5450$\pm$20 km s^{-1} (Sanders et al. 1988). The fainter knot in the Brγ image, is centered 0.95$\pm$.08 arcsecond east of the brighter nucleus and at a relative velocity of +200$\pm$25 km s^{-1}. This fainter knot is visible in all four of the individual K band spectra, ruling out its creation through inaccurate chopping or slit curvature. In the Paβ map, significant emission is found coincident with the Brγ knot, but is not as centrally concentrated at this second location. The position of this second peak matches that of the eastern infrared nucleus found in the high resolution K band image of Graham et al. (1990). Figure 3.2 shows spectra along the eastern and western nuclei respectively. The lines are essentially unresolved along a single spatial column (a resolution element corresponds to 285 km sec^{-1} for the J band and 375 km sec^{-1} for the K band), but appear slightly broadened in figure 3.2 because the apertures integrate over part of the velocity gradient discussed above. The velocity shift found in the hydrogen recombination lines, discussed above, is clearly visible. Through a 5" diameter aperture, Depoy et al. (1987) measured a Brα (4.05 μm) emission line which they fit both with one and two component Gaussian fits. The two component fit yielded a "narrow" component with an intrinsic FWHM of 1000

km sec^{-1} and a "broad" component with an intrinsic FWHM of 3300 km sec^{-1}. We do not see evidence for either of these line components in the Brγ line.

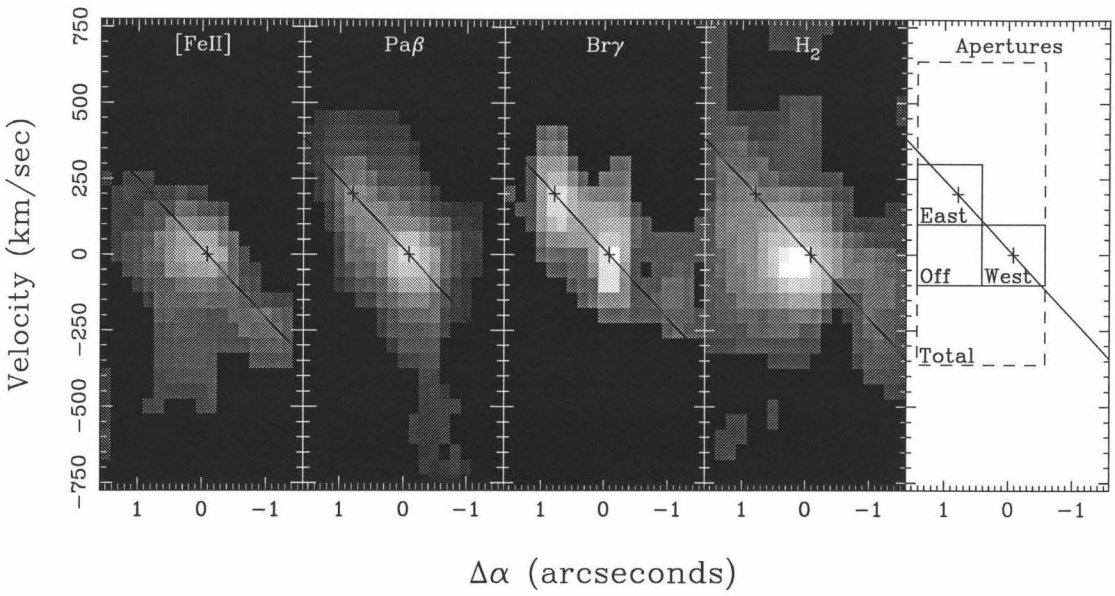

Figure 3.1: [FeII], Paβ, Brγ, and H_2 position-velocity plots along with a diagram showing the various apertures used to make table 3.1. The slit was oriented east-west to include both nuclei which are most visible in the Brγ plot. The western nucleus was selected as the zero-point offset for both axes. Black crosses mark the two Brγ centroids corresponding to the two nuclei and a straight line is drawn though them to show the velocity gradient. The lowest gray level corresponds to 2.5 sigma per resolution element which was 0.65 times the noise per pixel. The images are plotted from 0 (black) to two-thirds of their peak level (white).

In table 3.1, we present the fluxes, line ratios and calculated extinctions for the two nuclei. Four apertures, shown in the last panel of figure 3.1, were used on the position velocity plots to generate this table. First a 1"x200 km s^{-1} aperture was placed on the two nuclei respectively. A similar aperture was also placed at the spatial position of the eastern nucleus, but at the velocity of the western nucleus. The last aperture is 2"x1000 km s^{-1} and encompasses essentially all of the nuclear emission within our 0.75" slit. The extinctions are obtained by interpolating the interstellar extinction law of Rieke and Lebofsky (1985) at the rest wavelengths of Paβ and Brγ and using

Table 3.1
Line Fluxes[a], Ratios and Calculated Extinctions

Quantity	western nucleus[b]	eastern nucleus[b]	off eastern[b,c]	Total nuclear[d]
Brγ	0.65±.08	0.53±.08	0.38±.08	2.7±.3
H_2	1.32±.08	0.76±.08	1.03±.08	6.4±.3
Paβ	1.06±.05	0.56±.05	0.45±.05	3.8±.2
[FeII]	0.71±.05	0.21±.05	0.40±.05	2.1±.2
$\frac{Br\gamma}{Pa\beta}$	0.6±.1	1.0±.2	0.8±.3	0.7±.1
$\frac{H_2}{Br\gamma}$	2.0±.4	1.4±.4	2.7±.8	2.3±.3
$\frac{[FeII]}{Pa\beta}$	0.7±.1	0.4±.1	0.9±.2	0.6±.1
$\frac{H_2}{[FeII]}$	1.9±.2	4±1	2.6±.5	3.0±.3
A_V	10±1	13±2	12±2	11±1
int $\left(\frac{H_2}{[FeII]}\right)^e$	0.5±.1	0.6±.3	0.5±.2	0.6±.1

[a] Fluxes are in 10^{-15} ergs s^{-1} cm^{-2}, and are not corrected for extinction.
[b] Used a 1"x200 km s^{-1} aperture. The slit width is 0.75".
[c] "Off eastern" refers to the position of the eastern nucleus but with the same central velocity as the western nucleus.
[d] A 2"x1000 km s^{-1} aperture encompassing essentially all of the nuclear emission in the slit. The slit width is 0.75".
[e] Intrinsic ratio of H_2/[FeII] corrected for the extinction calculated from the hydrogen recombination lines as described in the text.

Table 3.1: Arp 220 line fluxes, flux ratios and calculated extinctions for the apertures marked in figure 3.1.

the case B intrinsic line ratio of 0.1647 (Osterbrock 1989). A foreground screen of dust is assumed for the extinction correction. If the dust and emitting sources are mixed, the effective extinction could be much larger. The intrinsic H_2 to [FeII] ratio is calculated by correcting the observed ratio for this extinction.

The observation that the Brγ emission is more peaked on the eastern nucleus than the Paβ emission is most easily explained by dust extinction. The calculated extinction at the western nucleus is $A_V \sim 10$ mag compared to $A_V \sim 13$ mag for the eastern nucleus (see table 3.1). Both of these numbers are consistent with the small aperture infrared measurements of Mazzarella et al. (1992), and Armus et al. (1994b). Note that the infrared extinctions for each line are interpolated from broad

band extinctions given in Rieke & Lebofsky (1985) where $A_J \sim 0.282\ A_V$, and $A_K \sim 0.112\ A_V$.

3.4.2 [FeII] and H_2

The measured fluxes for the [FeII] ($\lambda = 1.2567\mu$m) and H_2 ($\lambda = 2.1218\mu$m) lines at various locations in the central 2" are also summarized in table 3.1. The flux of the [FeII] emission in a 2" x .75" aperture, integrating over all velocities, is somewhat lower than that found in a 2" x .8" aperture by Armus et al. (1994b), being 2.1 x 10^{-15} ergs s^{-1} cm^{-2} compared to 3.5 x 10^{-15} ergs s^{-1} cm^{-2}. The Paβ emission, however, which was taken simultaneously with the [FeII], agrees very well with Armus et al. (1994b), being 3.8 versus 4.0 x 10^{-15} ergs s^{-1} cm^{-2}. A combination of different morphologies in the [FeII] and Paβ emission lines (the latter is more centrally concentrated) along with slightly improved seeing at the time of the new observations can explain these differences.

An important consideration in the flux calibrations is the accuracy of the stellar flat field at these wavelengths. At the redshift of Arp220, H_2 is close to the rest wavelength of Brγ and [FeII] is close to the rest wavelength of Paβ. The resolution is sufficient to separate possible Balmer contamination in the spectral standard by approximately two resolution elements from the extragalactic lines. As stated above, we also found no evidence for lines in the spectra of the spectral standard. The good agreement in fluxes with Armus et al. (1994b) also suggests that the effect is not significant for the current observations.

The [FeII] and H_2 lines show no significant shift between the two locations, although the H_2 emission is broadened towards higher velocities at the eastern nucleus. The position-velocity plots in figure 3.1 show that the H_2 peaks 1.5 pixels (0.25") to the east of the western nucleus. Such morphological and kinematic differences con-

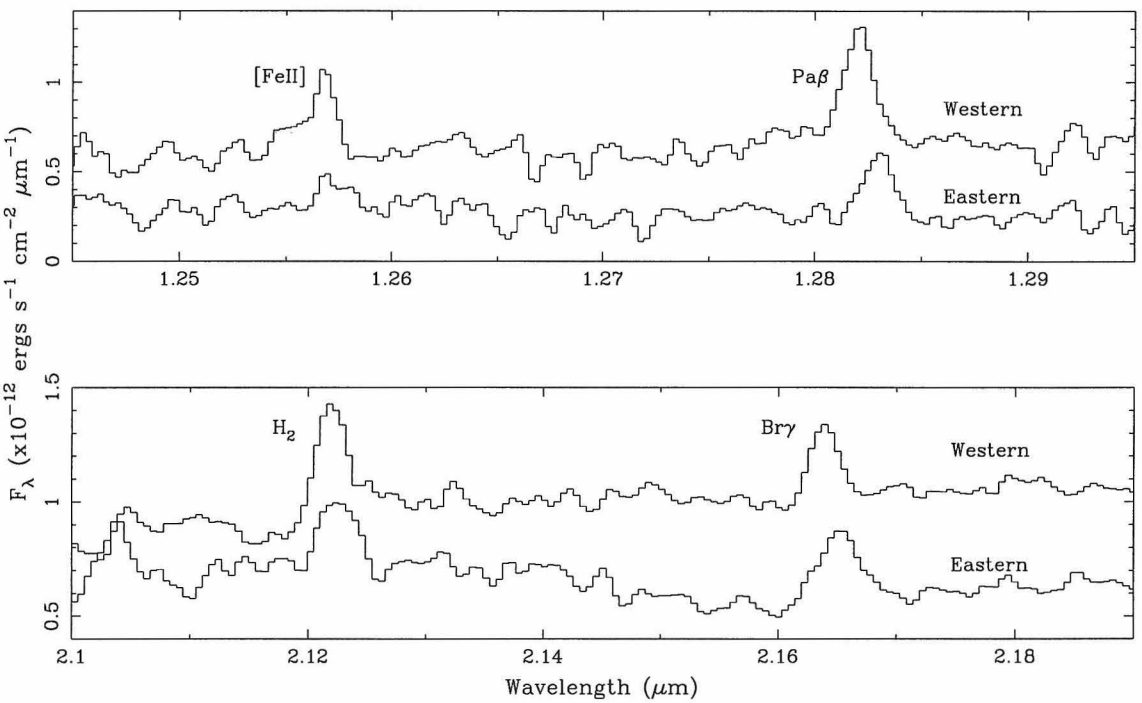

Figure 3.2: J and K-band spectra showing all four emission lines discussed in this paper. The spectra represent a synthetic 0.5" slice centered on the eastern and western nuclei, respectively. The spectra were taken with a 0.75" slit width with the slit oriented east-west. Note the wavelength shift of the hydrogen recombination lines between the two nuclei. The wavelength scale is given in the rest frame of the western nucleus. The Paβ and Brγ lines appear slightly broadened because the apertures integrate over the observed gradient. The lines are unresolved along an individual spatial pixel column.

tribute to the enhanced ratios of [FeII] and H_2 to the hydrogen recombination lines in the "off eastern" position (table 3.1), and the suppression of these ratios on the eastern nucleus. The [FeII] and the H_2 are kinematically and spatially distinct from the Paβ and Brγ lines.

3.5 Discussion

The spectra presented here have separated, both spatially and kinematically, the two nuclei within Arp 220. In the Brγ emission, the nuclei are found to be separated by 0.95" and 200 km s^{-1}. The Paβ emission shows a similar velocity shift, but is not strongly peaked at the location of the eastern nucleus. The centroid of the H_2 emission is not peaked on the western nucleus but is 0.25" towards the eastern nucleus. The H_2 also does not show the same velocity structure as the hydrogen recombination lines. The [FeII] emission shows a weak maximum at the location of the western nucleus along with emission in the direction of the eastern nucleus.

An important consideration is how much of the observed velocity shift in the recombination lines could be due to a spatial rotation of the emission line gas relative to the broad band emission which was used to position the slit. The recent narrow band Paβ image by Armus et al. (1994b.) appears to show a spatial displacement of the Paβ emission which would correspond to a rotation of <14 degrees (<0.25" over 1" separation). This could contribute up to ~95 km s^{-1} to the observed Paβ velocity shift making the actual velocity >105 km s^{-1}. This rotation is quite uncertain, however, since the image has had a very similar continuum image subtracted, and a small alignment error in continuum morphology could generate a fairly large spatial shift. The radio emission peaks (Becklin and Wynn-Williams 1987, and Norris 1986) are known to have a position angle of 102^o. If the infrared emission had the same

angle, it would reduce any observed velocity by $\sim$75 km s^{-1} making the actual velocity $\sim$275 km s^{-1}. The most likely angle, however, is that of the K band emission peaks which in Graham et al. (1990) was found to be 92^o which would only affect the measured velocity by 13 km s^{-1}, making the actual velocity 213 km s^{-1}. The fact that the observed shift is qualitatively and quantitatively consistent with recent CO millimeter wave velocities from Scoville et al. (1995) (see below), and the central mass estimates from this velocity shift are consistent with the stellar CO dispersion measurements of Doyon et al. (1994a,b) (see below) gives us confidence that the shift reported here is real, and the uncertainties due to spatial shifts in the nuclei are small. The velocity shift between the western and eastern infrared nuclei in Arp220 is likely to be close to our measured value of 200$\pm$25 km s^{-1}.

The most obvious question is whether the observed kinematic shift is due to the orbital motion of the nuclei. The excellent agreement of the spatial separation of the Brγ peaks with both the 2.2 μm (Graham et al. 1990) and the radio (Becklin & Wynn-Williams 1987; Norris 1988) peaks, argues that this shifted emission is closely associated with the nuclei. Recent CO measurements (Scoville et al. 1995 in preparation) at 1.3 mm, reveal a rotational gas motion of $\sim$300 km s^{-1} across the central 0.9" at $\sim$45^o position angle. Projecting this motion onto our slit (P.A.=90^0), and using our separation of 0.95", yields a rotation velocity of 220 km s^{-1}. This is very close to the observed Brγ velocity shift of 200 km s^{-1}. Both the spatial agreement with the nuclei, and the velocity agreement with the CO rotation rate, argue that we are measuring the rotation of the two nuclei. Since Arp220 has been shown to possess large scale outflows (Heckman, Armus, & Miley 1987,1990), it is possible, however, that the observed velocity shift may have some component due to non-rotational gas motions along the line of sight.

If the observed velocity shift is predominantly rotational in nature, then we may estimate the nuclear mass. Dynamical friction will circularize the nuclear orbits on a very short time scale. Assuming that the observed distance and rotation rate are the actual orbital radius and circular velocity, and that the orbit is seen edge on, gives a lower limit to the nuclear mass. We follow Graham et al. (1990) in assuming that the mass ratio can best be estimated by the K band flux ratio of 1.6, which when adjusted for our measured extinctions, becomes 1.2. Although the K band flux ratio may be affected by supergiants and nonstellar emission processes from the suspected circumnuclear starburst (Rieke et al. 1985), the mass calculation is not extremely sensitive to this ratio unless one of the nuclei completely dominates the mass. In that case the total mass would be twice that calculated below. With these assumptions, the lower nuclear mass limit is 1.5±0.4 x $10^9(H_o/75km\ s^{-1}\ Mpc^{-1})$ $M_\odot$, where the uncertainty is dominated by the uncertainty in the relative velocities. This estimate ignores the possible effects of position angle uncertainty as discussed above. Possible errors in the position angle could reduce our mass calculation by as much as a factor of 4 or increase it by almost a factor of 2. However, we have used the most likely velocity in this calculation, and both the velocity and the derived mass match very well to other estimates from other techniques. As an example, the nuclear mass calculated above is very consistent with the value of 1.8±0.8 x 10^9 $M_\odot$ within the central 2" (Shier, Rieke, & Rieke 1994), estimated from a CO bandhead (2.3μm) velocity dispersion of 125±30 km s^{-1} from a preprint of Doyon et al. (1994a). The final quoted velocity dispersion of 150±21 km s^{-1} (Doyon et al. 1994b) would predict a slightly higher value, but is easily reconciled with our value being a lower mass limit, and the uncertainties in the numbers.

The eastern nucleus has a K band magnitude of 13.7±0.2 mag within a 0.8" diameter aperture, while the western nucleus is 13.2±0.2 mag (Graham et al. 1990).

Using our calculated extinctions of $A_V = 13$ mag and 10 mag on the eastern and western nuclei, respectively, we derive a total nuclear K band luminosity of 3.3 x 10^{10} $L_\odot$. This gives an M/L = 0.05 within the K band, where we have used +3.41 mag for the absolute K band magnitude of the sun (Allen 1973). Most starburst models predict much lower values of M/L (K band), although the starburst calculations of Leitherer, & Heckman (1994), show that extreme models with an aging (10^8 years) burst can produce an M/L(K band) of ~0.05. This suggests our estimate of the M/L in the nucleus of Arp220 is only consistent with a starburst if the burst was isolated in time, occurring ~10^8 years ago. The strong CO band absorption seen in the nucleus of Arp 220 (Rieke et al. 1985, Ridgeway, Wynn-Williams & Becklin 1994), however, suggests that young red supergiant stars contribute significantly to the K band light, implying the age of the starburst is much less than ~10^8 years. The large M/L(K band) we have measured then suggests that a large fraction of the nuclear mass could be tied up in an older pre-existing stellar population. The fact that our dynamical mass estimate is only a lower limit would cause us to underestimate M/L and would enhance this effect.

Following Graham et al. (1990), the merging time scale can also be estimated from the rotational velocity using:

$$t_m = \frac{2\pi r}{v_c}\left(\frac{M}{m}\right) \tag{3.1}$$

derived from Binney & Tremaine (1987). Again we take the observed velocity and separation as the circular velocity and orbital radius, and a mass ratio of 1.2. This yields a merger time of 1.2 x 10^7 years, close to that found by Graham et al. (1990) from an estimated circular velocity of 150 km s^{-1} and a mass ratio of 1.6.

The kinematic differences between the [FeII] and H_2 compared to the H^+ lines suggests the [FeII] and H_2 may have an additional excitation source. The extended nature of the [FeII] and H_2 emission suggests that the nuclei may be surrounded by an extended shocked region. Fast shocks from supernovae remnants or from large scale winds could provide the energy required for this enhancement. Another excitation mechanism could be collisional shocks of interstellar clouds which, due to the ongoing merger process, may still have relative speeds of $\sim$300 km s^{-1}. Since the H_2 centroid lies between the two nuclei, and does not follow the hydrogen recombination lines, it may have a strong merger induced shock component. Similar morphology has been observed in NGC 6240 (Van Der Werf et al. 1993), and was used to argue that the H_2 emission was excited in shocks from collisions of interstellar material resulting from an ongoing merger. We cannot, however, at this point discriminate between interstellar cloud collisions and superwind driven shocks. The fact that the H_2/[FeII] ratio is higher than in most shocked environments may be explained by having some UV excitation of the H_2 by the central ionizing sources. Taking our extinction corrected Brγ luminosity to derive an ionizing photon luminosity and using the UV fluorescence models in Black & Dishoeck (1987), we find that the UV photon flux is only sufficient to power the observed H_2 emission with the most optimistic models. Most UV fluorescence models fall short by as much as a factor of 100 in generating the observed H_2 emission, suggesting that UV fluorescence is probably not a significant excitation source. Additional observations of other H_2 lines would be useful in discriminating between thermal excitation and UV fluorescence.

3.6 References

Allen, C. W., 1973, *Astrophysical Quantities* , (London & Atlantic Highlands: The Athlone Press).

Armus, L., Surace, J. A., Soifer, B. T., Matthews, K., Graham, J. R., & Larkin, J. E. 1994a, A.J., 108, 76.

Armus, L., Shupe, D. L., Matthews, K., Soifer, B. T., & Neugebauer, G. 1994b, Ap.J., in press.

Becklin, E. E., & Wynn-Williams, C. G. 1987, in *Star Formation in Galaxies*, ed. C. J. Lonsdale (Washington, D. C.: US Government Printing Office), p.643.

Binney, J., & Tremaine, S. 1987, *Galactic Dynamics* , (Princeton: Princeton University Press).

Black, J. H., & van Dishoeck, E. F. 1987, Ap.J., 322, 412.

Depoy, D. L., Becklin, E. E., & Geballe, T. R., 1987, Ap.J.(*letters*), 316, L63.

Doyon, Rene, Wells, M., Wright, G. S., & Joseph, R. D. 1994a, in "Mass Transfer Induced Activity in Galaxies", ed. Schlosman.

Doyon, R., Wells, M., Wright, G. S., Joseph, R. D., Nadeau, D., & James, R. A. 1994b, Ap.J.(*letters*), 437, L23.

Graham, J. R., Carico, D. P., Matthews, K., Neugebauer, G., Soifer, B. T., & Wilson, T. D. 1990, Ap.J.(*letters*), 354, L5.

Heckman, T. M., Armus, L., & Miley, G. K. 1987, A.J., 93, 276.

Heckman, T. M., Armus, L., & Miley, G. K. 1990, Ap.J.Supp., 74, 833.

Hoffleit, Dorrit 1964, Catalogue of Bright Stars, Yale University Observatory, Third Revised Edition.

Joseph, R. D., & Wright, G. S. 1985, M.N.R.A.S., 214, 87.

Joy, M., Lester, D. F., Harvey, P. M., & Frueh, M. 1986, Ap.J., 307, 110.

Larkin, J. E., Knop, R. A., Lin, S. Matthews, K., Soifer, B. T. 1994, P.A.S.P., in press.

Leitherer, C., Heckman, T. M. 1994, Ap.J., in press.

Mazzarella, J. M., Soifer, B. T., Graham, J. R., Hafer, C. I., Neugebauer, G., & Matthews, K. 1992, A.J., 103, 413.

Neugebauer, G., Elias, J., Matthews, K., McGill, J., Scoville, N., & Soifer, B. T. 1987, A.J., 93, 1057.

Norris, R. P. 1988, M.N.R.A.S., 230, 345.

Oliva, E., & Oliglia, L. 1992, A&A, 254, 466.

Osterbrock, D. E. 1989, *Astrophysics of Gaseous Nebulae and Active Galactic Nuclei*, University Science Books.

Ridgeway, S. E., Wynn-Williams, C. G., & Becklin, E. E. 1994, Ap.J., 428, 609.

Rieke, G. H., Cutri, R. M., Black, J. H., Kailey, W. F., McAlary, C. W., Lebofsky, M. J., & Elston, R. 1985, Ap.J., 290, 116.

Rieke, G. H., & Lebofsky, M. J. 1985, Ap.J., 288, 618.

Sanders, D. B., Soifer, B. T., Elias, J. H., Madore, B. F., Matthews, K., Neugebauer, G., & Scoville, N. Z. 1988, Ap.J., 325, 74.

Shier, L. M., Rieke, M. J., & Rieke, G. H. 1994, Ap.J.(*letters*), 433, L9.

Soifer, B. T., Sanders, D. B., Madore, B. F., Neugebauer, G., Danielson, G. E., Elias, J. H., Lonsdale, C.J., & Rice, W. L. 1987, Ap.J., 320, 238.

Van Der Werf, P. P., Genzel, R., Krabbe, A., Blietz, M., Lutz, D., Drapatz, S., Ward, M. J., & Forbes, D. A. 1993, Ap.J., 405, 522.

Chapter 4

Near Infrared Spectroscopy

Prologue: This chapter discusses the main focus of this thesis, namely infrared spectroscopy of a sample of 12 "classical" low luminosity LINERs, and 4 multiple nuclei galaxies with at least one LINER component. The spectra concentrate on the lines [FeII], and H_2 and the hydrogen recombination lines Paβ and Brγ. The majority of the LINERs show strong [FeII] and/or H_2 emission significantly stronger than typical Seyfert or starburst galaxies in comparison to hydrogen recombination lines. Both of these lines show a strong correlation with the optical [OI](6300Å) line across all galaxy types and for a range of more than 100 in flux ratio with hydrogen recombination lines. The LINERs are subdivided into two groups based on the strength of [FeII]/Paβ being larger of smaller than 2. The "weak" [FeII] LINERs exhibit Seyfert-like traits including some broad Hα detections, and strong x-ray emission. The "strong" [FeII] LINERs all have evidence for recent star formation and compact supernovae may be responsible for the enhanced [FeII] line. Comparisons with the IRAS 25 to 60 micron index show that for the flat spectrum LINERs (α(25:60) > -2), a starburst mechanism is incompatible with the infrared line ratios. Comparison of x-ray and infrared line luminosities show that the x-rays are strong enough to provide

sufficient energy for these lines in at least the majority of LINERs with x-ray detections, and for Seyferts. We therefore, argue that at least a large subgroup of LINERs (the "weak" [FeII] LINERS) have a power-law continuum source which excites the low ionization line emission.

4.1 Target Selection and Observing Strategy

The target list of classical LINERs began with the original sample of 30 LINERs (including several "transition" objects which have line ratios on the border between LINERs and Seyferts) from Heckman (1980). Heckman (1980) took optical spectra of a flux limited sample of the brightest galaxies above a declination of $+40^o$. Because Heckman (1980) was only able to obtain red spectra (required for LINER classification) during the spring, all of the available LINERs were concentrated on the sky in the range of right ascension between 8^h30^m and 13^h30^m. To extend the availability of targets, additional galaxies were selected from Keel (1983) and Ho et al. (1993). Because of bad weather during most of the spring runs, the objects observed with the infrared spectrograph are preferentially from these additional surveys. In the end 11 classical LINERs were observed in both the J and K bands and 1 additional galaxy had only J-band spectra taken. Table 4.1 lists the galaxies observed, the dates of observations, and the wavelengths covered.

In addition to the classical LINERs, we were interested in observing multiple nuclei galaxies in which at least one of the nuclei has line ratios consistent with the LINER definition. The goal was to investigate the LINER phenomenon over a range of luminosities and physical conditions to determine if these higher luminosity interacting systems are really members of the same class of objects as the low luminosity LINERs defined by Heckman (1980). Two ultraluminous infrared galaxies were selected with

Table 4.1
Near Infrared Spectroscopy Observing Log

Object (1)	RA(1950) (2)	Dec(1950) (3)	cz (km s^{-1}) (4)	Date (5)	Central λ (6)	Res. ($\frac{\lambda}{\Delta\lambda}$) (7)	P.A. (deg) (8)
NGC 0404	01h06m39.3s	+35d27m10s	-43	94/08/19	1.2567	1000	128
					2.1470	820	128
NGC 2685	08h51m40.7s	+58d55m33s	877	95/03/14	1.2683	1020	305
					2.1860	815	305
NGC 3992	11h55m00.8s	+53d39m11s	1051	94/05/22	1.2707	1020	270
					2.1532	800	270
NGC 3998	11h55m20.9s	+55d43m56s	1138	95/05/13	1.2671	1020	270
					2.1762	810	270
NGC 4258	12h16m29.8s	+47d34m51s	449	94/05/22	1.2707	1020	58
					2.1532	800	58
NGC 4589	12h35m29.0s	+74d27m59s	1825	95/03/14	1.2683	1020	343
					2.1501	800	343
NGC 4736	12h48m31.9s	+41d23m32s	307	95/03/12	1.2683	1020	35
					2.1801	820	35
NGC 4826	12h54m16.9s	+21d57m18s	350	95/03/13	1.2683	1020	270
					2.1801	820	270
NGC 5194	13h27m46.0s	+47d27m22s	467	94/05/23	1.2707	1020	170
					2.1532	800	170
				94/07/26	1.2837	1020	170
					2.1649	810	170
NGC 7217	22h05m37.9s	+31d06m52s	1400	94/07/26	1.2679	1020	270
NGC 7479	23h02m26.41s	+12d03m11s	2800	94/08/21	1.2837	1060	55
					2.1649	810	55
NGC 7743	23h41m48.6s	+9d39m25s	1710	94/07/27	1.2693	1020	270
					2.1515	780	270
Arp 220	15h32m47.0s	+23d40m02s	5450	94/07/27	1.2845	1050	270
					2.1784	800	270
IR 17132	17h13m14.1s	+53d13m14s	15249	94/08/19	1.3424	750	60
					2.2551	870	60
Mrk 848	15h16m19.4s	+42d55m38s	12065	94/08/20	1.3217	1100	160
					2.2320	850	160
Mrk 928	23h15m47.2s	-4d41m22s	7511	94/08/20	1.3027	1060	96
					2.1970	830	96

Table 4.1: Log of the galaxies observed, their coordinates, redshifts, observation dates, wavelength settings, resolution, and position angle of the slit.

double LINER nuclei: Arp 220 and IRAS 17132+5313. Also two Markarian galaxies were selected: Mrk 848 (1 Zw 107) and Mrk 928. Mrk 848 is a LINER, starburst system, while Mrk 928 is a triple system with LINER, Seyfert 2 and starburst nuclei. Spectra were taken with the slit aligned so both nuclei could be measured simultaneously; in the case of Mrk 928, the Seyfert 2 and LINER nuclei were measured. All four of these galaxies were selected because a wealth of observations are available at other wavelengths to aid in our understanding of the infrared lines. These galaxies are also listed at the bottom of table 4.1.

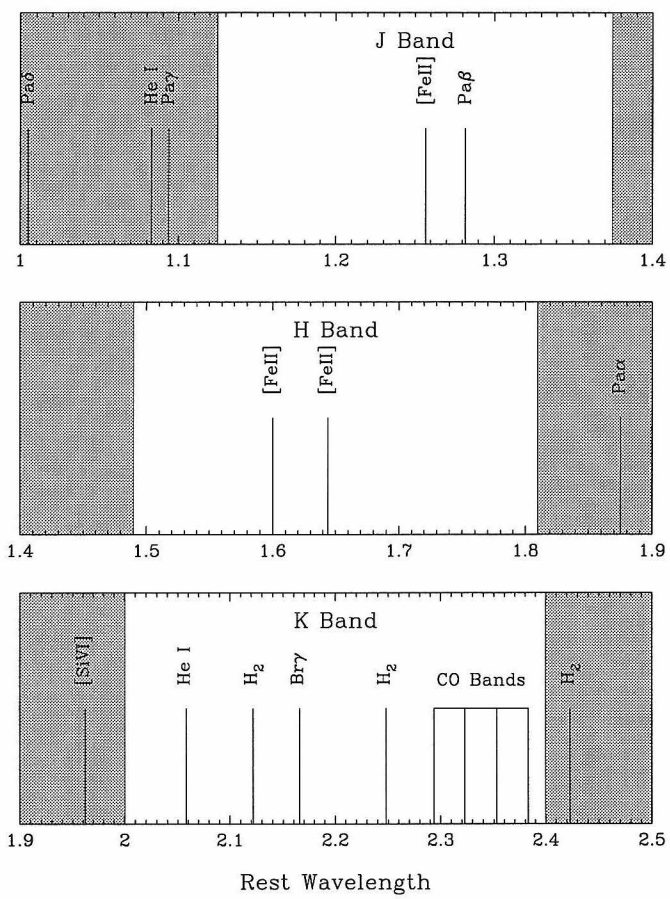

Figure 4.1: The panels show the locations of many of the brightest infrared lines. The gray areas are unavailable at zero redshift because of atmospheric absorption. The wavelength coverage of the spectrograph is ~0.06 μm within the J band, ~0.07 μm within the H band, and ~0.11 μm within the K band.

Since LINERs typically have faint emission features, it was important to concentrate the observations on the potentially brightest near infrared lines. Figure 4.1 shows the locations of a selected sample of potentially bright infrared lines. Among those lines accessible at zero redshift, Paβ is typically the brightest feature in AGN and starburst galaxies. Brγ is fainter by a factor of about 6 from Paβ but is still usually one of the brightest lines. The brightest Fe^+ line is at 1.2567 μm which is only 0.0251 μm away from Paβ, making this an obvious pair of lines to observe simultaneously. The strongest H_2 line available at zero redshift is from the 1-0 S(1) transition at 2.1218 μm. This line is 0.0437 μm away from Brγ again creating an obvious pair of lines to observe simultaneously. In order to maximize the number of LINERs observed, only these two settings were observed at a resolution of $\sim$1000.

4.2 Observing Procedures and Data Reductions

4.2.1 Near Infrared Spectroscopy at the 200 Inch Hale Telescope

Near infrared spectra were obtained using the 200 inch Hale telescope at Palomar Observatory from 1994 April to 1995 May. The spectra were taken with a new near infrared longslit spectrometer, described in chapter 2. For all observations, the lower resolution grating was used with the slit set at 0.75" x 40". To center the objects on the slit, images were first taken through a wide open slit (10" x 40") and the telescope was moved to place the nuclear centroid onto the slit center. The position angle of the slit was selected either by aligning the slit along a position angle of known extended optical emission observed in optical Hα images obtained at the 60 inch telescope at Palomar (Larkin et al. 1995, in preparation) or by orienting the slit along the minor

axis. For all but one object (Markarian 928) the galaxy was moved back and forth along the slit between two locations 10" from the opposite ends of the slit (20" between the two positions). In this way, each spectrum in a pair could serve as the sky frame for image subtraction for the other mated spectrum. In the case of Markarian 928, the separation of the two nuclei (12.5") was too great to allow this paring of spectra, and a separate sky spectrum was taken 120" away. Two grating angles were typically used to give rest frame wavelength coverages from 1.245 to 1.300 μm (R$\sim$1050), and 2.087 to 2.207 μm (R$\sim$800). These wavelength ranges were selected to include the redshifted [FeII] ($\lambda = 1.2567\mu$m), and Paβ ($\lambda = 1.2818\mu$m) spectral lines, and the redshifted H_2 ($\lambda = 2.1218\mu$m) and Brγ ($\lambda = 2.1655\mu$m) lines. All wavelengths quoted in this thesis are values in air.

The Yale Bright Star Catalog (Hoffleit 1964) was used to select main sequence G stars that were observed close in time and airmass to the galaxies in order to remove telluric absorption from the galaxy spectra and to serve as flat fields. The chopping secondary of the telescope was driven with a triangular waveform to move the star back and forth along the slit to uniformly illuminate the array. The stars represent a good approximation to an ideal blackbody at these wavelengths except for weak hydrogen absorption lines. In order to properly correct the galactic spectra, these lines must first be removed from the stellar spectra. Simple interpolation on the two dimensional spectra is unsatisfactory at removing the absorption features due to a ripple pattern that is especially strong in the K-band. This ripple is thought to be caused by interference in the sapphire substrate of the NICMOS 3 chip inside the camera. The level of the ripple can be as much as 20% of the signal and is often stronger than the stellar absorption features. Panel (a) in figure 4.2 shows an uncorrected spectrum of the G star BS 4277. In panels (a), (c) and (e), the strength of the recombination line has been doubled to make its location more obvious. Interpolat-

ing over the hydrogen lines, removes the ripple from the stellar spectra making them inappropriate for direct division into the galaxy spectra. Robert Knop has identified the location of the ripple pattern in Fourier transforms of similar spectra. By interpolating over this location (shown in panel (b) of figure 4.2), I have found that the ripple in the stellar spectrum can be greatly reduced. In this cleaned image (panel (c)), the absorption line can be properly removed by linear interpolation (panel(d) shows the interpolated frame). Once the line has been removed, the strength of the absorption can be determined at every pixel by dividing the cleaned image(c) by the interpolated image(d). This ratioed frame (shown in panel (e)) can then be multiplied to the original frame to remove the line absorption without affecting the ripple pattern. Since only those pixels covering the absorption line are affected, it is not important if some residual ripple remains in the corners of the cleaned image such as in panel (c) of figure 4.2. The final spectral flat is show in panel (f).

The galaxy spectra were reduced by first subtracting image pairs. The galaxy frames were then divided by the interpolated star frames described above. The interpolation in the stellar frames does increase the noise at the affected wavelengths especially in the K band, where some residual fringing problems may persist. Bad pixels were then replaced by the median of their neighboring pixels. Atmospheric OH emission lines in the stellar spectrum were fit with third order polynomials in order to remove a slight curvature in the spectral lines and to wavelength calibrate the spectra. Wavelengths for the OH lines were obtained from Oliva and Origlia (1992). Slight spatial curvature was removed by fitting spectra taken of a calibrator star which was moved in 5" steps along the slit.

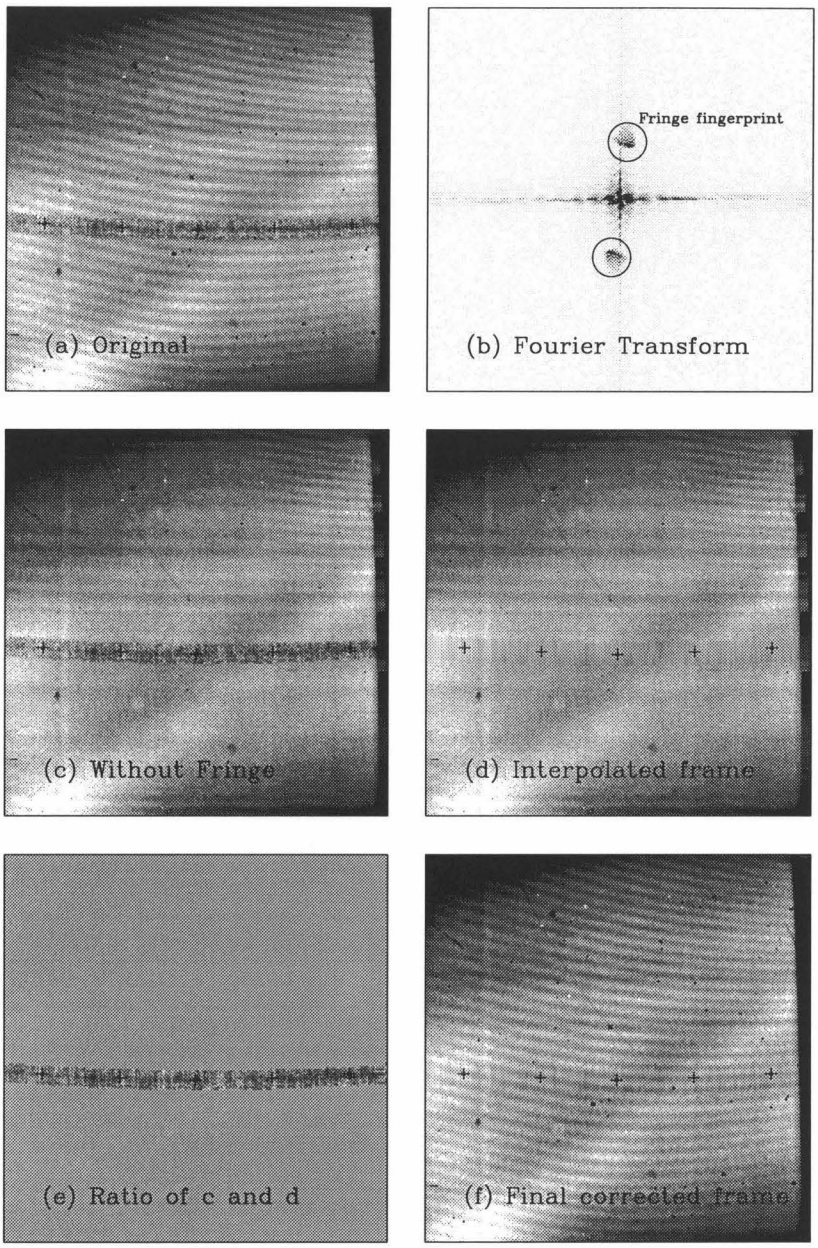

Figure 4.2: This figure shows the K-band spectrum of the G star bs 4277 in various stages of preparation. In the spectral frames, the crosses trace the approximate location of the Brγ line. In the spectral frames, position is horizontal and wavelength is vertical. Frame (a) shows the original sky subtracted spectrum. Frame (b) is the Fourier transform of this original spectrum showing the location (circled) of the fringing pattern's Fourier transform. Frame (c) is the spectrum after interpolating vertically over the comma shaped mark in the Fourier transform, and computing an inverse Fourier transform. Frame (d) is the same as (c) except the Brγ line has been interpolated over. Frame (e) is the ratio of the images in frames (c) and (d) showing only the Brγ line which was removed. Frame (f) is the final processed frame which is the ratio of the images in frames (a) and (e), thus removing the line but preserving the fringe pattern.

4.2.2 Near Infrared Imaging at the 200 Inch Hale Telescope

Broad band 1.25μm (J-band) and 2.2μm (K-band) images were also taken in order to flux calibrate the spectra. These images, were themselves flux calibrated by matching synthetic aperture fluxes in the images with aperture photometry from either Neugebauer et al. (1987), Aaronson (1977), or Willner et al. (1985). A 0.75" x 3" synthetic aperture on the same broad band images was then used to determine the flux densities within the slit for the spectroscopic observations. These "slit" measurements were then used to scale the counts in the spectra to actual flux.

4.3 Results: Classical LINERs

The flux calibrated spectra for the 12 classical LINERs observed at ~1000 resolution are shown in figures 4.3 to 4.14. In the figures, the locations of expected emission lines are labeled above each spectrum even if undetected. Below each spectrum, the locations of the stellar absorption features are also marked, even if they are undetected in the particular object. The most obvious result is that the [FeII] line at 1.2567μm is the most common emission line detected, being present in 8 of the 12 galaxies. H_2 is also a common feature, being found in 4 of the 11 galaxies with K-Band spectra. Paβ, which is typically the strongest near infrared line available at zero redshift, is only found in 2 galaxies, NGC 5194 and NGC 7479. Brγ is undetected in all 11 galaxies with K-Band spectra. Lines as faint as 1.0×10^{-15} ergs s^{-1} cm^{-2} were detected in some objects making these among the faintest lines ever detected with infrared spectroscopy. Table 4.2 gives the measured fluxes and uncertainties for the infrared lines. In most cases a 3" by 1000 km s^{-1} aperture was placed on the continuum subtracted spectra to determine the fluxes making the true aperture on the sky 3" by 0.75" (the slit width). The uncertainties were determined by placing the same

aperture at several locations on the spectra above and below each emission line. In many cases, Paβ is detected in absorption, and the strength is listed as a negative value in the table.

Table 4.2
Measured Line Fluxes ($\times 10^{-15}$ ergs s^{-1} cm^{-2})

Object (1)	[FeII] (2)	Paβ (3)	H_2 (4)	Brγ (5)
NGC 0404	7.8±0.2	-1.3±0.3	2.4±0.7	0±1
NGC 2685	0±1	-1.5±1	0±1	0±1
NGC 3992	0±1	-2±1	0±0.5	0±0.5
NGC 3998	3.1±0.7	-1±1	0±1	0±1
NGC 4258	3.5±0.6	-0.4±0.6	0±0.9	0±0.9
NGC 4589	0±2	-2.6±2	0±0.8	0±0.8
NGC 4736	10±4	-8±3	0±2	0±4
NGC 4826	4±2	-2.6±2	0±0.5	0±2
NGC 5194[a]	5.8±0.9	1.0±0.7	3.9±0.6	0±1
	7.8±0.9	1.5±0.4	4.7±0.7	0.5±.3
NGC 7217	2.3±0.7	-1.5±0.7	-	-
NGC 7479	0±0.3	1.3±0.4	2.8±0.6	0±0.6
NGC 7743	4.5±1	-1.2±1	3.7±0.4	0±0.5

[a] NGC 5194 was observed twice, the may 94 values are given above the July 94 values.

Table 4.2: Raw fluxes from the calibrated spectra. No stellar absorption, reddening or other factors have been considered in this set of numbers. In the case of NGC 7217, where no K-band spectrum was taken, dashes are used. For Paβ, where absorption was seen in many of the galaxies, a negative value is allowed. For other features, however, if no line was seen, zero is listed with the calculated uncertainty.

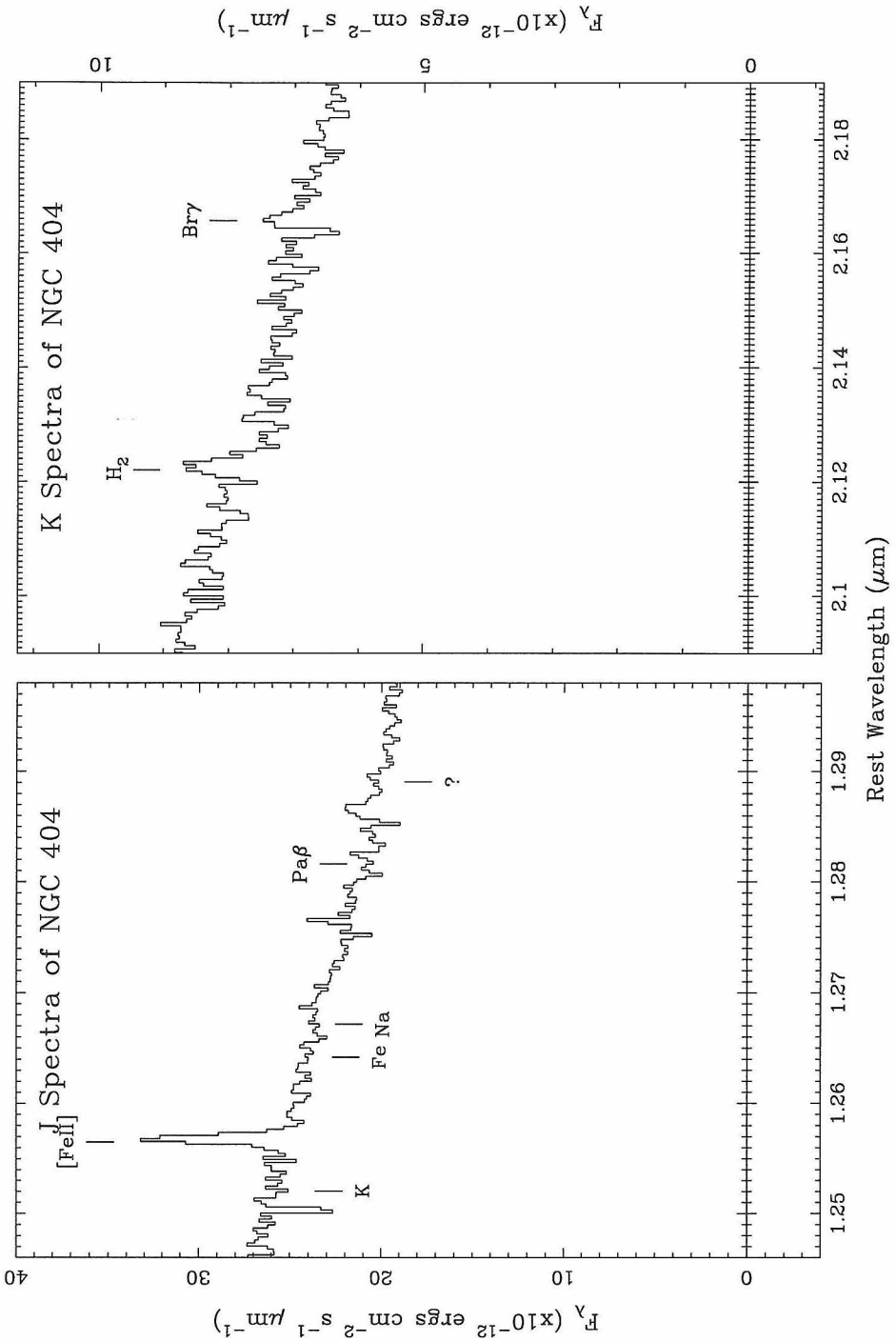

Figure 4.3: Flux calibrated spectra of NGC 404: The left spectrum is in the J-band window and covers the wavelengths of [FeII] (λ_{rest}=1.2567μm) and Paβ at a resolution of ~1100. The right spectrum is in the K-band window and covers the wavelengths of H_2 (λ_{rest}=2.1218 μm) and Brγ at a resolution of ~900.

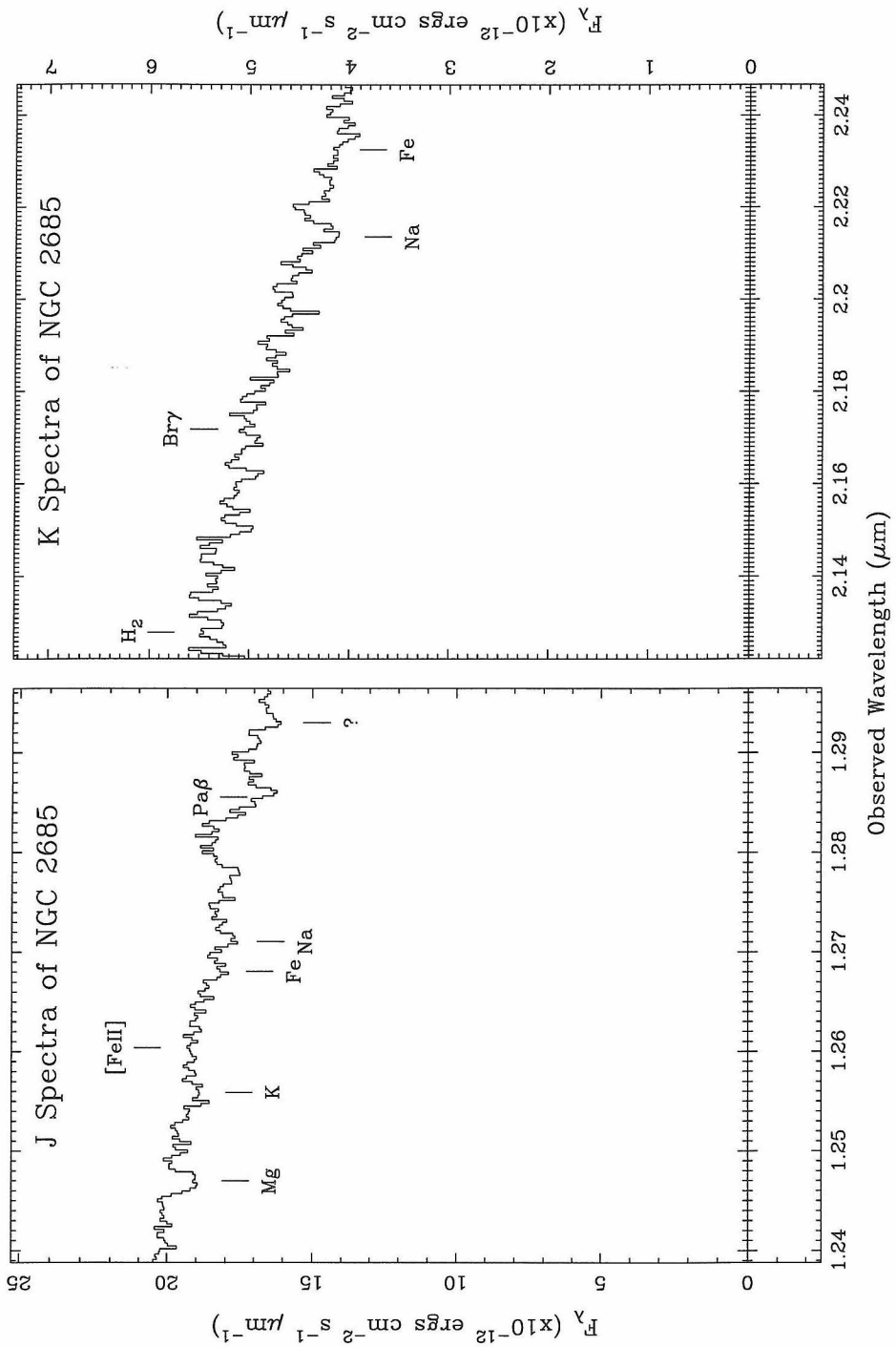

Figure 4.4: Similar spectra of NGC 2685 as in figure 4.3

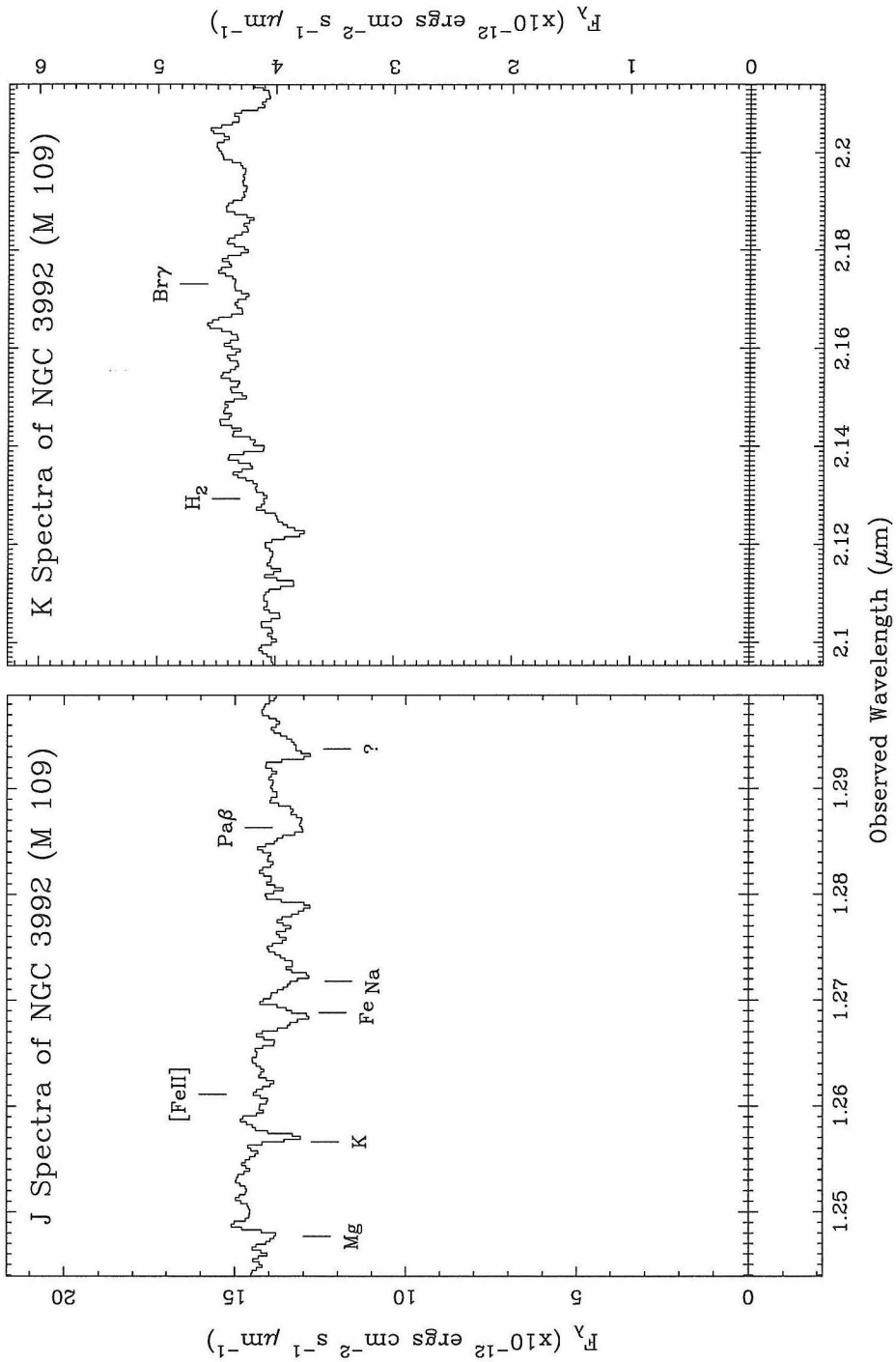

Figure 4.5: Similar spectra of NGC 3992 as in figure 4.3

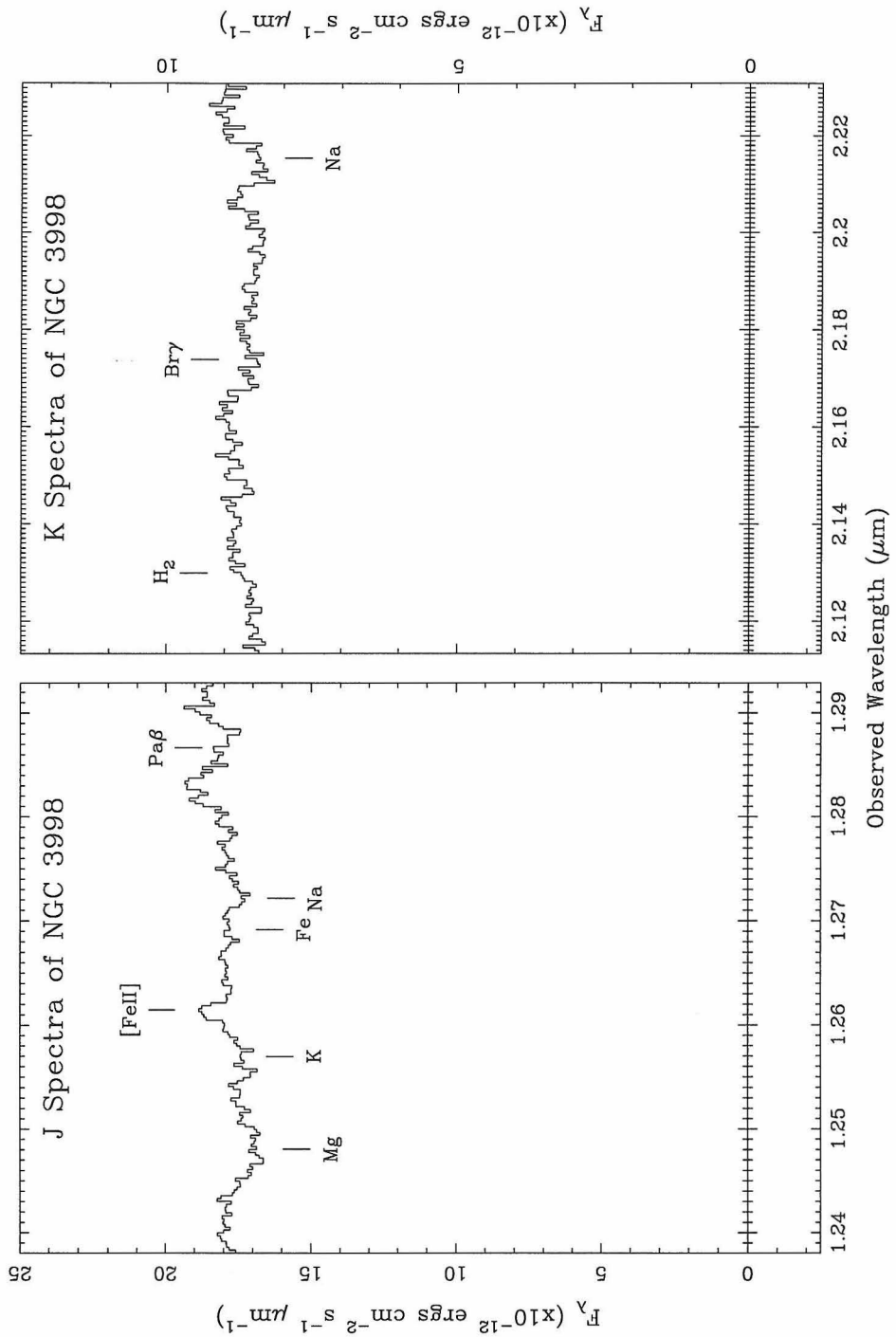

Figure 4.6: Similar spectra of NGC 3998 as in figure 4.3

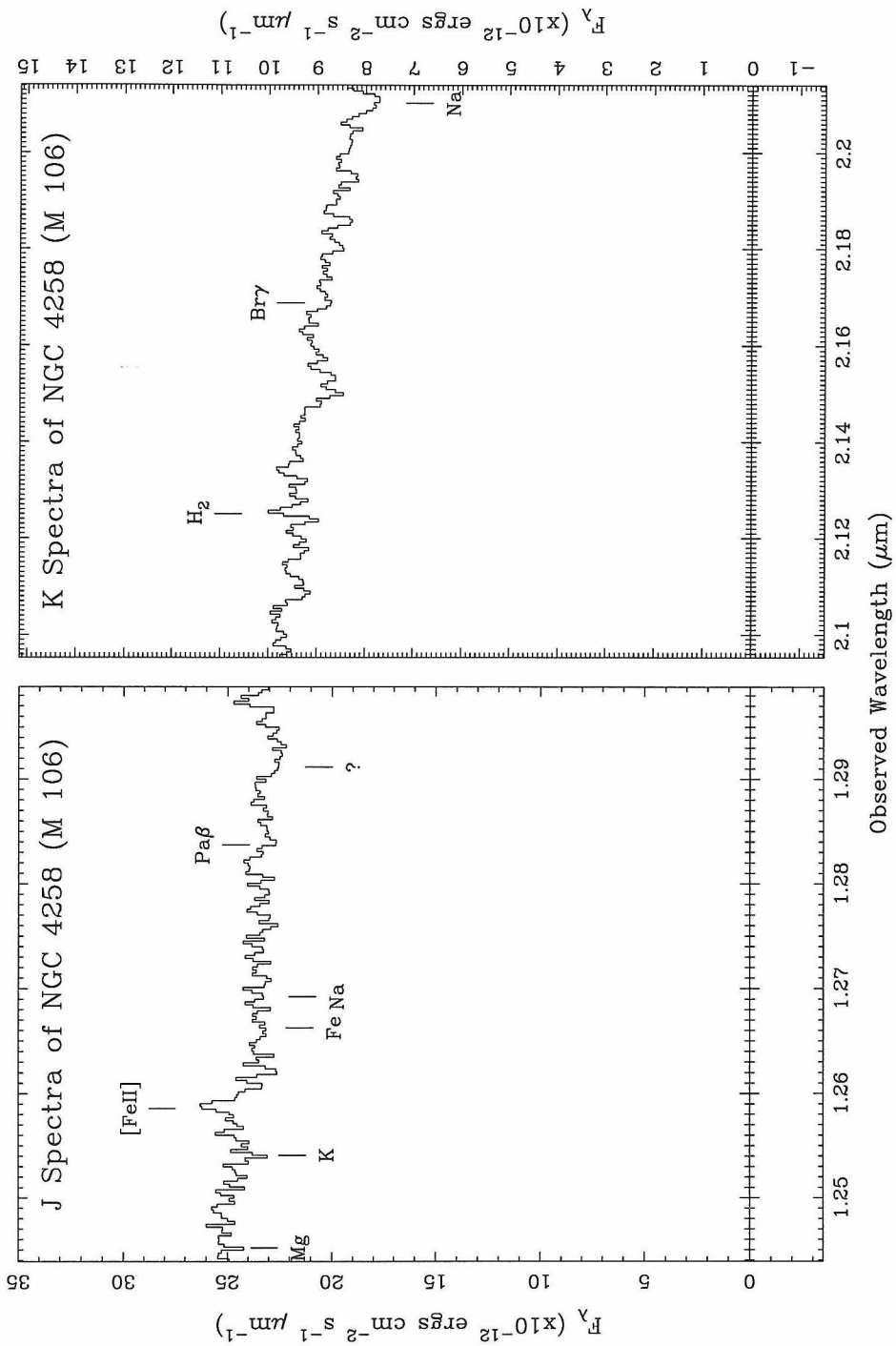

Figure 4.7: Similar spectra of NGC 4258 as in figure 4.3

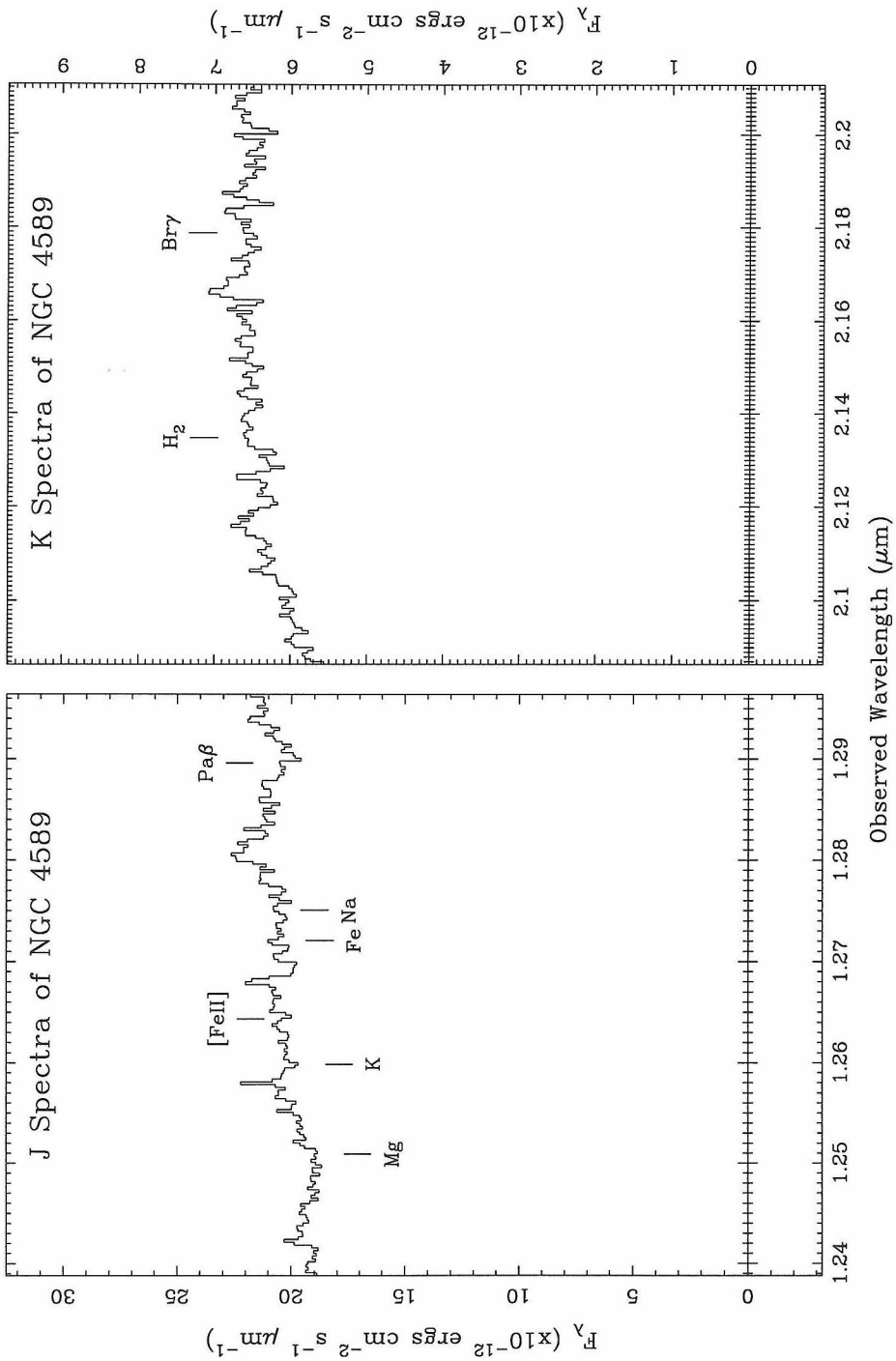

Figure 4.8: Similar spectra of NGC 4589 as in figure 4.3

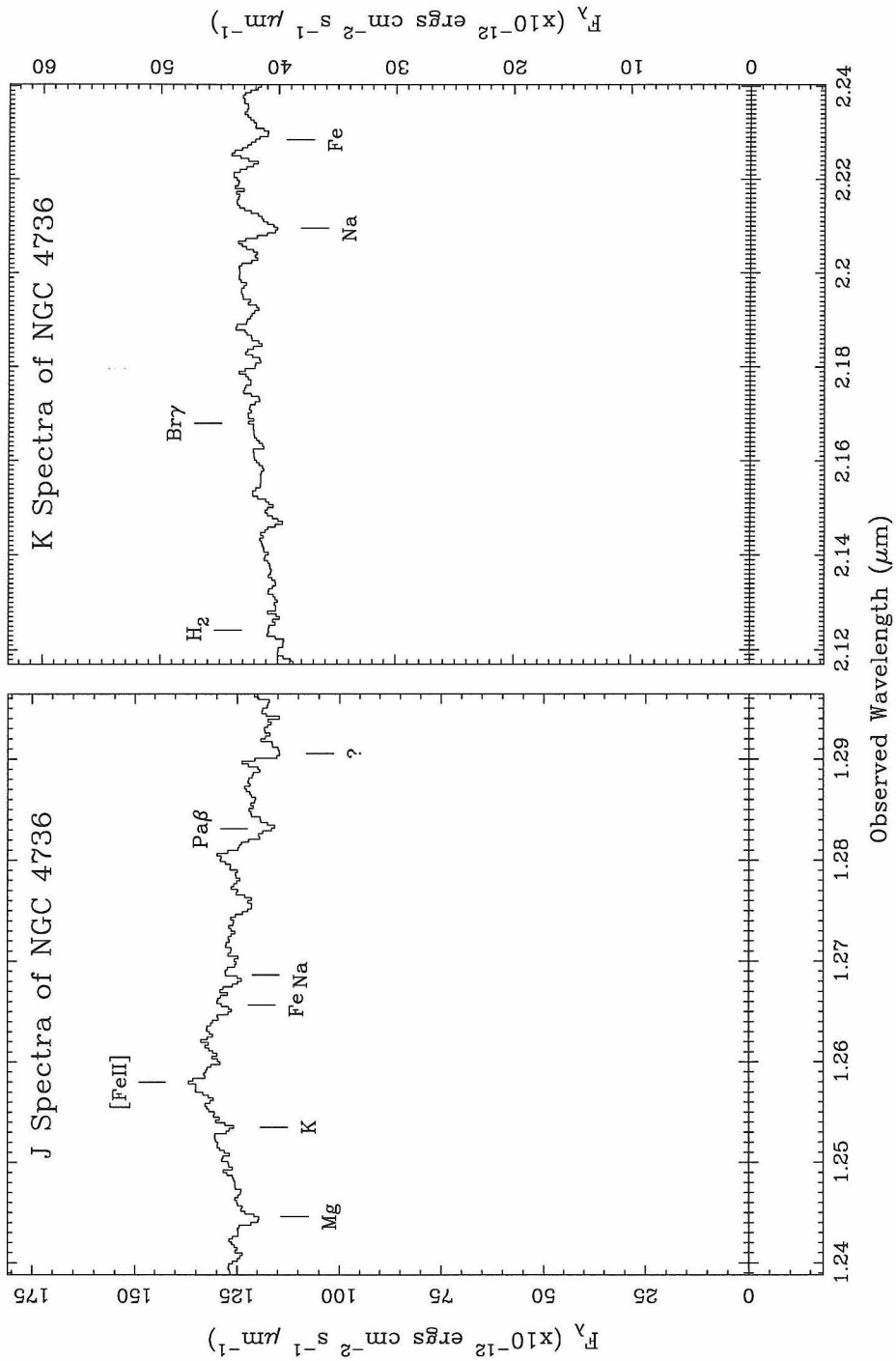

Figure 4.9: Similar spectra of NGC 4736 as in figure 4.3

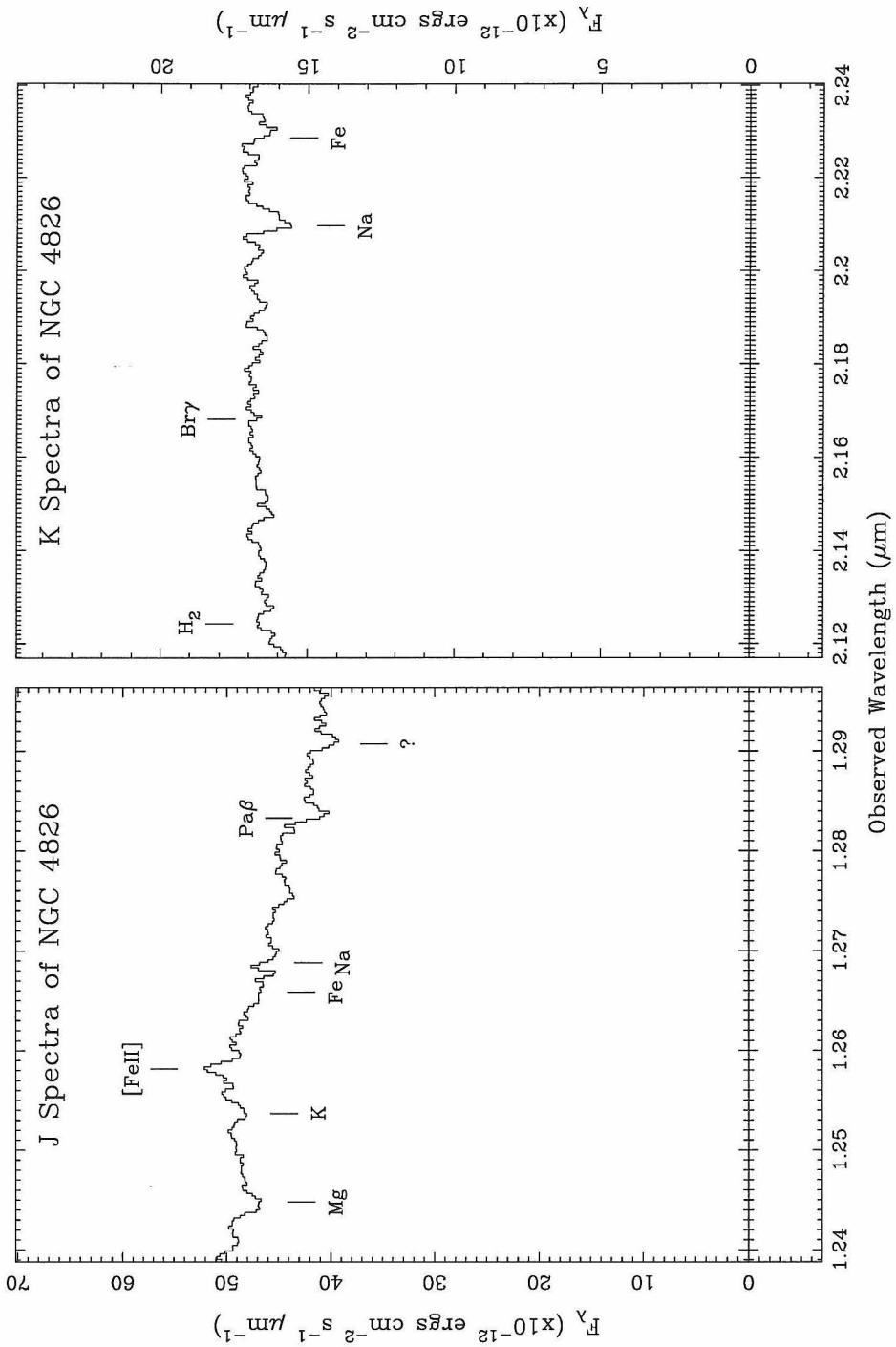

Figure 4.10: Similar spectra of NGC 4826 as in figure 4.3

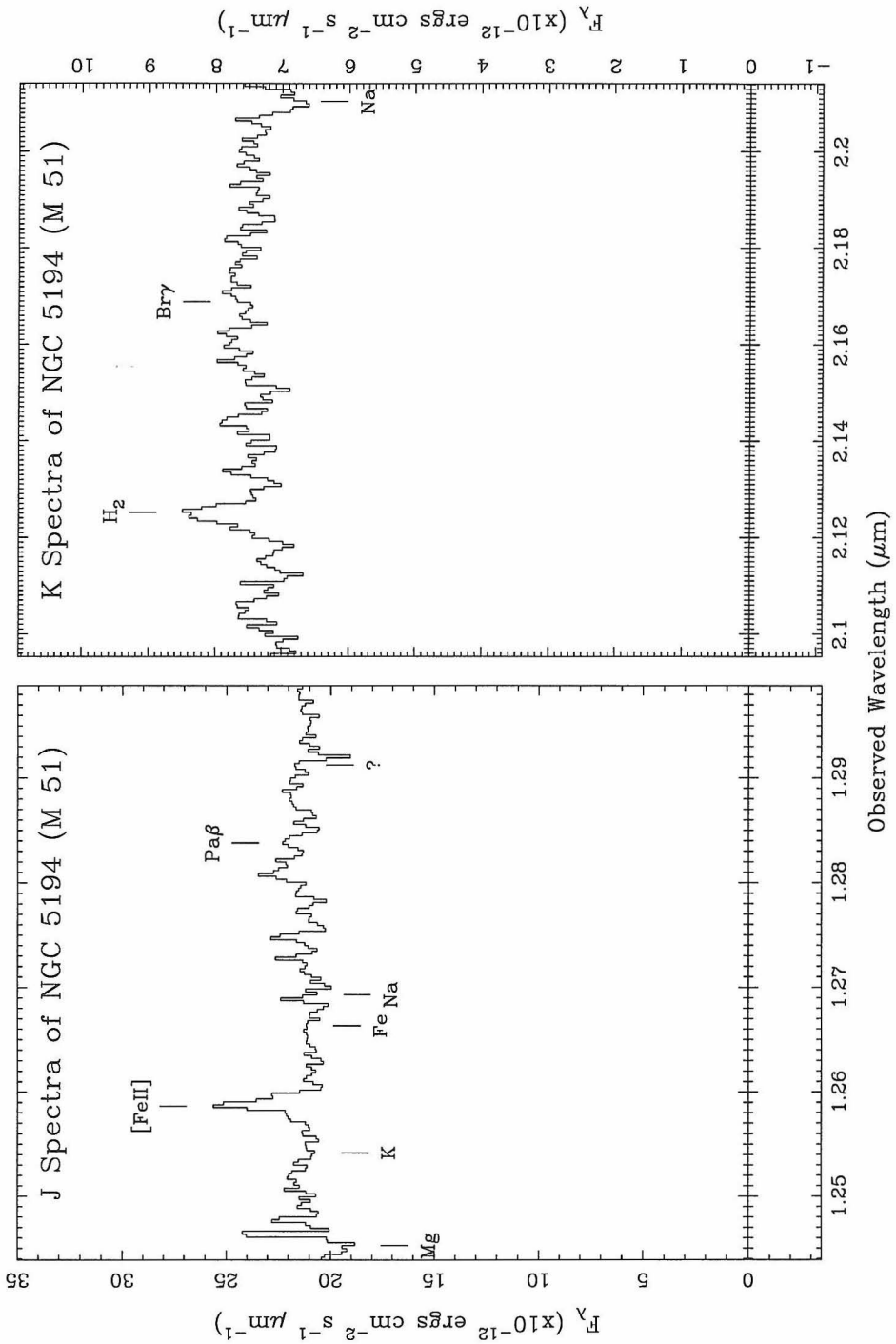

Figure 4.11: Similar spectra of NGC 5194 as in figure 4.3

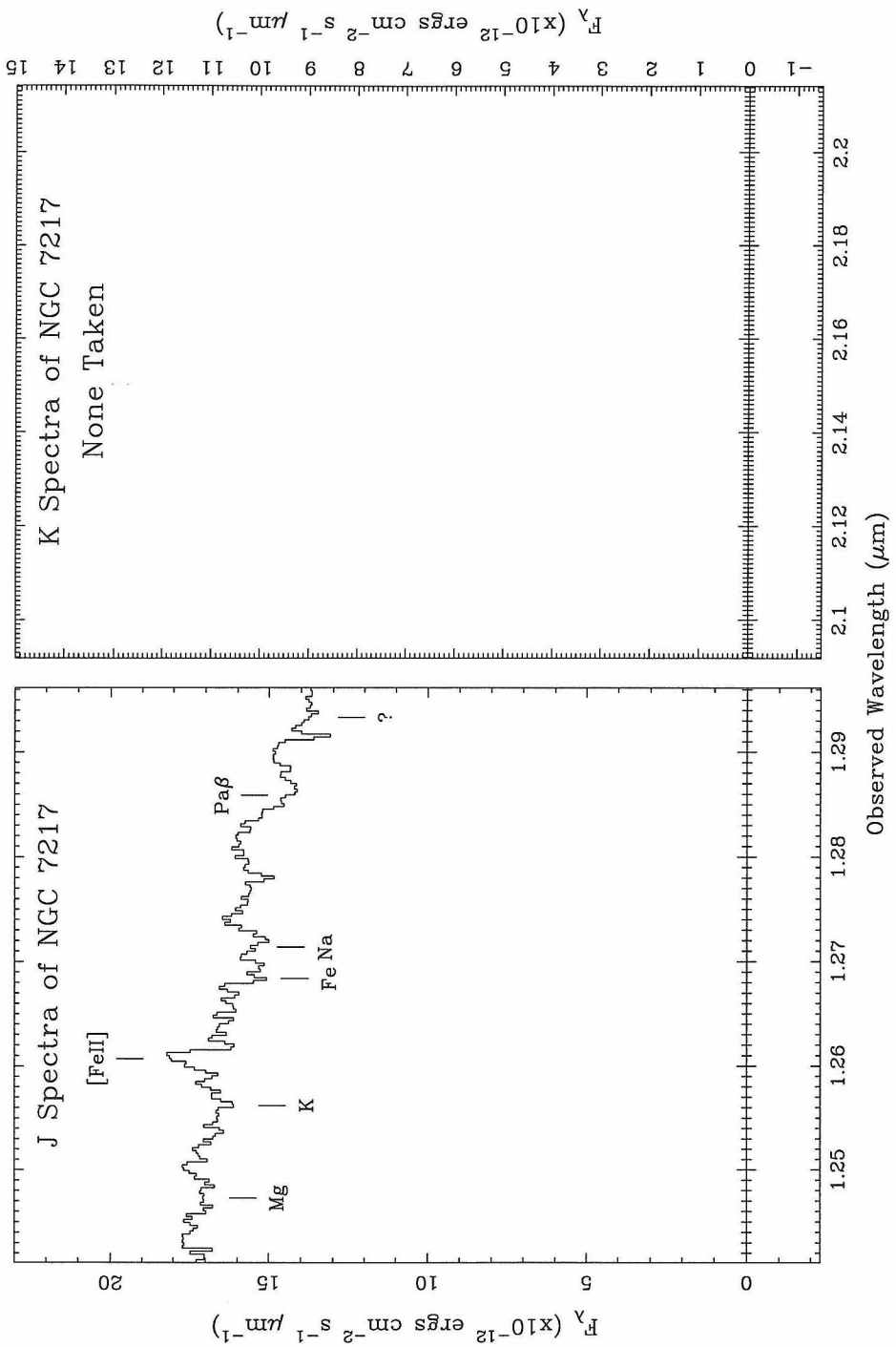

Figure 4.12: Similar spectra of NGC 7217 as in figure 4.3 , except no K band spectrum was taken.

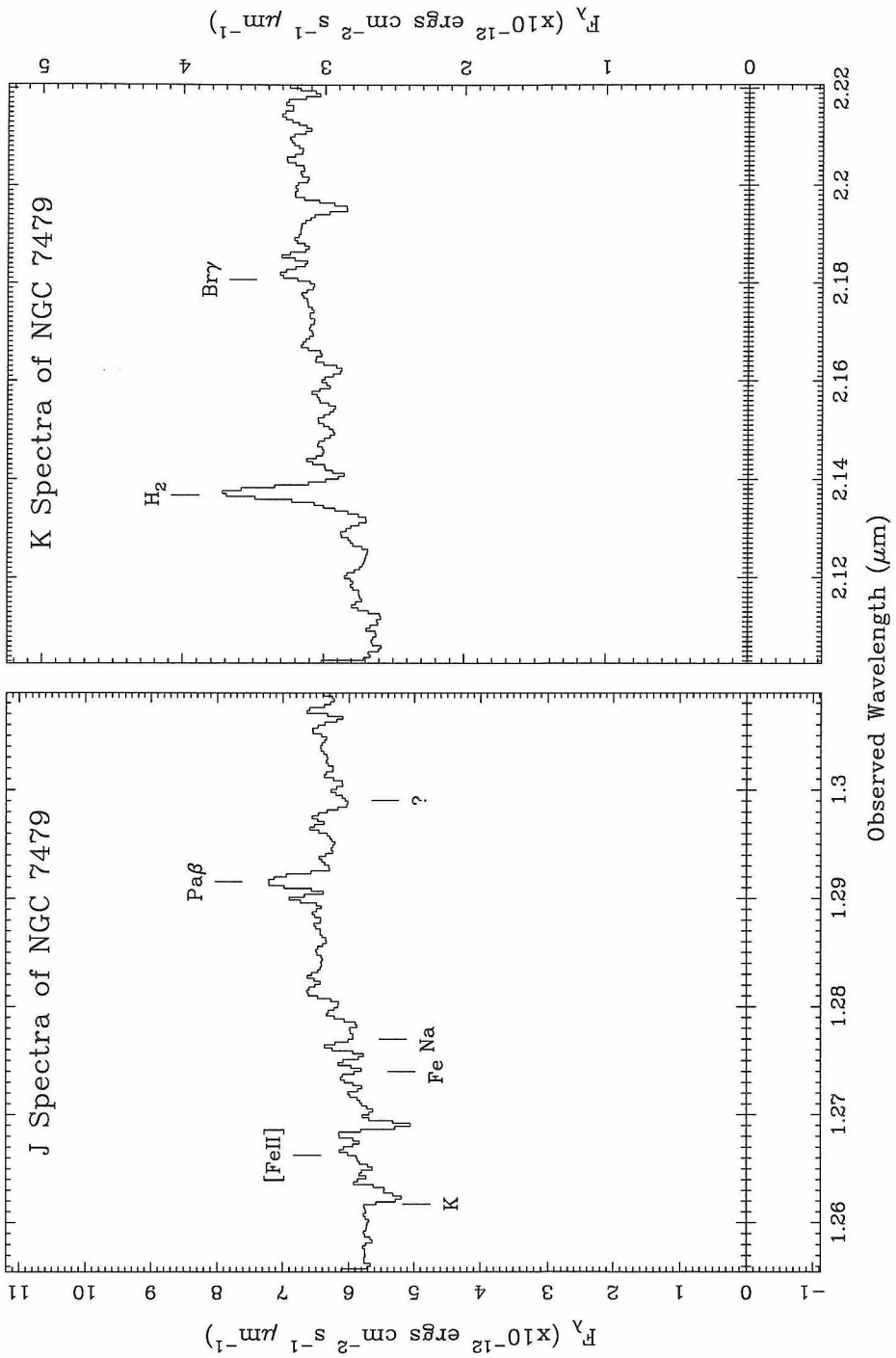

Figure 4.13: Similar spectra of NGC 7479 as in figure 4.3 .

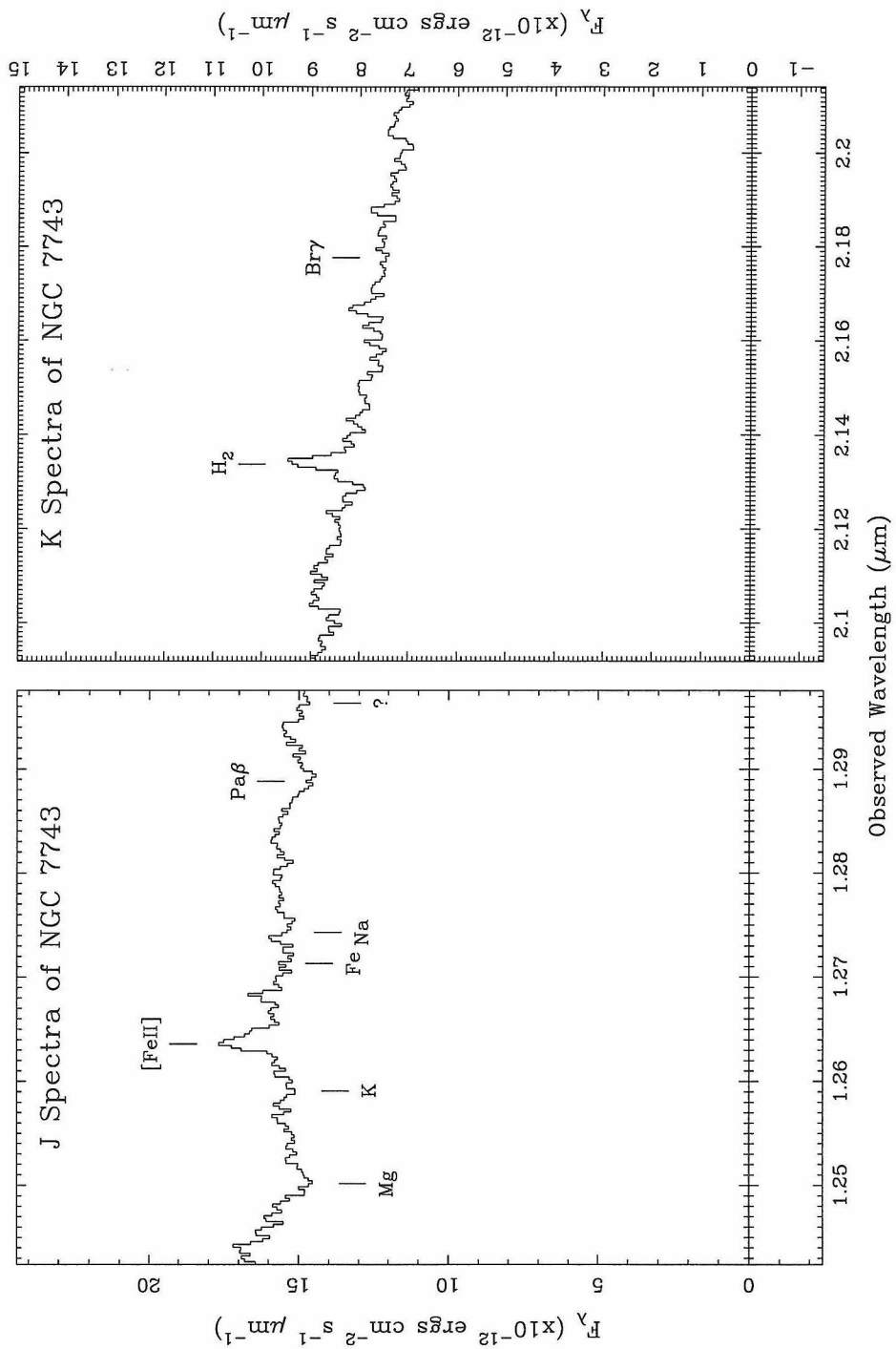

Figure 4.14: Similar spectra of NGC 7743 as in figure 4.3 .

4.3.1 The estimated Paβ and Brγ strengths

Even though Paβ and Brγ are usually not detected in emission, it is important to try and estimate their strengths because these lines are directly proportional to the ionizing photon flux, and provide useful reddening insensitive ratios with the [FeII] and H_2 lines. The fact that strong Paβ absorption is seen in many of these galaxies and that the expected Paβ emission line strengths are comparable, makes a direct determination of the true Paβ emission line flux difficult. Instead, we use an extrapolation from the optical recombination lines to estimate the infrared recombination line emission strengths. This technique uses the case B recombination ratios for hydrogen (Osterbrock 1989) modified to take into account the enhancement of Hα due to collisional excitation typical in AGN resulting in an intrinsic Hα to Hβ ratio of 3.1:

$$
\begin{aligned}
&ModifiedCaseB: \\
&\qquad I(H\alpha) = 3.1 \times I(H\beta) \\
&\qquad\qquad = 16.8 \times I(Pa\beta) \\
&\qquad\qquad = 102 \times I(Br\gamma)
\end{aligned}
\tag{4.1}
$$

where I(x) is the intrinsic (without extinction) flux of line x. Differential reddening between Hα and Paβ was removed with the extinction coefficients of Cardelli et al. (1989). This technique was also applied to estimate Brγ even though the flux should in most cases be below our detection limits. The basic equations relating Hα and Hβ observed line fluxes to Pβ and Brγ observed line fluxes are:

$$\begin{aligned} A_V &= 5.81 \times log\left(\frac{1}{3.1}\frac{f(H\alpha)}{f(H\beta)}\right) \\ &= 5.81 \times log\left(\frac{f(H\alpha)}{f(H\beta)}\right) - 2.85mag \end{aligned} \tag{4.2}$$

$$\begin{aligned} \frac{f(Pa\beta)}{f(H\alpha)} &= \frac{I(Pa\beta) \times 10^{-.105 \times A_V}}{I(H\alpha) \times 10^{-.324 \times A_V}} \\ &= 0.0596 \times 10^{0.219 \times A_V} \end{aligned} \tag{4.3}$$

$$\begin{aligned} \frac{f(Br\gamma)}{f(H\alpha)} &= \frac{I(Br\gamma) \times 10^{-0.046 \times A_V}}{I(H\alpha) \times 10^{-0.324 \times A_V}} \\ &= 0.0098 \times 10^{0.278 \times A_V} \end{aligned} \tag{4.4}$$

where f(x) is the observed flux of line x, and A_V is the magnitude of visual extinction. Combining these equations, and adding an aperture correction factor, AC, between the optical and infrared apertures generates the final equations:

$$f(Pa\beta) = 0.0141 \times AC \times f(H\alpha) \times \left(\frac{f(H\alpha)}{f(H\beta)}\right)^{1.272} \tag{4.5}$$

$$f(Br\gamma) = 0.0016 \times AC \times f(H\alpha) \times \left(\frac{f(H\alpha)}{f(H\beta)}\right)^{1.615}. \tag{4.6}$$

If Hα/Hβ was not known, the median Hα to Hβ ratio of 3.81 (A_V = 0.53 mag) from the other galaxies was used. In these cases the estimated values are given in parenthesis in the table. The aperture correction between our 3" by 0.75" slit and the larger apertures in the other papers depends on the spatial extent of the line emission. We used the Hα+[NII] images obtained at the 60 inch telescope at Palomar (Larkin

et al. 1995 in preparation), to determine the appropriate aperture correction for each object. For the larger circular apertures used in Heckman et al. (1980) and Keel et al. (1983), the average correction is 0.34±0.04, while the average corrections to Ho et al.'s (1993) 1" by 4" and 2" by 4" apertures were 0.73±0.03 and 0.44±0.05 respectively. The final estimated Paβ and Brγ fluxes are given in columns (4) and (5) respectively of table 4.3. It is important to remember that these predicted fluxes are for Paβ and Brγ as they would be measured, not corrected for extinction. The only corrections are for the difference in reddening between the optical and the infrared lines.

4.3.2 Paβ absorption strength

Since many of the predicted Paβ emission line strengths are within the range of detectability, it is important to understand why these lines were not seen. The most likely possibility is that stellar absorption lines in the galaxies are equal to or stronger than the emission lines. In order to evaluate this possibility, we looked at the three galaxies, NGC 2685, NGC 3992, and NGC 4589, which have the weakest predicted Hα emission line strengths (all have only upper limits on their optical Hα and Hβ fluxes). In these three galaxies, the measured absorption is much larger than the upper limit on emission, and the emission can be assumed to have little impact on the measured values. The average equivalent width of the Paβ absorption in these three objects is 1.2±0.25 Å, comparable to a late G type star (see the appendix). Assuming that the other galaxies in this sample have comparable or stronger absorption, column (2) of table 4.3 gives the lower flux limit on Paβ absorption for each galaxy. Adding this to the measured Paβ fluxes in table 4.2 gives the lower limit on the true Paβ emission line strength and these values are listed in column (3) of table 4.3. For all of the galaxies with negative measured Paβ fluxes, this fiducial absorption is sufficient to make the

corrected values positive or zero, indicating that absorption is at least comparable to the emission line strengths, and is a plausible explanation for the nondetections.

Six of the galaxies (NGC 404, NGC 3998, NGC 4258, NGC 4826, NGC 5194, and NGC 7743) have expected Paβ fluxes from the optical (in column (4) of table 4.3) significantly higher than these absorption corrected values. This probably indicates that the absorption correction is too small, and these galaxies have absorption strengths closer to that found for A type stars. These galaxies may, therefore, have younger stellar populations than the three galaxies used in determining the amount of absorption. It is interesting to note, that all of these six are among the galaxies with strong [FeII] detections. It is possible that recent star formation plays a role in these objects, and that supernova remnants could increase the gas phase iron abundance, and enhance the level of [FeII] emission.

4.3.3 [FeII] and H_2 line ratios

As a first step in the analysis of the [FeII] and H_2 emission lines, their ratios to the estimated Paβ and Brγ hydrogen recombination lines are calculated respectively. Each of these ratios is extinction insensitive (although the Paβ and Brγ line fluxes are dependent on the ratio of Hα to Hβ used to infer A_V) and provides a good way of comparing the [FeII] and H_2 line strengths with other objects in the literature. Since we don't have direct measurements of Paβ and Brγ in most cases, we use the extrapolations from the optical data given in table 4.3. The ratios of [FeII] to Paβ are shown in column (6) of table 4.3, and the H_2 to Brγ ratios are similarly given for each galaxy in column (7). In principle, these values can be treated as ratios to the optical Hα fluxes corrected for extinction, and aperture size and then scaled to the relative Paβ or Brγ to Hα intensity. This also allows for easy comparison with other emission line ratios which use Hα or Hβ.

Table 4.3
Estimated Paβ and Brγ Fluxes and Ratios

Object (1)	flux (x10^{-15} erg cm^{-2} s^{-1}) <Paβ abs.> (2)	est. Paβ (3)	<Paβ > (4)	<Brγ > (5)	$\frac{[FeII]}{<Pa\beta>}$ (6)	$\frac{H_2}{<Br\gamma>}$ (7)
NGC 0404	2.5±0.5	1.2±.6	3.1[b],2.7[c]	.55[b],.49[c]	2.7±.3	5±2
NGC 2685	2±.6	.5±1	(<.4)[a]	(<.06)[a]	-	-
NGC 3992	1.7±.6	-.3±1	(<.3)[a]	(<.05)[a]	-	-
NGC 3998	2.2±.7	1.2±1	3.6[a],7.9[b],4.3[c]	.61[a],1.5[b],.72[c]	.6±.3	< 2
NGC 4258	2.8±.9	2.4±1	(5.7)[a]	(1.0)*a*	.6±.3	< 2
NGC 4589	2.5±.8	0±2	(<.24)[a]	(<.04)[a]	-	-
NGC 4736	15±5	7±6	(1.9)[c]	(.35)[c]	5.3±2.5	< 20
NGC 4826	5±1	2.5±2	(6.0)[c]	(1.1)[c]	.7±.4	< 1
NGC 5194	2.6±.9	3.6±1	(3.1)[b],(2.7)[c]	(.55)[b],(.48)[c]	2.3±.6	8±3
NGC 7217	1.8±.6	.3±.8	.98[b]	.16[b]	2.3±.9	-
NGC 7479	.7±.3	2±.5	1.2[b]	.26[b]	<.5	11±4
NGC 7743	1.8±.6	.6±1	3.4[b]	.74[b]	1.3±.4	5±2

[a] Flux estimated from Heckman et al. (1980).
[b] Flux estimated from Ho et al. (1993).
[c] Flux estimated from Keel et al. (1983).

Table 4.3: Estimated Paβ and Brγ fluxes and ratios. Column (2) lists the expected strength of Paβ absorption based on the levels seen in NGC 2685, NGC 3992 and NGC 4589 (see text). Column (3) lists the estimated Paβ emission strength by adding the expected absorption from column (2) to the observed flux from table 4.2. Column (4) contains the expected Paβ emission through our slit as determined from optical lines corrected for the differential extinction derived from the Hα to Hβ ratio if known. If the reddening is not known, the median Hα to Hβ ratio of 3.81 from the other galaxies is used, and the value is given in parenthesis. An aperture correction has also been applied. Column (5) is the same as column (4) except that it lists the expected Brγ fluxes. Column (6) then gives the [FeII] to Paβ ratio for the estimated Paβ fluxes listed in column (4). If [FeII] and all hydrogen recombination lines are undetected, then a dash is given. Column (7) lists the H_2 to Brγ ratio using the estimated Brγ fluxes in column (5).

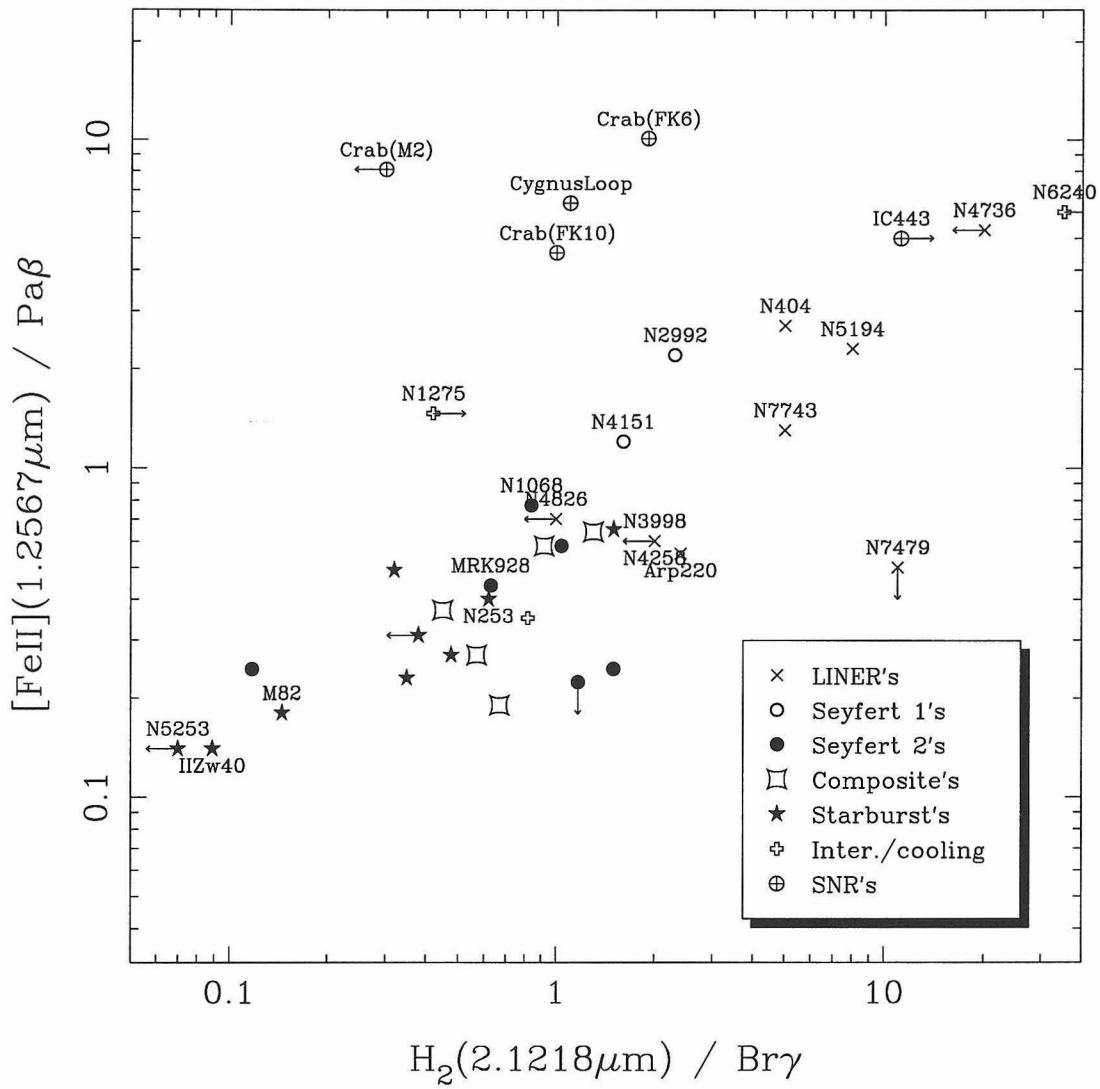

Figure 4.15: For all of the objects in this sample plus many objects from the literature, the ratio [FeII]/Paβ is plotted against the ratio H_2/Brγ. There is a strong linear correlation between these two ratios for the galaxies included, regardless of class, even though some of the Seyfert 2's lie significantly below the correlation. Several galactic SNR's are also plotted and usually have unusually strong [FeII]/Paβ flux ratios as compared to galaxies with similar H_2/Brγ ratios. Also, NGC 7479, which is often classified as a Seyfert 2, is much weaker in [FeII] compared to H_2 than this curve.

Figure 4.15 plots [FeII]/Paβ versus H_2/Brγ for the LINERs and many objects from the literature. It is immediately apparent that several of the LINERs have both ratios significantly higher than most other objects. For all included galaxies, regardless of galaxy type, a linear correlation is also evident over a range in ratios of more than 100. The one exception is the LINER NGC 7479 which has weaker [FeII] emission than other LINERs given its large H_2/Brγ.

The SNR points in figure 4.15 are for small apertures on individual filaments and may not represent the global ratios in these objects. One of the SNR's located at the middle top of figure 4.15 is the Cygnus Loop, where the excitation is thought to arise from an unusually fast shock with a magnetic precursor penetrating a low density environment (2 cm^{-3})(Graham et al. 1991). The other SNR points at the middle top of the figure are from various locations in the Crab Nebula, where Graham et al. (1990) argue photoionization, not shock heating is the dominant emission source. The SNR with the largest H_2/Brγ is IC 443 which is believed to be shock heated (Graham et al. 1987).

Figure 4.16 plots H_2/Brγ versus OI/Hα for all of the classical LINERs and for many galaxies in the literature. Mouri et al. (1989) found a linear correlation for starburst and Seyfert galaxies between the H_2 and OI(6300Å) lines, and the LINERs in this sample appear to extend the linear correlation to higher values by a factor of 2 or more. NGC 7479, however, is a factor of several stronger in H_2/Brγ than the correlation predicts, and NGC 3998 is at least a factor of three below the main correlation. The galaxies NGC 4258 and NGC 4826 fall in the middle of the Seyfert galaxies, which is not unexpected since both are considered prime candidates for dwarf Seyferts (Filippenko and Sargent 1985). Four of the LINERs in this sample have an H_2/Brγ ratio above 3, as do the LINERs NGC 5128 and NGC 6240 from the literature. These are the only known objects with such a large ratio of H_2 to Brγ.

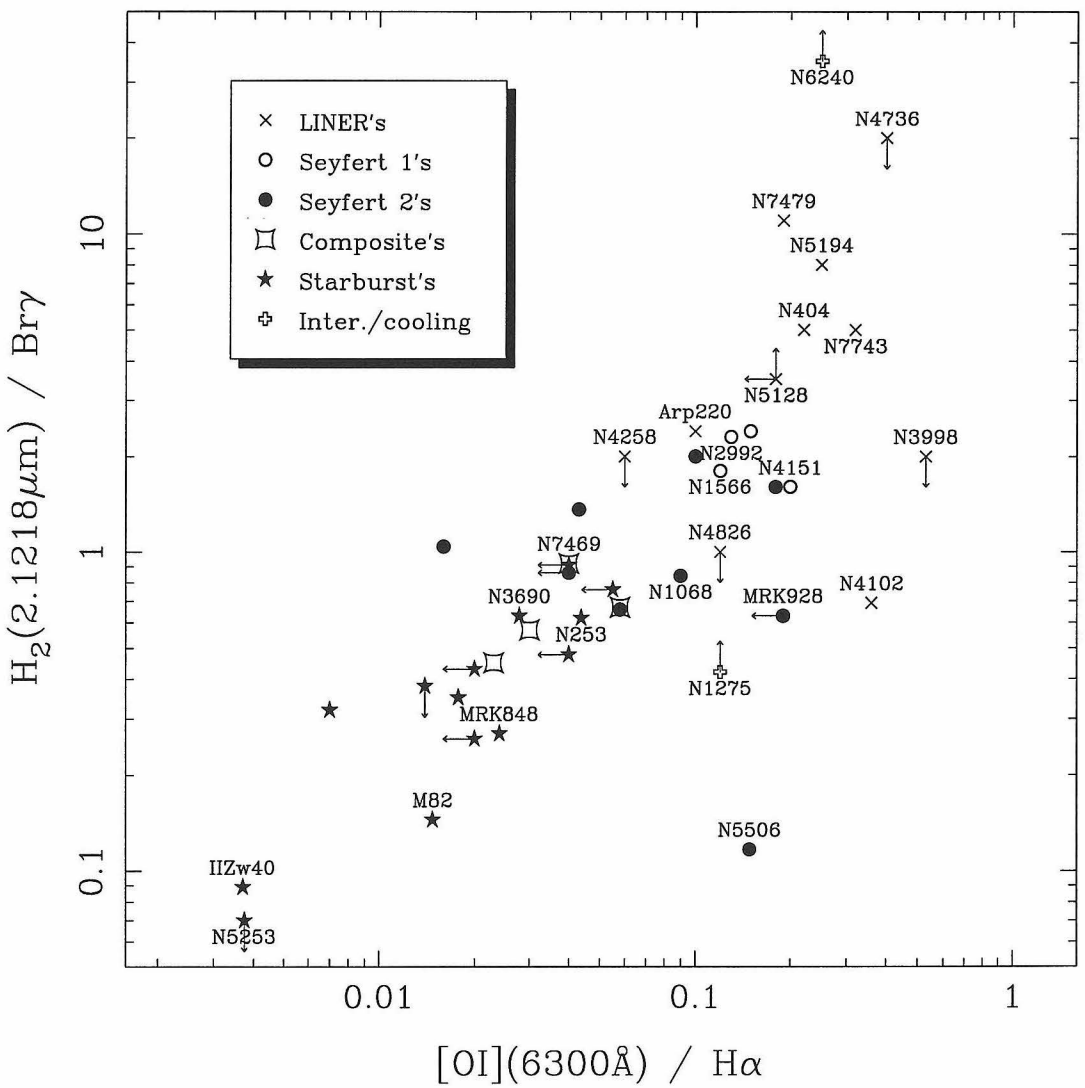

Figure 4.16: For all of the objects in this sample plus all available objects in the literature, the ratio $H_2/Br\gamma$ is plotted against the ratio OI/Hα.

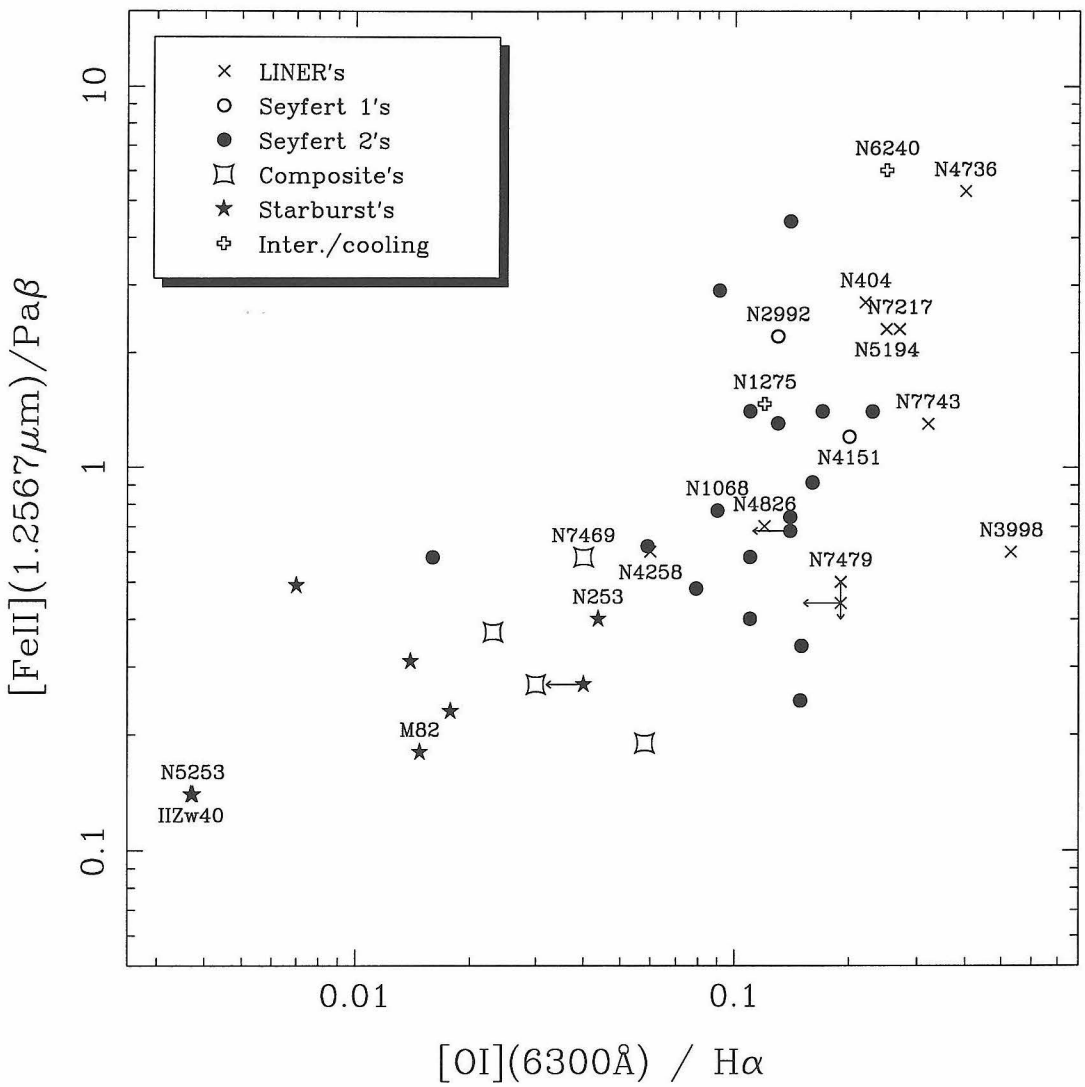

Figure 4.17: For all of the objects in this sample plus all available objects in the literature, the ratio [FeII]/Paβ is plotted against the ratio OI/Hα.

Figure 4.17 plots [FeII]/Paβ versus OI/Hα for all of the classical LINERs and for all of the available galaxies in the literature. Again, many of the LINERs have both ratios significantly higher than both starbursts and Seyfert galaxies, and for several the [FeII]/Paβ ratio is stronger than the general correlation predicts. Only the merger NGC 6240, which does satisfy the LINER definition, has a higher measured [FeII]/Paβ ratio than the strongest LINERs. Seyfert's show a large spread in [FeII]/Paβ ratio from $\sim$0.2 to $\sim$3.0. Only a handful of objects have [FeII]/Paβ greater than 2, including four of the LINERs in this sample (NGC 4736, NGC 404, NGC 7217, and NGC 5194). These strong [FeII] LINERs have some other common properties which set them apart from the weaker [FeII] LINERs as will be discussed below.

Figures 4.18 and 4.19 plot the optical [OIII]/Hβ ratio against H_2/Brγ and [FeII]/Paβ for the objects in this sample and the available objects in the literature. Unlike figures 4.15-4.17, no obvious correlation is evident, however, figure 4.18 shows a clear separation between the LINERs and Seyfert galaxies primarily due to the difference in H_2/Brγ. As mentioned above, the six known objects with H_2/Brγ ratios above 3 have LINER type spectra. Starburst galaxies are located in the lower left corner of these figures and are well separated from the other types. The [FeII]/Paβ ratio is significantly poorer at separating the various galaxy classes. The H_2/Brγ ratio is probably better at separating the classes than low ionization optical lines, because H_2 traces the colder molecular gas and is therefore less closely coupled with the high ionization lines like [OIII]. The three LINERs which are not grouped with the others in figure 4.18, all have unusual activity. NGC 4258 is a transition object with a great deal of recent evidence for a central black hole (see discussion of individual objects below). It is not unexpected, then that it falls within the Seyferts in this figure. NGC 4826 has an extrapolated Paβ flux almost twice as strong as can be accounted for with the fiducial absorption applied in section 4.3.2. This may imply a young

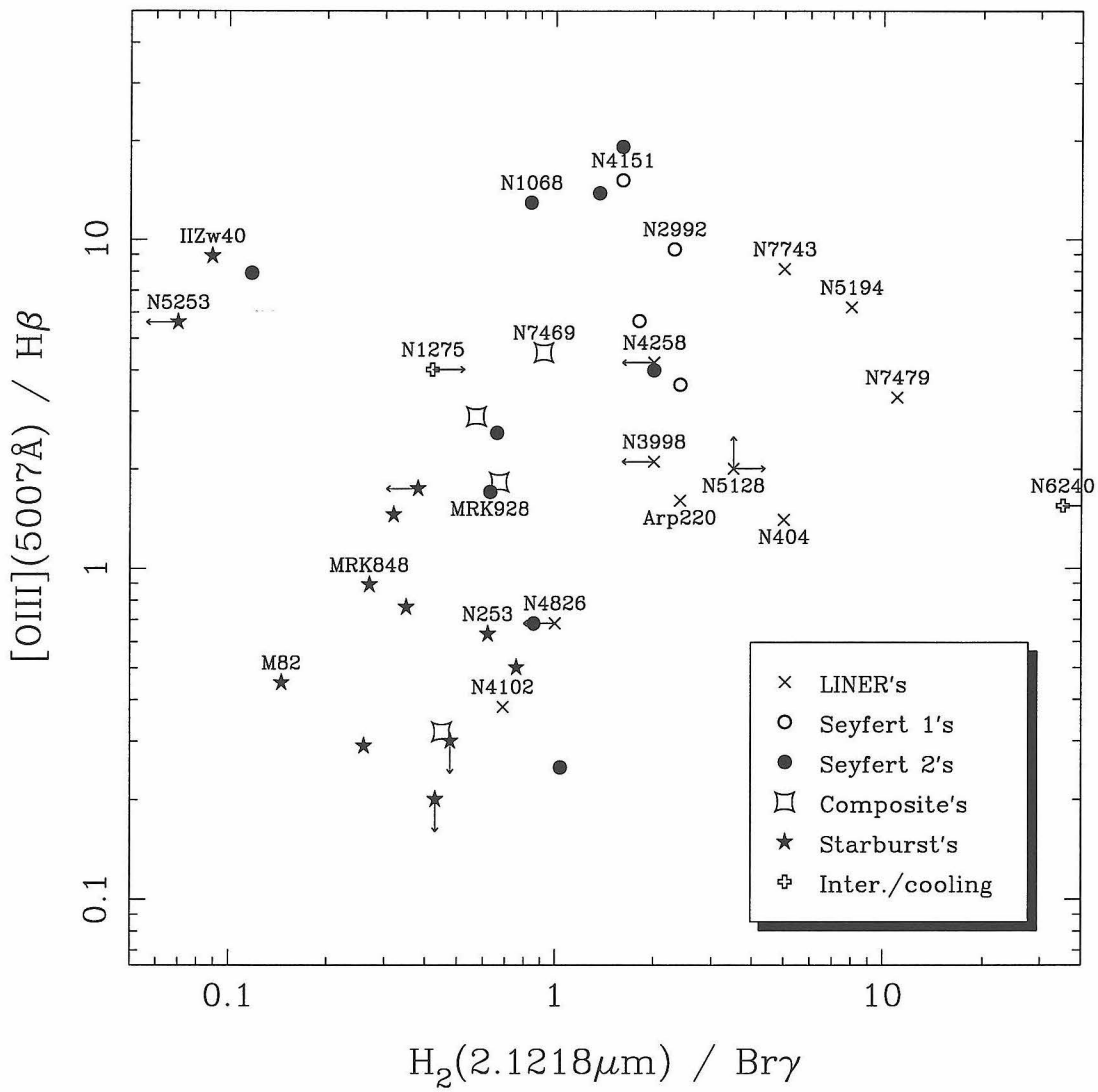

Figure 4.18: For all of the objects in this sample plus objects in the literature, the ratio [OIII]/Hβ is plotted against the ratio H_2/Brγ.

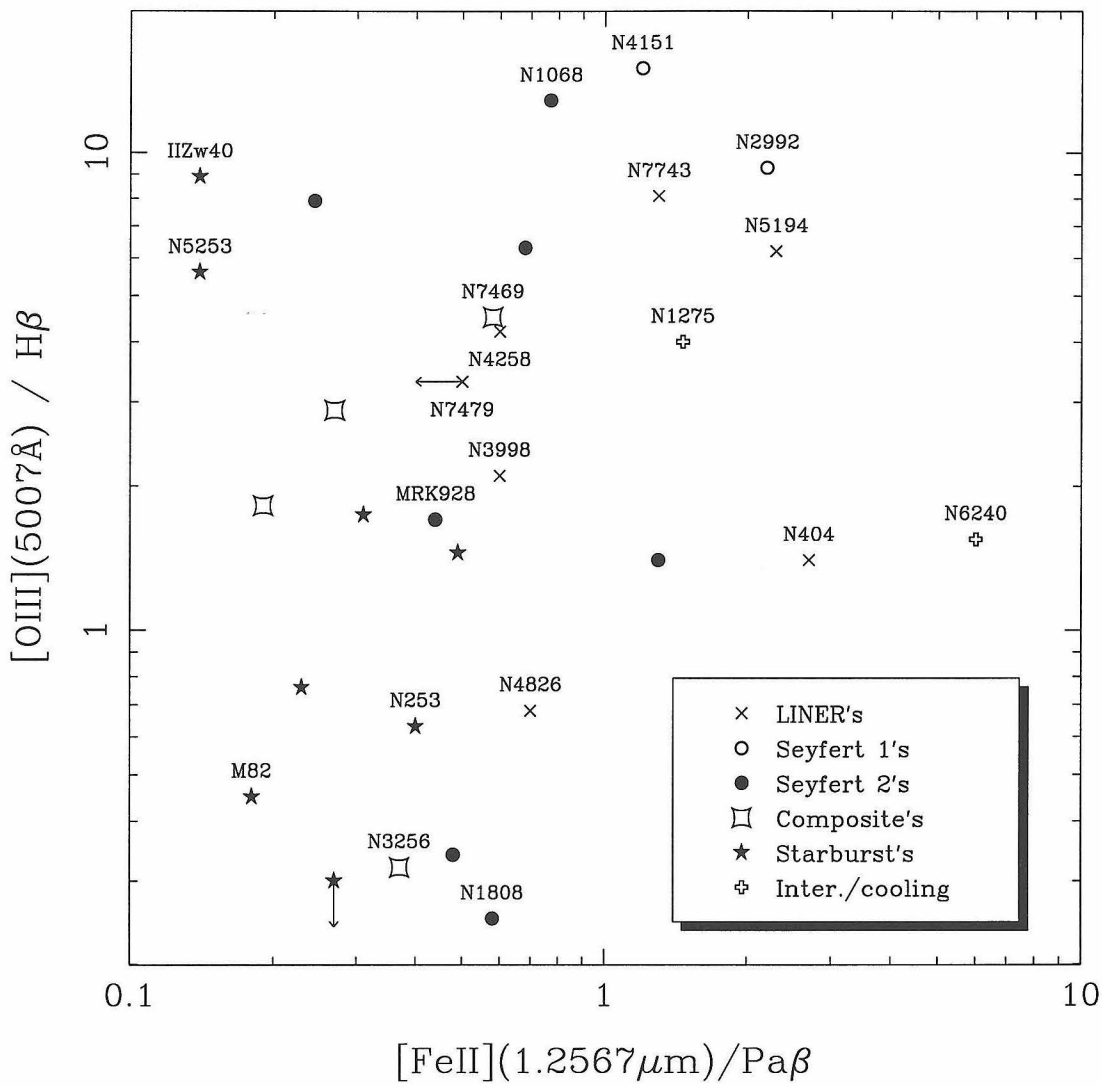

Figure 4.19: For all of the objects in this sample plus objects in the literature, the ratio [OIII]/Hβ is plotted against the ratio [FeII]/Paβ.

stellar population and recent star formation, and could explain why it is consistent with the starburst galaxies in the figure. NGC 3998, as argued below has a central source with Seyfert-like ratios, while in large apertures (D$\sim$5") the low ionization lines are stronger and it appears to be a true LINER. This could explain why our small aperture shows such a low $H_2/Br\gamma$ ratio, and why it lies within the range of Seyfert values.

4.3.4 Comparison with IRAS α(25:60) index

In this subsection, the IRAS 25 to 60 μm index (α(25:60)) is compared with the infrared line ratios. The index is defined as:

$$\alpha(25:60) = \frac{-log(f_{25\mu m}/f_{60\mu m})}{log(25\mu m/60\mu m)}. \tag{4.7}$$

The IRAS indices measure the shape of the far infrared continuum and α(25:60) in particular is thought to reflect the relative importance of warm (30-50 K) dust which dominates the 60μm band to hot (100-150 K) dust which dominates the 25μm band. In figures 4.20 to 4.24, the IRAS 25 to 60 micron index is plotted against the H_2/Brγ, [FeII]/Paβ and [OI]/Hα, respectively for the LINERs in our sample as well as many starbursts, Seyferts, composites (Seyfert + starburst), ULIRGS, and LINERs from the literature. For reference, non-active galaxies have a large range of α(25:60), but are typically between -2 and -3. Mouri and Taniguchi (1992) found that starburst galaxies and to a lesser extent, infrared ultraluminous galaxies, showed a linear correlation between this IRAS index and H_2/Brγ. They further found that Seyfert galaxies showed no such correlation, and although some Seyferts have α(25:60) comparable to starbursts, most Seyferts had a shallower 25 to 60 μm slope than the starburst correlation predicts. In fact, the α(25:60) index has been found to be an efficient identifier of Seyfert galaxies, especially the most luminous objects where the host galaxy colors play less of a role (De Grijp, et al. 1992). The LINERs show a large spread in α(25:60) from NGC 3998 at -1.15 to NGC 4826 at -3.23, while showing little variation in H_2, and [OI]. The plot of α(25:60) vs. [FeII]/Paβ (figure 4.22) shows more scatter for starbursts and ULIRGS than the other plots. LINERs also show a weak trend that the objects with flatter α(25:60) have weaker [FeII] than the steeper index LINERs. Some of the LINERs and Seyferts are close to the starburst correlations of

Mouri and Taniguchi (1992), but most have flatter indices than either the $H_2/Br\gamma$ of [OI]/Hα would predict. ULIRGs show the opposite trend with more of them on the steeper side of the relationship, indicating an unusually large ratio of warm to hot dust.

Unlike starbursts which are heated by young stars and produce sharply bounded ionized regions, the power-law Seyfert nucleus produces large amounts of x-rays. Since hard x-rays can penetrate very deeply into molecular clouds, the transition regions between ionized and neutral gas are thicker than in star forming regions, and so as the hydrogen recombination lines get stronger, so does the x-ray flux and the size of the transition region. This may explain why the lower ionization lines stay strong relative to the hydrogen lines in these objects. Mouri and Taniguchi (1992) use this model to explain why Seyferts have flatter α(25:60) and maintain a relatively high H_2 and [OI] flux and why starbursts show the linear trend. This model may also apply to LINERs, although the relationship between the IRAS index and the line ratios is complicated since the IRAS beam, in most cases, included virtually the entire galaxy while the spectrograph's slit only includes the nuclear fluxes. Also the grain temperatures may be affected by several mechanisms including dust grain processing. Nevertheless, the LINERs and Seyfert galaxies do not follow the same trend as the starbursts.

For the galaxies with the flattest α(25:60) it is likely that the central source is strong enough to affect the global dust properties. It is plausible then, that the flattest objects which are far from the starburst correlation have dust that is heated by a different mechanism than star formation. It is interesting to point out that the LINERs with the flattest α(25:60) (NGC 3998, NGC 7479, NGC 7743, and NGC 4258) have lower [FeII]/Paβ than the steeper spectrum sources. These four objects are also the strongest candidates in the sample to have Seyfert-like nuclei (in fact NGC 7479 and NGC 4258 are often classified as Seyfert 2's). Also NGC 3998 is the strongest

x-ray sources among the LINER sample, and has recently been found to have an unobscured hard (1-12 keV) compact, power-law, x-ray source by ASCA (Serlemitsos 1995). For the LINERs with steep α(25:60) the IRAS index provides little information except that the central source does not alter the global infrared colors significantly. The majority of these sources, however, do have the highest ratios of [FeII]/Paβ (see figure 4.22). As a final emphasis of how different LINERs and starbursts are in these quantities, α(25:60) versus [OI]/Hα is plotted for starbursts and LINERs from the literature. For the flattest objects where the nucleus is altering the global IRAS index, the ratio of [OI]/Hα for starbursts and LINERs are different by up to a factor of 100, while towards steeper indices, the [OI]/Hα ratios are converging.

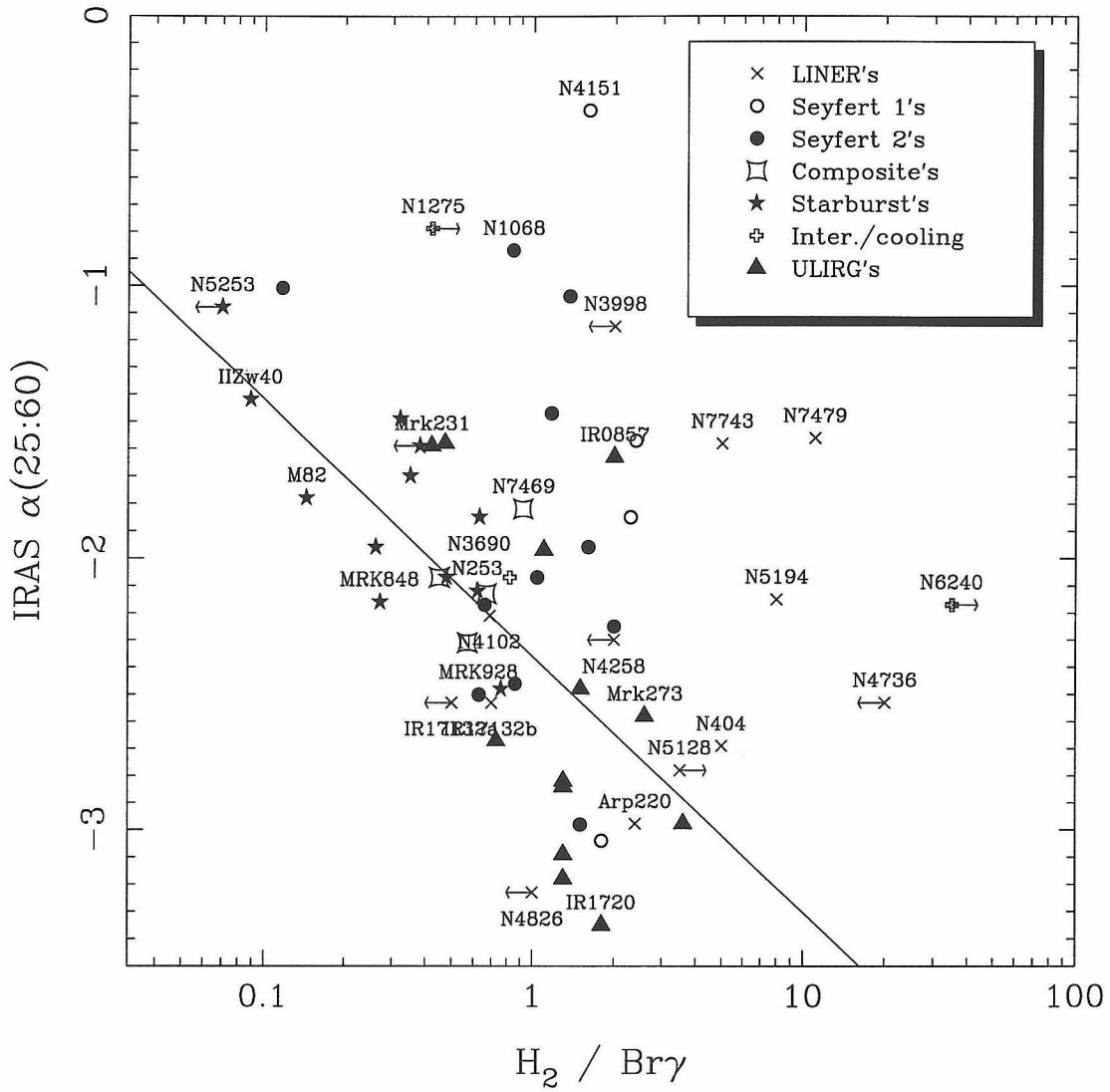

Figure 4.20: For all of the objects in this sample plus objects in the literature, the infrared spectral index from 25 to 60 μm is plotted against $H_2/Br\gamma$. A line is drawn showing the correlation between these two parameters found for starburst galaxies and ultraluminous IRAS galaxies in Mouri and Taniguchi (1992). The LINERs, like the Seyferts, do not in general follow this correlation.

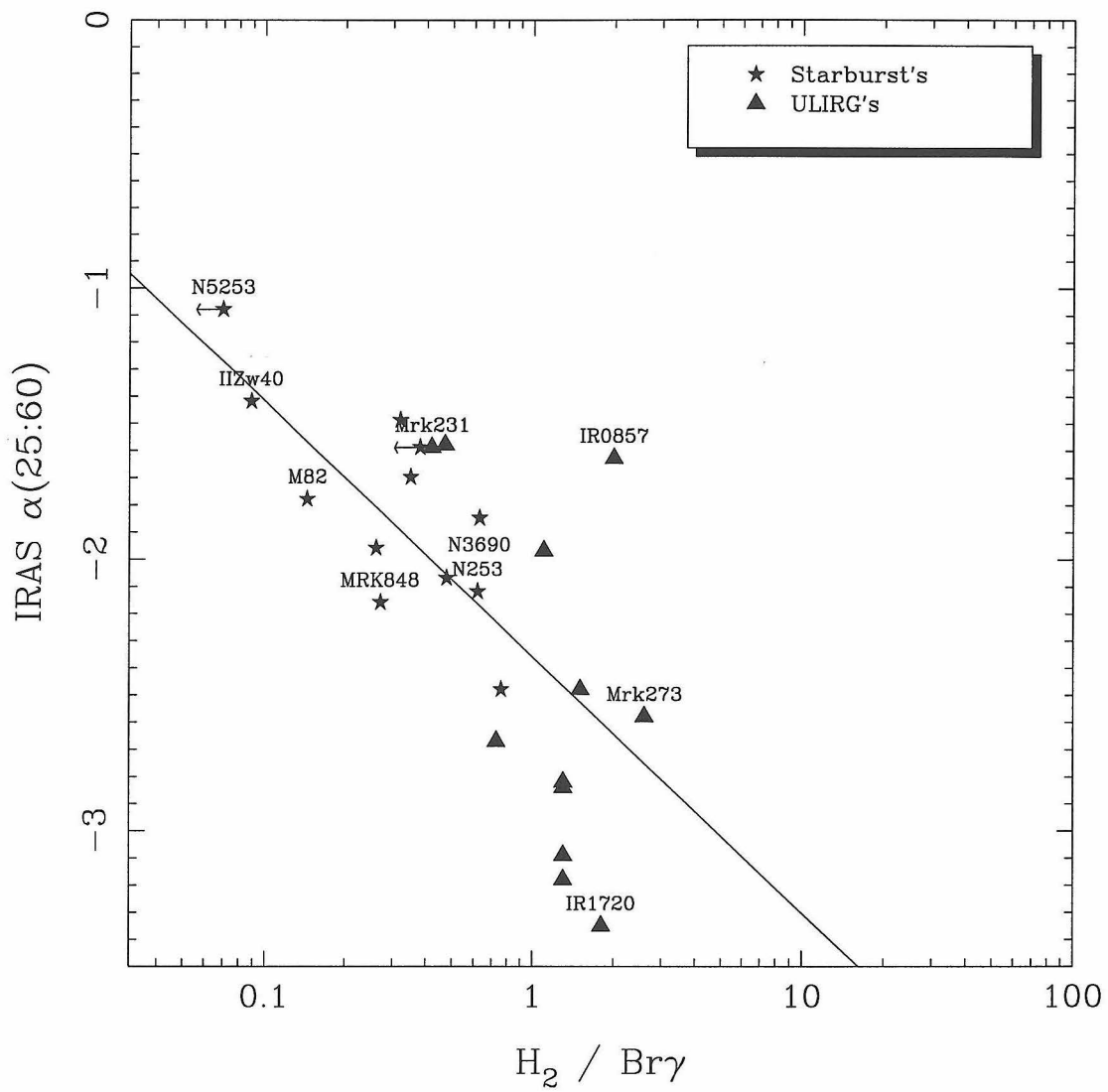

Figure 4.21: For starbursts and ultraluminous IRAS galaxies in the literature, the infrared spectral index from 25 to 60 μm is plotted against $H_2/Br\gamma$. This figure is to point out the known correlation between infrared index and $H_2/Br\gamma$ ratio for these galaxy types (Mouri and Taniguchi 1992).

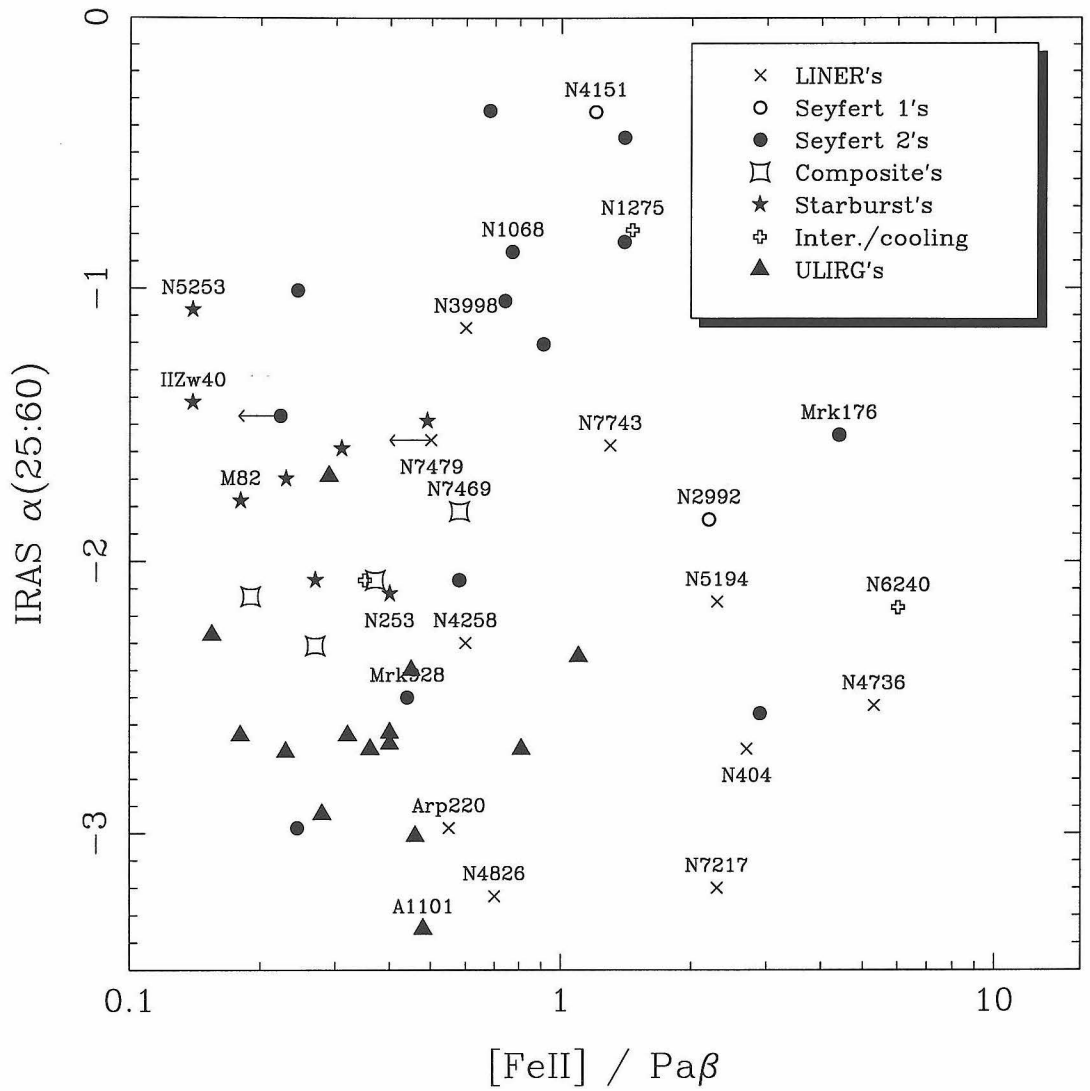

Figure 4.22: For all of the objects in this sample plus objects in the literature, the infrared spectral index from 25 to 60 μm is plotted against [FeII]/Paβ. The correlation between these two parameters for starburst galaxies and ultraluminous IRAS galaxies is significantly weaker than between α(25:60) and H_2/Brγ. The flatter index LINERs do have lower [FeII]/Paβ compared to most of the steep spectrum LINERs.

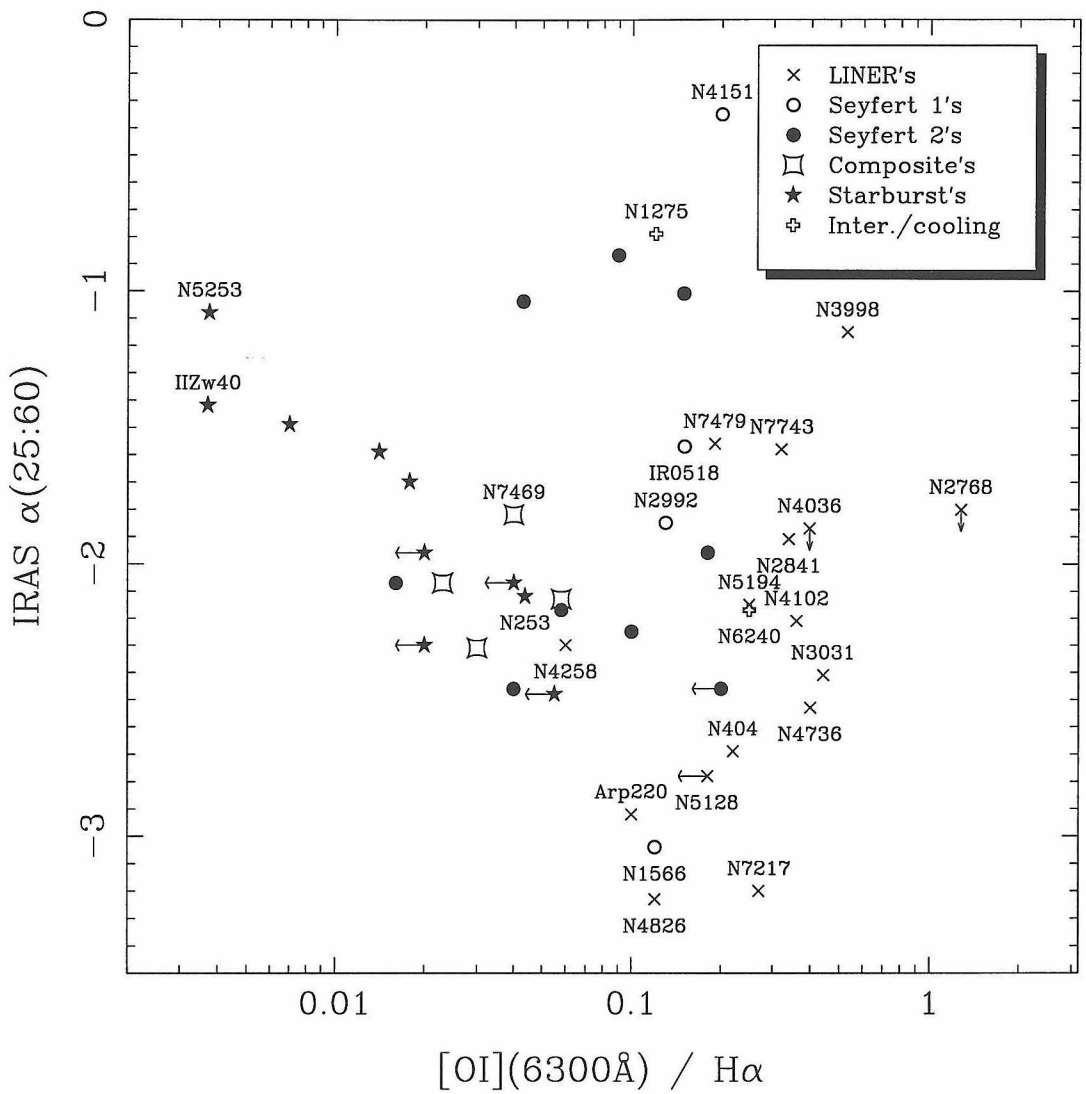

Figure 4.23: For a collection of galaxies in the literature, the infrared spectral index from 25 to 60 μm is plotted against [OI]/Hα. A linear correlation between these two parameters was found for starburst galaxies in Mouri and Taniguchi (1992). The LINERs, like the Seyferts, do not appear consistent with this correlation.

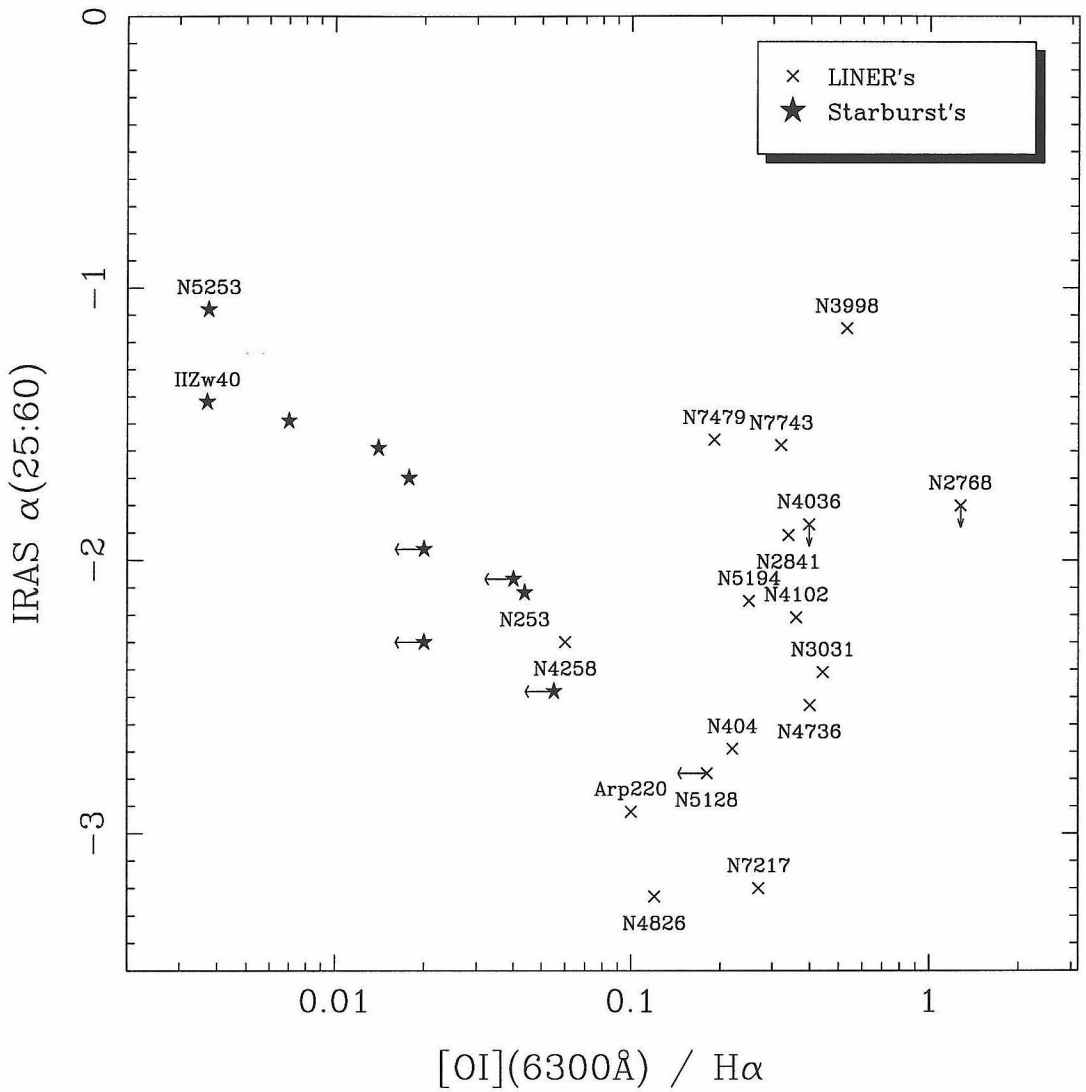

Figure 4.24: For LINERs and starbursts the infrared spectral index from 25 to 60 μm is plotted against [OI]/Hα. This figure is to emphasize the linear correlation found for starbursts by Mouri and Taniguchi (1992), and the very different behavior of LINERs.

4.3.5 Comparison with Einstein x-ray measurements

If the LINERs with the flattest α(25:60), and the lowest [FeII]/Paβ are x-ray heated by a power-law source, as suggested in the previous subsection, there should be sufficient x-rays to power the observed infrared line emission. The ratio of [FeII]/Paβ is not trivial in these objects, however, and some degree of grain destruction to increase the gas phase iron abundance is probably necessary. A successful x-ray heating model must therefore include a significant hard x-ray flux. Unfortunately, very little is known about the hard x-ray output of LINERs. The best survey for comparison is from the Einstein satellite which operated out to 3.5 keV. For Seyfert 1's the luminosity in the range 0.5 to 3.5 keV is thought to be comparable to the hard x-ray luminosity (Van Der Werf et al. 1993).

Figures 4.25 plots the Einstein luminosity (0.2 to 3.5 keV) for the available LINERs in the sample against the [FeII] luminosity. Notice that both the x-ray luminosity and the [FeII] luminosity is much lower for the LINERs compared to the Seyferts in the figure. Models predict that in hard x-ray heating, about 1% of the 1 to 10 keV energy can come out in the 1.2567μm [FeII] line. In the figure the 1% curve is plotted as a rough approximation of the minimum efficiency of x-ray to [FeII] conversion. The fact that many of the Seyfert 2's are below this line probably results from dust obscuration of the soft x-ray flux. For the LINERs with Einstein detections near to or above the 1% line, there are probably sufficient x-rays to power the the iron lines. As in Seyfert 2's, dust obscuration may have a significant effect on the soft x-ray fluxes of many of the LINERs making it difficult to estimate the role of x-ray heating in those objects without x-ray detections and those below the 1% line. The apparent correlation between x-ray luminosity and [FeII] luminosity is greatly reduced in figure 4.26 where the fluxes are plotted instead of the luminosities.

The Einstein luminosity is plotted versus the H_2 luminosity in figure 4.27. The models of Lepp and McCray (1983) predict that .25% of the x-ray energy can come out in the 2.1218μm H_2 line, although some more recent models imply that x-ray heating may not be this efficient at stimulating this transition. The .25% line is drawn in the figure, and again, most of the LINERs are at or above this line. In general then, the LINERs in our sample with Einstein detections do appear to have sufficient x-ray energy to power the line emission.

The Einstein satellite used a large beam, so much of the measured x-ray flux could arise from outside the nuclear region, making the amount of energy available for line emission much lower. Also the extrapolation from the Einstein fluxes to the hard x-rays is highly uncertain for LINERs. The better resolution available with ROSAT is offset by the softer range of x-rays measured. The ASCA satellite and the future AXAF mission will greatly improve our knowledge of hard x-ray emission from LINERs and other sources. It is very intriguing that the first few LINERs (NGC 3998, NGC 4579, NGC 3031 (M81), NGC 4258, NGC 5194 (M51)) observed with ASCA all require a power-law x-ray source out to 12 keV, which appears to be point-like (Serlemitsos 1995). Although the current ASCA sample is not a randomly selected sample and the result is only preliminary, it does support x-ray heating in at least some LINERs.

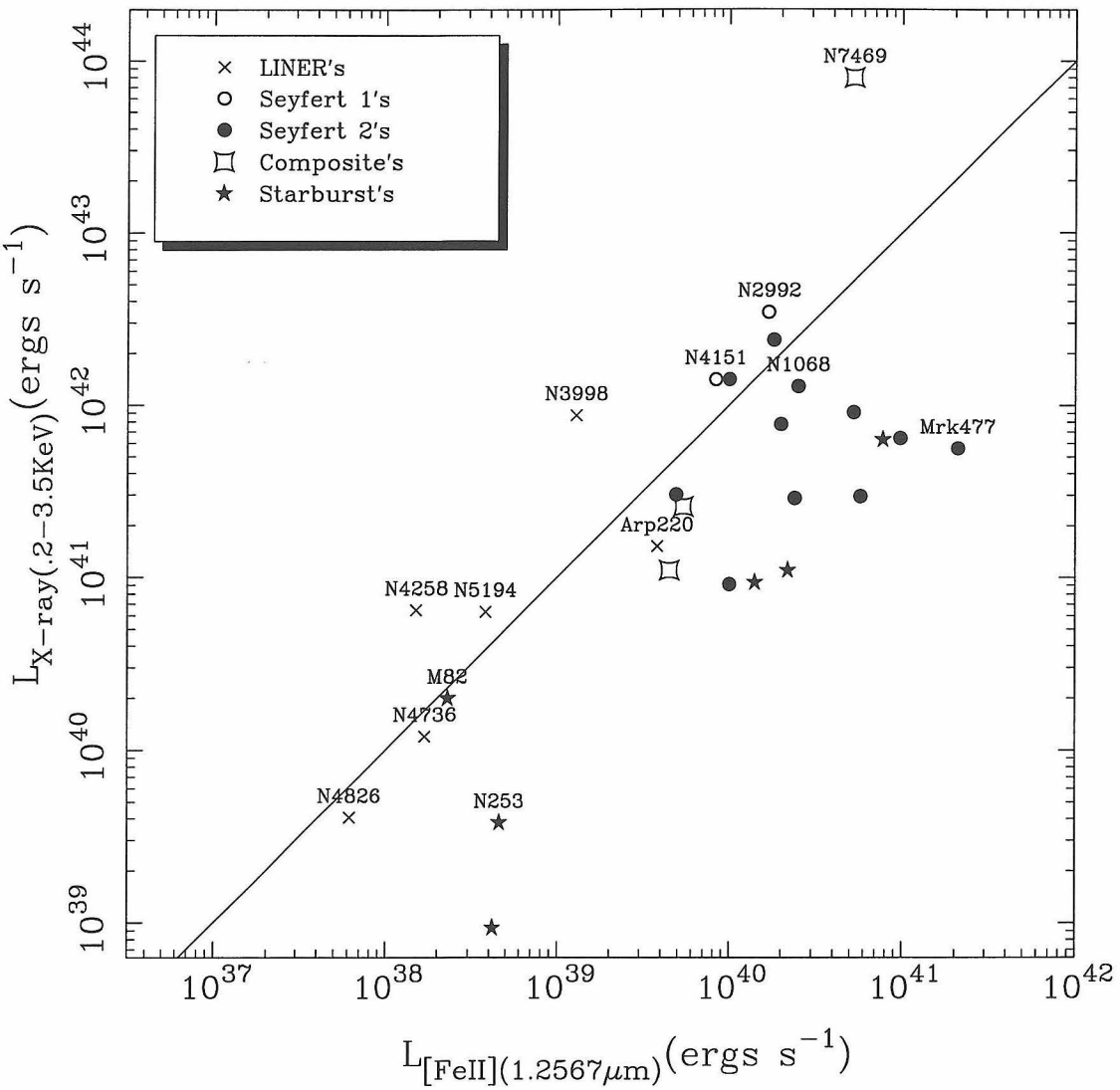

Figure 4.25: For all of the objects in this sample plus objects in the literature, the Einstein x-ray luminosities (.2-3.5 keV) are plotted against the [FeII] luminosity. A line is drawn at $L_{x-ray} = 100\ L_{[FeII]}$ which is approximately the fraction of [FeII] emission expected for a given L_{x-ray}. Most of the LINERs are close to or above this line.

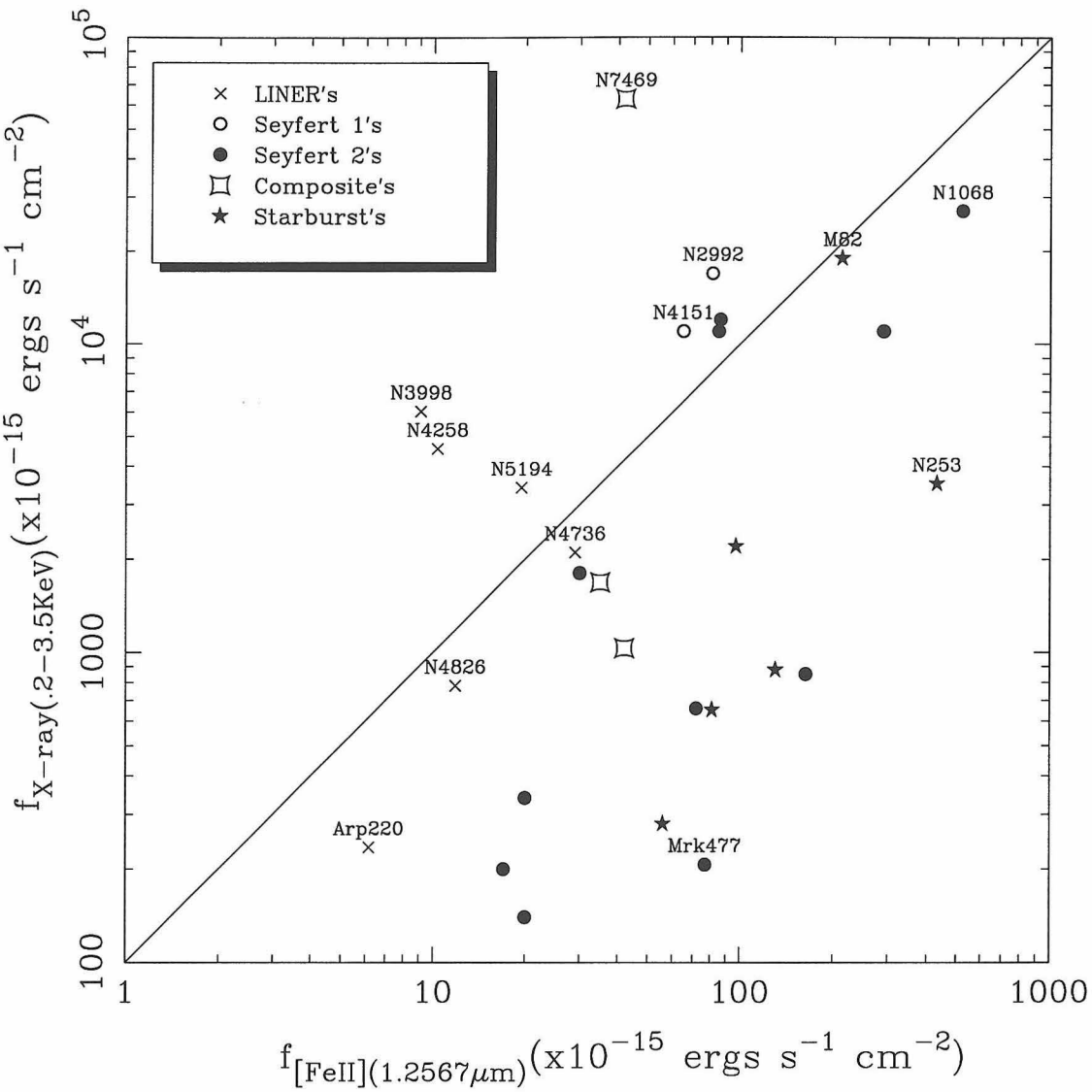

Figure 4.26: For all of the objects in this sample plus objects in the literature, the observed Einstein x-ray fluxes (.2-3.5 keV) are plotted against the [FeII] fluxes. A line is drawn at $f_{x-ray} = 100\ f_{[FeII]}$ which is approximately the fraction of [FeII] emission expected for a given f_{x-ray}. Note that the apparent linear correlation between x-ray and [FeII] luminosities in figure 4.25 is not present here, indicating that the main effect was the stretching of the graph by including the distances to the objects.

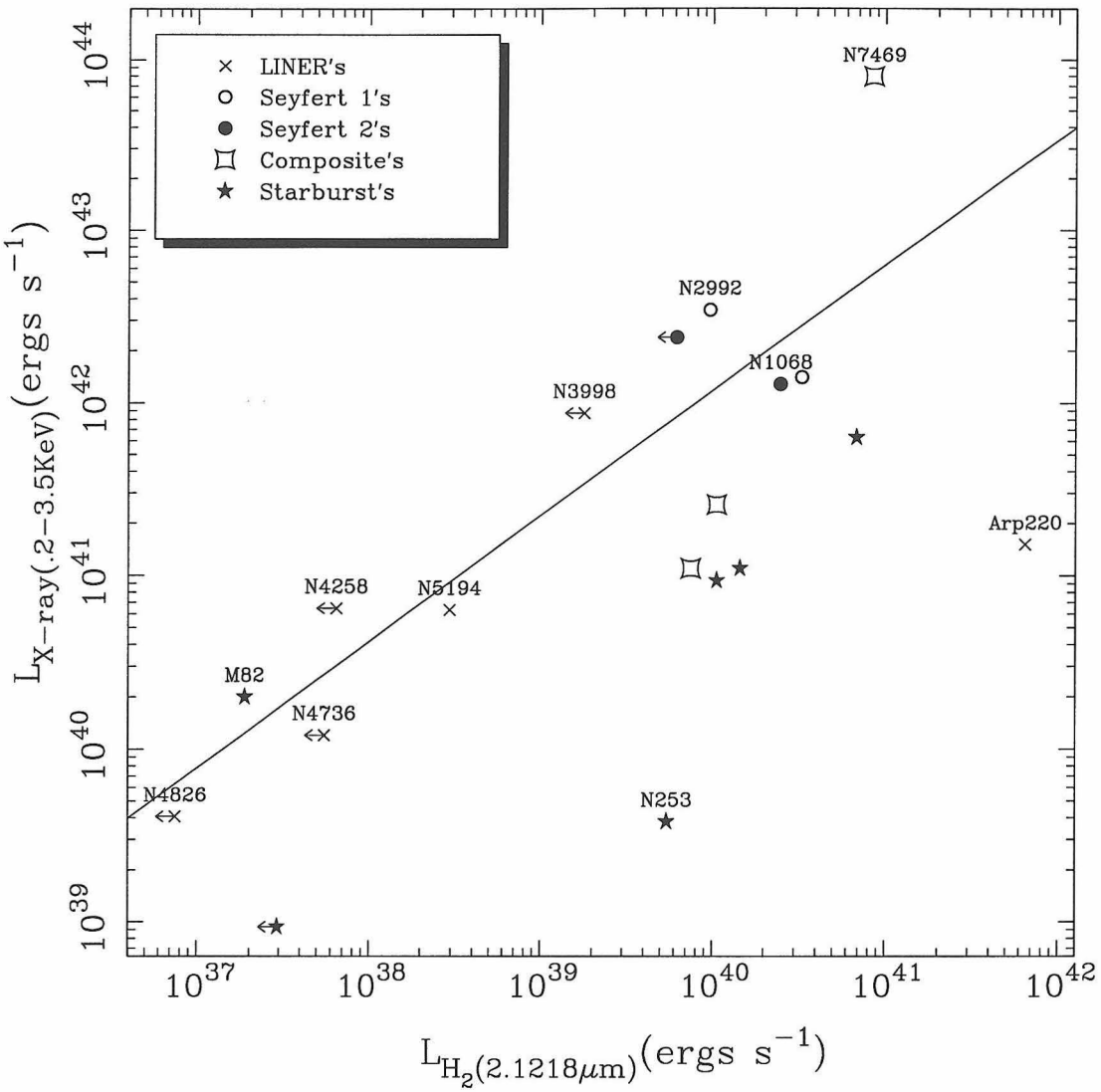

Figure 4.27: For all of the objects in this sample plus objects in the literature, the Einstein x-ray luminosities (.2-3.5 keV) are plotted against the H_2 luminosity. A line is drawn at $L_{x-ray} = 400\ L_{H_2}$ which is approximately the fraction of H_2 emission expected for a given L_{x-ray}. Most of the LINERs are close to or above this line. Arp 220 is the obvious exception. In chapter 3, it's argued that the line emission in Arp 220 most likely comes from shocks due to cloud-cloud collisions resulting from the merger.

4.3.6 Unexpected Atomic Absorption Features

In addition to the emission lines, several atomic absorption features are seen in many of the galaxies. These features were found by shifting the spectra to the rest frame and noting that several of the galaxies showed the same features. Further confidence that they are real features in the galaxies' spectra and are not a reduction artifact comes from a comparison with optical spectra in Filippenko and Sargent (1985) which show that the galaxies with the strongest infrared absorption lines also have the strongest optical absorption lines. In figures 4.3 to 4.14, these suspected absorption lines are marked by vertical marks below each spectrum with the most likely identification given. The line identifications were found by comparing the spectra with a very high resolution (R $\sim$ 100,000) spectrum of the solar photosphere (Hall 1973). Among the strongest lines present in the galaxies spectra are a Na doublet ($\lambda\lambda$2.2062,2.2090μm) and a Mg doublet ($\lambda\lambda$1.2423,1.2433μm). The Na doublet is seen in all seven galaxies where the spectra extend to this wavelength. One feature at $\lambda_{rest} = 1.2893 \pm 0.0003$ μm is still not identified, although it is detected in 5 or 6 of the galaxies. It is possible that this line is from a molecular species present in cool giants but not in the Sun.

4.3.7 Individual Galaxies

NGC 404 : A classical LINER fully satisfying Heckman's criterion. The infrared spectra show a very prominent [FeII] emission and a strong detection of H_2. NGC 404 has the largest [FeII] line to continuum ratio for any of the LINERs in this sample. It is plausible that the estimated Paβ flux is too high and that the calculated [FeII]/Paβ flux is significantly higher than the value of 2.7 in table 4.3. Even with this large estimated Paβ flux, NGC 404 has one of the highest ratios of [FeII] to Paβ of any extragalactic object. A ripple at the location of Brγ is due to residual ripple in the G

star which is most apparent in NGC 404 because it is at essentially zero redshift. Since the expected Brγ is below the detection limit, and there is an obvious explanation for the feature, we do not regard this as a real detection in NGC 404. All of the line emission is spatially unresolved with a seeing of 1". At a distance between 1.8 and 2.4 Mpc, this corresponds to only 10pc. At this distance, the aperture corrected [FeII] luminosity is 1.1×10^{37} ergs s^{-1} which is only a few times the expected luminosity for a single supernova remnant (Moorwood and Oliva 1988). It is an interesting possibility that the emission within NGC 404 could be generated in a single SNR in a high density medium, see the discussion below. The Paβ absorption correction estimated in 4.3.2 is about a factor of two too low to explain why Paβ is undetected. The most obvious explanation is that it contains a significant population of young stars which increase the amount of Balmer absorption. This is supported by Keel (1983), who considered NGC 404 a peculiar member of the LINER class due to the presence of a blue continuum and strong Balmer absorption lines. NGC 404 shows none of the atomic absorption features. The optical spectrum in Filippenko and Sargent (1985) also shows a relatively smooth continuum spectrum. Although the emission lines are very narrow, a strong UV point source and several fainter ones has been detected with HST (Maoz 1993), and this was used to suggest that a non-stellar source is present in the nucleus. It is possible, however, that the UV sources are a young star cluster.

NGC 2685 : Classified as a LINER based upon only the [OII]/[OIII] ratio, this object has very weak optical lines. No emission lines are detected in the infrared spectrum. There appears to be a strong Paβ absorption feature, although the continuum around it has residual features from the night sky and the G star division. It does show most of the atomic absorption features, especially the Mg ($\lambda\lambda$1.2423,1.2433μm) and Na ($\lambda\lambda$2.2062,2.2090μm) lines. Optically it has strong Balmer absorption, weak NII and strong atomic absorption lines (Filippenko and Sargent 1985).

NGC 3992 (M 109) : Like NGC 2685, it was classified only on the basis of [OII]/[OIII], without knowing the [OI] ratio. No emission lines are detected in the infrared spectrum. There is an obvious strong Paβ absorption line. NGC 3992 also shows the strongest atomic absorption features of the classical LINERs in this sample. The spectrum in Filippenko and Sargent (1985) also shows prominent atomic absorption features and weak emission lines.

NGC 3998 : A true LINER which shows increasing ratios of [OI] and [OII] to [OIII] with increasing aperture size. The only detected infrared emission line is [FeII] which is detected at the 4 to 5 sigma level. Using the estimated Paβ flux, the ratio of [FeII] to Paβ is 0.6, which is one of the lowest in the sample. Also since H_2 is undetected, both its H_2/Brγ and [FeII]/Paβ ratios are significantly lower in comparison to the OI/Hα ratio than the other LINERs in the sample. The ratio of H_2 to [FeII], however, does lie along the main correlation for LINERs and other galaxies. In Larkin et al. (1995, in preparation), it is argued that the NII emission is significantly extended in comparison to the Hα. It is probable that the OI, and also probably the [FeII] and H_2, are also more extended than the H recombination lines, and that the optical ratio calculated in the larger aperture is enhanced in comparison to the infrared ratios in a much smaller aperture. If true, then the infrared ratios in a larger aperture would probably be greater and NGC 3998 would lie closer to the main correlations shown in figures 4.16 to 4.15. In principle, this says that the low ionization lines are more extended than Hα, and that the unresolved core has more Seyfert-like line ratios. The Na and Mg absorption features may be present at a very low level. Optical spectra show prominent broad Hα wings and even a broadened OI line (700 km sec^{-1}). Optical absorption features, if present, are weak and broadened (Filippenko and Sargent 1985). Like NGC 404, NGC 3998 has had a strong UV point source detected by HST (Fabbiano et al. 1994). Coupled with the broad Hα, this makes

NGC 3998 a prime candidate for a weak Seyfert galaxy. Its [FeII] and H_2 ratios are comparable to Seyferts.

NGC 4258 (M 106) : One of Heckman's original two transitional objects. Its optical line ratios are actually typical of Seyferts. Its infrared spectra are similar to those of NGC 3998; only a fairly weak detection of [FeII] in emission. Also has a similar ratio of [FeII] to Paβ ratio of 0.6, which is low for this sample. Optically, also very similar to NGC 3998, with faint broad wings of Hα and slightly broadened OI. The Na absorption feature is detected weakly. Unlike NGC 3998, NGC 4258 shows several strong optical absorption features (Filippenko and Sargent 1985). A wealth of high resolution observations have focused on NGC 4258, showing it to have a rotating ring of water masers (e.g. Nakai et al. 1993), optical jets (e.g. Ford et al. 1986) and a steeply rising velocity curve (Miyoshi et al. 1995), all of which make NGC 4258 one of the best candidates for harboring a central black hole. Its [FeII] and H_2 ratios are comparable to Seyferts.

NGC 4589 : Classified as a LINER based on only the [OII] to [OIII] ratio. This is the most featureless of the LINERs in the infrared, showing no emission or absorption lines, except weak Paβ absorption. Mollenhoff and Bender (1989) showed that NGC 4589 had a peculiar velocity field with evidence for large streaming motions, and a warped dust lane. They argued that NGC 4589 was the result of a recent merger.

NGC 4736 : A true LINER satisfying both of Heckman's (1980) criterion. NGC 4736 is one of the strongest continuum sources in the sample making the expected weak lines difficult to detect. The [FeII] to Paβ ratio is the highest of any object in this sample, and the second largest of any extragalactic object measured (only NGC 6240 has a higher ratio). This ratio is, however, uncertain by 50% due to the strong continuum surrounding the [FeII] line. The ratio is supported by the strong optical ratio

of [OI]/Hα which, as discussed above, is correlated with [FeII]/Paβ. The H_2/Brγ is only a very poor upper limit, but based on the other two line ratios, is probably also very high ($\sim$10). Like NGC 404, NGC 4736 is very close (4.3 Mpc) making the [FeII] luminosity only a few times higher than an individual SNR. The estimated Paβ absorption in table 4.3 is not sufficient to reconcile optical line strengths and the observed Paβ flux. This may indicate the presence of a younger stellar population. Atomic absorption features are reasonably strong in the infrared spectra, and in the optical spectra of Filippenko and Sargent (1985). NGC 4736 was found to have two compact UV sources separated by 2.5" in its nucleus by HST (Maoz et al. 1993). It also had UV arcs at 2", 4" and 6" suggestive of bow shocks. At much larger scales, NGC 4736, has a strong ring of Hα emission (Larkin et al. 1995, in preparation). All of these features suggest that NGC 4736 is the result of a recent merger event or recent star formation.

NGC 4826 (M 64): Probably a true LINER since [OI]/[OIII] = 0.65 (Keel 1983), but [OII] is not measured. The infrared spectra look very similar to NGC 4736, with the relatively weak [FeII] detection, and fairly strong atomic absorption features. A strong Paβ absorption line is also apparent. Optical spectra from Filippenko and Sargent (1985) show strong emission lines, many atomic absorption features, but no broad Hα. Along with NGC 4258 and NGC 3998, it has the lowest ratios of [FeII] and H_2 to hydrogen lines of this sample, and their ratios are actually located within the range typical of Seyferts.

NGC 5194 (M 51) : One of Heckman's (1980) original transition objects with oxygen line ratios comparable to Seyferts. Among the most famous LINER galaxies, M 51 is one of only two in this sample to show Paβ in emission (although it is very weak). M 51 also shows strong [FeII] and H_2 emission and has estimated ratios among the highest in this data set, significantly above any Seyfert or starburst galaxy.

A bubble of Hα emission is seen just off of the nucleus (Larkin et al. 1995, in preparation). Known as the whirlpool galaxy, it has an obvious interaction with NGC 5195 which may contribute to any nuclear activity. No broad lines are detected by Filippenko and Sargent (1985). The only obvious atomic absorption feature in M51 is the Na doublet, although Mg may also be present.

NGC 7217 : A true LINER satisfying both of Heckman's criteria. Only a J-band spectra is available for NGC 7217. It shows strong [FeII] in emission, and Paβ in absorption, along with faint atomic absorption features. It ranks among the top four LINERs in [FeII]/Paβ ratio. In Hα, an inner ring of radius 10" is visible suggesting some form of recent tidal interaction or star formation (Larkin et al. 1995, in preparation). Filippenko and Sargent (1985) found no broad Hα component and only weak atomic absorption.

NGC 7479 : NGC 7479 does not meet the full LINER classification of Heckman (1980) in the small aperture of Ho et al. (1993) since [OI]/[OIII] is below 1/3rd, but it has [OI]/[OIII] of $\sim \frac{2}{3}$ in Keel's larger 6" aperture. It is also often classified as a Seyfert 2 in the literature. NGC 7479 is the only galaxy in this sample to be detected in H_2 but not in [FeII]. It also has a strong Paβ emission line detected. Filippenko and Sargent (1985) found no broad Hα, although many of the lines showed a complex velocity field which suggests a fuel supply of molecular gas. Since the [OI] may be more extended than the [OIII] emission, the central source may have Seyfert-like line ratios.

NGC 7743 : It has a [OI]/[OIII] ratio of 0.14 which is below the cutoff of $\frac{1}{3}$ of Heckman (1980) but it has strong [OII] emission. The infrared spectra show strong [FeII] and H_2 emission lines, and perhaps broadened Paβ and Mg absorption lines. Its [FeII] and H_2 ratios are significantly stronger than Seyfert and starburst galaxies.

Filippenko and Sargent (1985) found no broad Hα component and a fairly smooth continuum with little atomic absorption.

4.4 Results: Double and High Luminosity LINERs

Figures 4.28 to 4.31 show the J and K band spectra of the four multiple nuclei objects in this sample. For Arp 220, a 3" cut across both nuclei was used to make figure 4.28. The Arp 220 spectra are discussed in detail in chapter 3. For the other three objects, IRAS 17132+5313, Mrk 848 and Mrk 928, the spectra of each nucleus is shown along with the grayscales of the two-dimensional spectra to show the spatial separation of the nuclei. For IRAS 17132+5313 and Mrk 848, the J-band spectra are on the long wavelength end of the band, and telluric features make the spectra very noisy.

The line fluxes and ratios for the multiple nuclei objects are listed in table 4.4. An obvious difference between these objects and the low luminosity LINERs in the previous section is that [FeII] is not the strongest line detected in any of the objects. Actually, only one of the LINER nuclei, Arp 220 has a confident detection of [FeII]. The other strong [FeII] lines are in the starburst and Seyfert nuclei of Mrk 848 and Mrk 928, respectively. Also, unlike the classical LINERs, Paβ is a strong line in Arp 220, and Mrk 928, which are the only galaxies with a clear view of this line. Brγ is detected in all of the nuclei except for the LINER sources in the Markarian galaxies. All four galaxies have steep IRAS α(25:60) index ($<$ -2.1 for all). The starburst and Seyfert components of Mrk 848 and Mrk 928, have H_2/Brγ and in the case of Mrk 928, [FeII]/Paβ consistent with other starburst and Seyfert galaxies, and much lower than the group of LINERs with strong [FeII].

Table 4.4
Measured Line Fluxes and Ratios

Object	flux ($\times 10^{-15}$ erg cm^{-2} s^{-1})				$\frac{[FeII]}{<Pa\beta>}$	$\frac{H_2}{<Br\gamma>}$
	[FeII]	Paβ	H_2	Brγ		
(1)	(2)	(3)	(4)	(5)	(6)	(7)
Arp 220[a]	2.1±0.2	3.8±0.2	6.4±0.3	2.7±0.3	.55±.06	2.4±.3
IRAS 17132+5313[b]	0.8±0.8	-	0±0.3	1.2±0.3	-	<.5
	0±1	-	0.7±0.5	1±0.2	-	.7±.5
Mrk 848[c]	0±1	-	0.5±1.5	0±0.5	-	-
	5±2	-	1.5±0.2	5.6±0.3	-	.27±.04
Mrk 928[d]	0±1	4±1	0±0.5	0±0.5	<.5	-
	4±1	9±2	1.5±0.5	2.4±0.3	.44±.15	.6±.2

[a] For Arp 220, both nuclei were combined for this table. For a detailed discussion of the relative fluxes of the two nuclei see chapter 3 of this thesis.
[b] For IRAS 17132+5313, the western most nucleus is listed above the eastern most.
[c] For Mrk 848, the LINER is listed above the starburst nucleus.
[d] For Mrk 928, the LINER is listed above the Seyfert 2 nucleus.

Table 4.4: Raw fluxes from the calibrated spectra. No stellar absorption, reddening or other factors have been considered in this set of numbers. In the case of the highly redshifted objects, where Paβ is inaccessible, dashes are used. If no line was seen, zero is listed with the calculated uncertainty, and a two sigma limit is given for any calculated ratios.

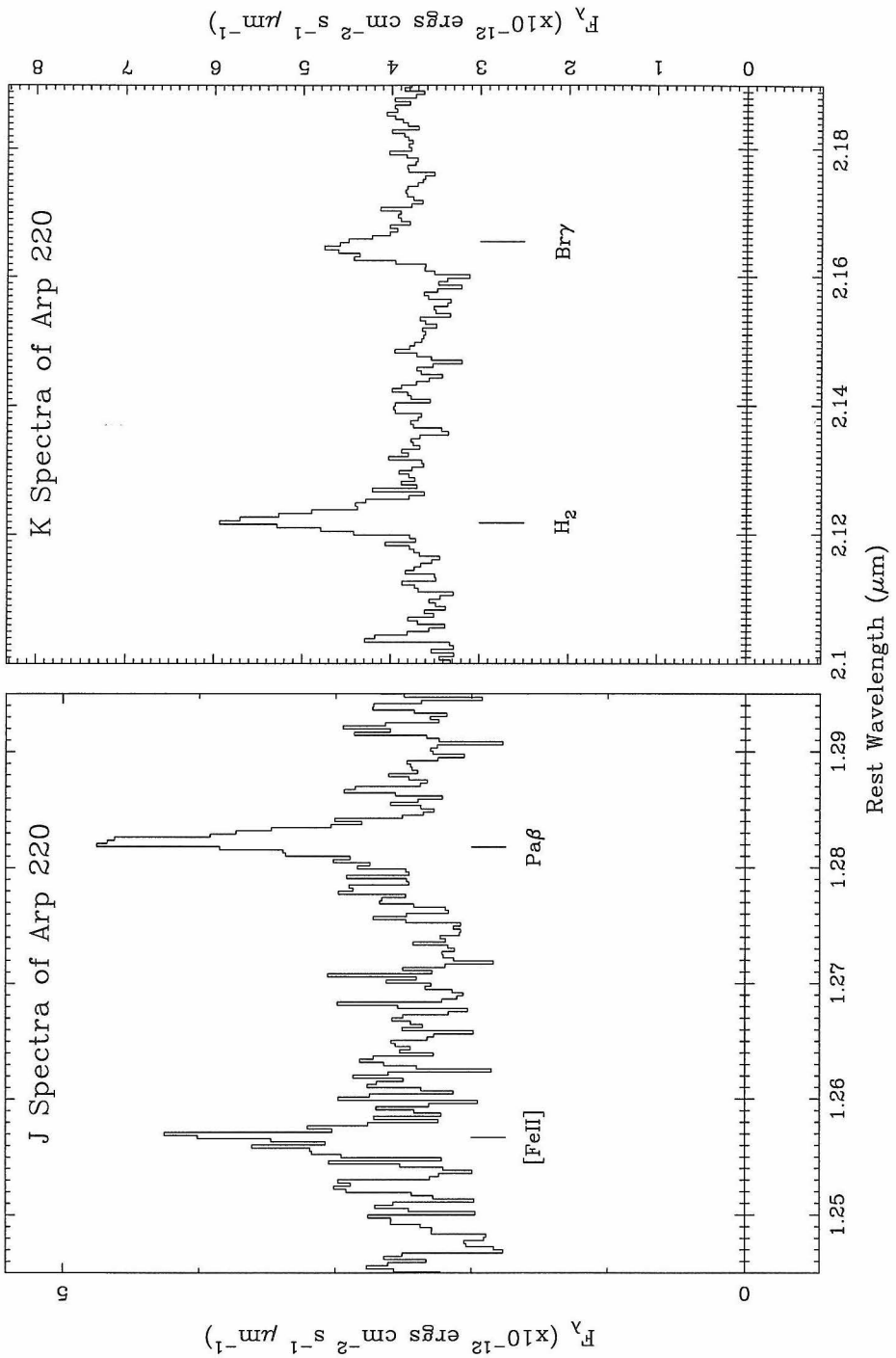

Figure 4.28: Flux calibrated spectra of Arp 220: The left spectrum is in the J-band window and covers the wavelengths of [FeII] (λ_{rest}=1.2567 μm) and Paβ at a resolution of ~1100. The right spectrum is in the K-band window and covers the wavelengths of H_2 (λ_{rest}=2.1218 μm) and Brγ at a resolution of ~900.

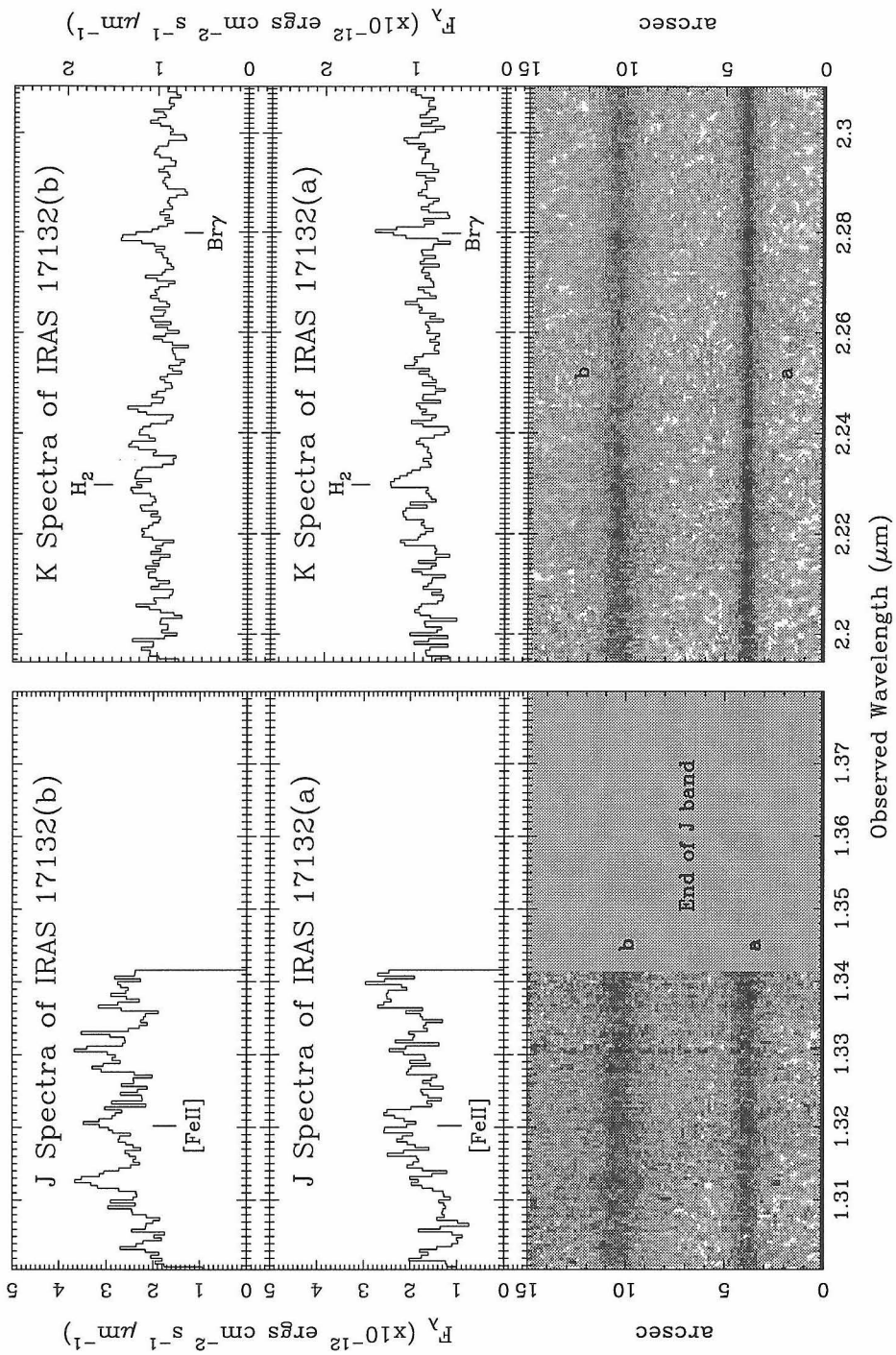

Figure 4.29: The left three panels show the J band spectra of the two nuclei (labeled a and b) of IRAS 17132+5313. The lower left panel is a grayscale of the long slit spectrum shown as position along the slit versus wavelength. The two upper left panels are 3" slices centered on the two nuclei respectively. Note that the J window cuts off at ~1.342 μm so Paβ was not observable. The three panels on the right are similar except for the K band spectra.

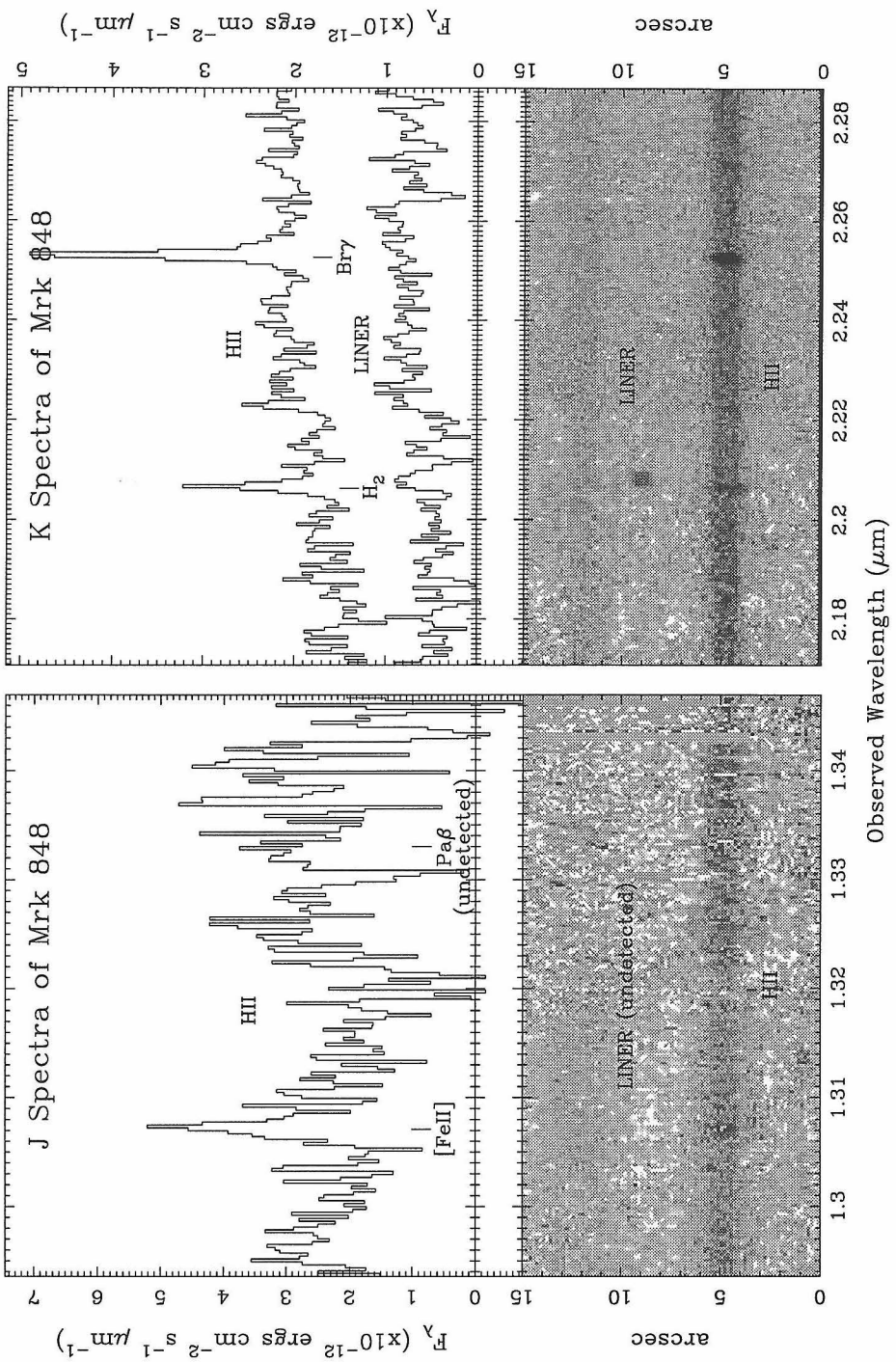

Figure 4.30: The left two panels show the J band spectra of the two nuclei (labeled LINER and HII) of Mrk 848. The lower left panel is a grayscale of the long slit spectrum shown as position along the slit versus wavelength. The upper left panel is a 3" slice centered on the starburst nucleus (HII). The LINER nucleus is too faint in the J band to detect. The two panels on the right show the K band spectra in a similar manner to the left panels. Note that both the starburst nucleus and the LINER are plotted in the upper left panel.

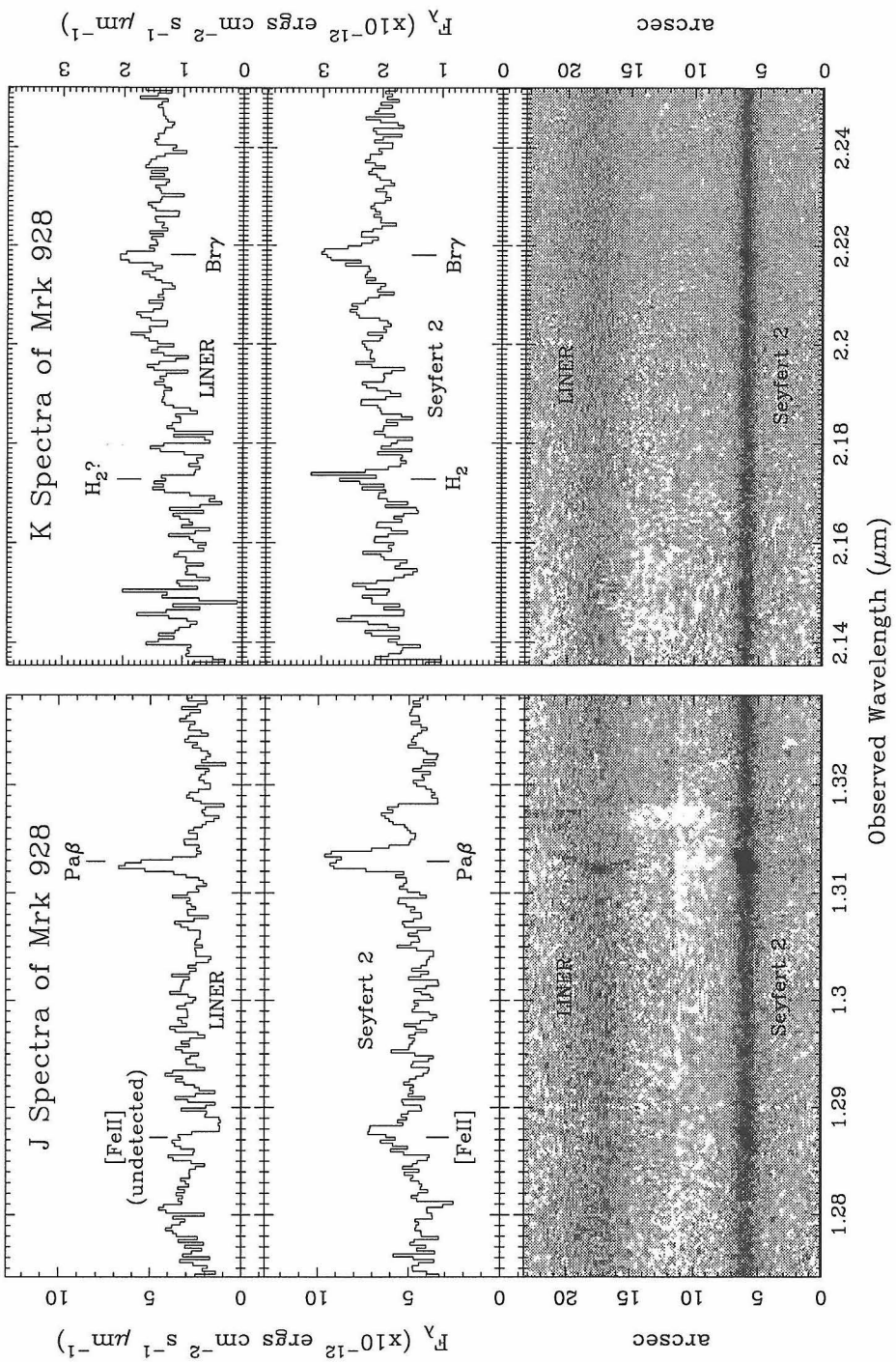

Figure 4.31: The left three panels show the J band spectra of the two nuclei (labeled LINER and Seyfert 2) of Mrk 928. The lower left panel is a grayscale of the long slit spectrum shown as position along the slit versus wavelength. The two upper left panels are 3" slices centered on the two nuclei respectively. The three panels on the right are similar except for the K band spectra.

4.4.1 Individual Galaxies

Arp 220 : Arp 220 is discussed in great detail in chapter 3, but some important comparisons can be made to the classical LINERs in this chapter. The ratios of [FeII]/Paβ and H_2/Brγ are 0.55 and 2.4 respectively, which places Arp 220 in between the Seyfert galaxies and the strong LINERs in figure 4.15. In chapter 3, it is shown that off of the nuclei, both of the ratios are enhanced and are more consistent with the high ratios among the classical LINERs. In the case of Arp 220, this probably results from cloud-cloud collisions due to the on-going merger. It is probable that the two nuclei themselves are Seyfert-like with the LINER-like spectrum resulting from the collision driven shocks.

IRAS 17132+5313 : Due to the high redshift of this object ($\sim$15,000 km s^{-1}), [FeII] and Paβ are shifted to a poor location in the atmospheric window. Brγ and H_2, however, are in a good portion in the K window, and Brγ is strong in both nuclei. The eastern nucleus, labeled (a) in figure 4.29 has a H_2/Brγ ratio of 0.7 which is at the break between Seyfert's and starburst galaxies, while the western nucleus (b), has a ratio below 0.5 (two sigma) making it consistent with the starburst galaxies.

Mrk 848 : Unfortunately, no emission lines were confidently identified in the LINER component of this double system. The starburst nucleus, however, has several strong emission lines. The H_2/Brγ ratio is 0.27, and the [FeII]/Paβ ratio (calculated by estimating Paβ from Brγ) is probably close to 0.15. Both of these ratios place this nucleus almost in the dead center of the starburst galaxies displayed in figure 4.15. The [OI]/Hα ratio of 0.024 (Mazzarella and Boroson 1993) is also consistent with the other starburst systems in figures 4.16 and 4.17. The [OI]/Hα upper limit for the LINER nucleus of 0.014 (Mazzarella and Boroson 1993) is not, however, typical of any

LINERs in the classical sample. This may explain why [FeII] and H_2 are undetected in this nucleus.

Mrk 928 (NGC 7592): As in Mrk 848, the LINER nucleus does not show [FeII] or H_2 emission, although a strong Paβ line is detected, and there is a hint of a weak Brγ line. This makes the LINER nucleus unusual compared to the classical LINERs because the [FeII]/Paβ two sigma upper limit is 0.5 which is below all of the LINERs except NGC 7479 which is an unusual case (see above). The Seyfert 2 component has [FeII]/Paβ and H_2/Brγ ratios of 0.44 and 0.63 respectively, which is fairly typical for the Seyferts in the literature (see figures 4.16-4.18).

4.5 Discussion

The most striking feature of the infrared spectra is the strength of the [FeII] and H_2 features in relation to hydrogen recombination lines, and the correlation of H_2 and to a lesser extent [FeII] with the optical [OI] line. Ho et al. (1993) found that there was a clear separation between LINERs and transitional objects at [OI]/H$\alpha \sim \frac{1}{6}$. We find a similar separation between the majority of LINERs in this sample and Seyferts at [FeII]/Paβ of $\sim$ 1, and H_2/Brγ ratio of $\sim$ 3. This transition is clearer than the difference in [OI]/Hα ratios for LINERs and Seyferts. The one galaxy which does not satisfy this is NGC 3998, which as argued above, satisfies the LINER criterion only for larger apertures than employed here, and which is Seyfert-like in small apertures. In this object at least, the LINER classification may be based solely upon circumnuclear emission lines which may be photoionized or shock heated by a central AGN.

The H_2/Brγ ratio also divides the Seyfert's from the starburst galaxies in the literature at $\sim$ 0.6, although several exceptions are evident. It is therefore, interesting to consider that H_2/Brγ can alone be used to classify galaxies as either starbursts,

Seyferts (and transitional LINERs), and LINERs. Figure 4.18 shows that by including the [OIII]/Hβ ratio, the divisions between these classes become even clearer. It must, however, be remembered that these trends apply only when the true Paβ and Brγ emission line fluxes free of stellar absorption are available or can be estimated with reasonable precision. This is particularly important for LINERs where the stellar features often dominate the nuclear activity even for small apertures.

The multiple nuclei LINERs, unfortunately resulted in few line detections on the LINER nuclei. In Arp 220 the nuclear line ratios are more consistent with Seyfert galaxies, while the strong [FeII] and H_2 emission is more extended (see chapter 3) indicating that circumnuclear activity (probably shocks from the outflowing wind, or cloud-cloud collisions) creates the LINER-like ratios. IRAS 17132 also has low ratios of H_2/Brγ consistent with either starbursts of Seyferts. All four multiple nuclei objects have fairly steep 25 to 60 μm index consistent with ULIRGs from the literature, indicating a large ratio of warm to hot dust. A significant possibility is that the LINER-like spectra of these merger objects seen in large optical apertures is a circumnuclear phenomenon. The dust obscuration towards the nuclei in these merging systems may also be very high, so the optical observations may only measure the circumnuclear activity.

4.5.1 Possible Sub-Classes

An interesting result of this work is that the LINERs with infrared detections break up into basically two groups in figure 4.22 based on the ratio of [FeII] to Paβ. In the following, LINERs with [FeII]/Paβ above 2 will be referred to as "strong" [FeII] LINERs, while the ones below 2 will be called "weak" [FeII] LINERs.

The "weak" [FeII] LINERs include NGC 4826, NGC 3998, NGC 4258, NGC 7479 and NGC 7743. All three of the LINERs with relatively flat far infrared spectra

(α(25:60)>-2) are "weak" [FeII] LINERs. Although the interpretation of the α(25:60) index is complicated, a flatter spectrum probably indicates a strong nuclear source that is able to alter the global dust temperatures and affect the IRAS colors. The only two LINERs with detected broad Hα lines (NGC 3998 and NGC 4258) are "weak" [FeII] LINERs. These two LINERs are also the strongest x-ray sources in the sample. The other three "weak" [FeII] LINERs also show evidence for Seyfert-like activity. Technically, NGC 7479, should actually be classified as a Seyfert 2 based on its optical line ratios. NGC 7743 also has unusual line ratios with the highest [OIII]/Hβ ratio in the sample indicating a relatively high state of ionization. The last "weak" [FeII] LINER, NGC 4826 is technically a "weak" [OI] LINER since [OI]/Hα is less than $\frac{1}{6}$, and it has the lowest H_2/Brγ ratio in the sample.

The "strong" [FeII] LINERs are NGC 404, NGC 4736, NGC 5194 and NGC 7217. None of the "strong" [FeII] LINERs has a detected broad Hα line, and none are known as strong x-ray sources. Among the "strong" [FeII] LINERs, NGC 404 and NGC 4736 are particularly noteworthy for having unusually strong Balmer absorption lines indicative of recent star formation. NGC 4736 and NGC 7217 also have inner rings or arcs of Hα emission probably resulting from circumnuclear star formation. NGC 5194 was classified by Heckman (1980) as a transition object (its oxygen line ratios are on the border between Seyfert and LINER classifications). It does, however, have a high ratio of [FeII]/Paβ (2.3) and a very strong H_2 line (H_2/Brγ = 8). Because NGC 5194 is closer to a Seyfert in optical line ratios, and because it has a good x-ray detection, however, it is not as consistent with star formation as the other "strong" [FeII] LINERs. All of the "strong" [FeII] LINERs have steep (α(25:60)<-2) IRAS indices.

An appealing model is that the two groupings reflect different excitation mechanisms. The "weak" [FeII] LINERs may be low luminosity Seyferts, while the "strong"

[FeII] LINERs may be powered by compact starbursts. Compact supernova remnants (pressure confined) are likely to enhance the [FeII] line in the latter group. The [FeII] luminosity of several of the galaxies, in particular the "strong" [FeII] LINERs NGC 404 and NGC 4736, is only a few times that expected for individual supernova remnants, making supernovae, an attractive excitation source. Although this model of "strong" and "weak" [FeII] LINERs is attractive it is by no means definitive, since none of the objects in either sample is unambiguously a Seyfert-like or starburst-like nucleus. Also many of the diagnostics used here are relatively weak, especially the IRAS α(25:60) index. The next subsection also shows that x-ray heating from a central Seyfert-like source can reproduce the large [FeII]/Paβ ratios of "strong" [FeII] LINERs under special conditions. It is, however, suggestive that the LINERs with the strongest indications or recent star formation have the greatest [FeII]/Paβ ratios. It is possible that the "strong" [FeII] LINERs have a Seyfert-like core, but also have a surrounding star formation region where supernova remnants enhance the [FeII] emission.

4.5.2 Excitation of the [FeII] and H_2 emission

The main goal of this study is to determine the source of the strong, low ionization emission lines in LINER spectra. The observation that both the molecular line H_2 1-0 S(0) and the [FeII] line are strong, places even more stringent requirements on the excitation mechanism since (1) H_2 is relatively easy to destroy, and (2) 98% of iron is tied up in dust grains in the local ISM. In order for a common mechanism to power both lines, as well as the optical [OI] line, it must not destroy all of the H_2 molecules and yet must free up iron through dust grain destruction. The strength of the [FeII] line is much harder to explain through increased metallicity, since the

oxygen, nitrogen and sulfur lines in the optical are not consistent with extremely high metallicities.

A general equation for the strength of [FeII] versus Paβ is derived from Blietz et al. (1994) and is given by:

$$\frac{[FeII](1.2567\mu m)}{Pa\beta} = \frac{22 \times \delta \times \left(\frac{f_{II}}{\xi}\right) \times T_4^{0.07} \times exp\left(\frac{-1.57}{T_4}\right)}{\left[1 + 4.2 \times \left(\frac{T_4^{0.69}}{n_4}\right)\right]} \tag{4.8}$$

where T_4 is the temperature in units of 10^4 K, n_4 is the electron density in units of 10^4 cm^{-3}, δ is the fraction of iron in the gas phase, f_{II} is the fraction of gaseous iron that is singly ionized, and ξ is the ionization fraction of hydrogen. This equation is of course only valid if both lines arise within the same parcel of gas. If multiple excitation mechanisms exist, then the equation can still be used to try and constrain the dominant mechanism. Equation 4.8 can be also be written in a two part form:

$$\begin{aligned} \frac{[FeII](1.2567\mu m)}{Pa\beta} &= coef \times \delta \times \left(\frac{f_{II}}{\xi}\right) \qquad (4.9) \\ \text{where} & \\ coef &= \frac{22 \times T_4^{0.07} \times exp\left(\frac{-1.57}{T_4}\right)}{\left[1 + 4.2 \times \left(\frac{T_4^{0.69}}{n_4}\right)\right].} \end{aligned}$$

The advantage of equation 4.9 is that it separates the temperature and density dependence from the dependence on iron abundance and ionization states. Figure 4.32 plots the parameter coef as a function of density for a variety of temperatures.

Since δ is $\sim$0.02 in the local ISM, figure 4.32 shows that even for the most extreme possible temperature and density for these objects, coef $\times$ δ is only 0.5. So unless the gas phase abundance of iron is much greater than locally, and/or the ionized fraction

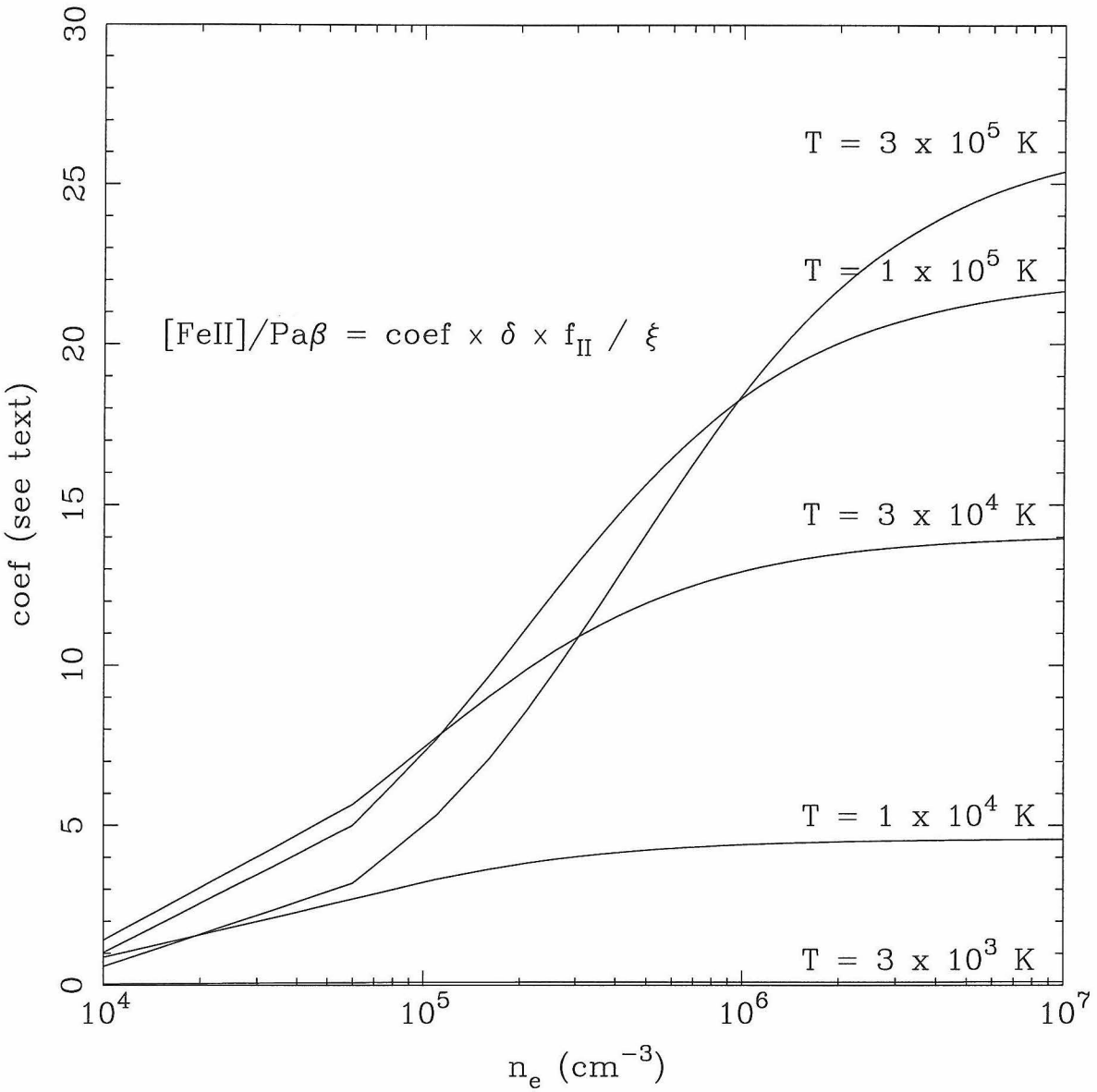

Figure 4.32: From the equations of Blietz et al. (1994), the temperature and density dependence of the ratio of [FeII]/Paβ is parameterized into the variable coef. This figure plots coef as a function of density for a range of temperatures given above each curve. The formula in the left of the figure gives the theoretical relationship between coef and [FeII]/Paβ.

of iron to hydrogen is much greater than 1, then [FeII]/Paβ cannot reach the level of the "strong" [FeII] LINERs.

Several types of environments can immediately be ruled out based on equation 4.8. Standard HII regions have an ionized fraction of iron to hydrogen of less than $\sim$0.2 (Oliva et al. 1989). In order to reach [FeII]/Paβ of even the values of $\sim$0.6 seen in the "weak" [FeII] LINERs requires the gas phase abundance of iron (δ) to be 0.12 (a six fold increase in gas phase iron) for even the most extreme conditions (T = 10^5 K and n = 10^5 cm^{-3}). For more reasonable conditions (T = 10^4 K and n = 10^4 cm^{-3}), δ must be greater than 1, which is unphysical. Even δ of 0.12 is difficult to explain in an HII region, since there are no strong mechanisms to process dust grains. Since Galactic HII regions are observed to have very weak [FeII] emission, it is expected that extragalactic HII regions should have [FeII]/Paβ ratios much less than unity.

The photodissociation region around strong UV sources were also examined by Blietz et al. (1994) since these regions can produce strong H_2 and other low ionization lines. The temperatures in the photodissociation regions are always below 2000 K, however, which greatly reduces the [FeII] flux (coef $<$ 1). Also these regions tend to be very thin, so the ratios of low ionization lines to hydrogen recombination lines (which are generated interior to the ionization fronts) is in general very low.

X-ray heating from a nonthermal power-law source can produce an extended ionization front if very hard x-rays are present (Halpern and Grindlay 1980). In such extended regions, the fraction of ionized iron to hydrogen can reach 100, although the temperature may be only $\sim$3000 K (Blitz et al. 1994). For this temperature, the coef parameter is about 0.11 for any density over $\sim 10^4$ cm$^-3$. For a ratio of [FeII]/Paβ as high as 2, δ must be at least 18%. Although high, this is not unfeasible since the hard x-rays can destroy dust grains. For the "weak" [FeII] LINERs, the ratio of [FeII]/Paβ of $\sim$0.6, δ need only be 0.055, which is very reasonable. X-rays are

therefore an attractive emission source for the "weak" [FeII] LINERs and may play a part in powering the infrared emission lines in the "strong" [FeII] LINERs as well.

Another possible excitation mechanism is a J-type shock (jump discontinuity shocks without magnetic precursors). Shocks can produce large fractions of ionized iron to hydrogen and provide a natural mechanism for dust grain processing. Seab and Shull (1983) find that fast shocks (40 to 120 km s^{-1}) can increase the gas phase iron abundance (δ) up to 60%. For an expected ionization fraction of iron to hydrogen of around 2, J-shocks then require coef to be greater than 1.7 for [FeII]/Paβ around 2, and 0.5 for [FeII]/Paβ of 0.6. These values are possible for virtually any temperature above 10^4 and density above 10^4. This fact makes shocks a very attractive mechanism for the "strong" [FeII] LINERs, and they may also produce the [FeII] emission in the "weak" [FeII] LINERs. If present in "weak" [FeII] LINERs, the effect of shocks is probably diluted by other mechanisms. Although fast shocks will destroy H_2 and cannot explain the H_2 lines, there should exist a range of densities making a variety of shock speeds possible. The strong H_2 lines may then result from the same shock mechanism, but in slightly different parts of the gas.

Both hard x-ray heating, and fast shocks are plausible mechanisms for all of the LINERs, although the "weak" [FeII] LINERs are easier to explain by x-ray heating while "strong" [FeII] LINERs are more consistent with shock excitation. Both mechanisms are also able to generate the H_2 emission, but shocks are more efficient at [FeII] production, and are better able to explain the "strong" [FeII] LINERs. If shocks are present, either compact supernova remnants (pressure confined), or other mechanisms such as cloud-cloud collisions, or outflowing winds are plausible shock sources. Supernova remnants are the likely source for the "strong" [FeII] LINERs since many of these show other evidence for recent star formation. The multiple nuclei objects

like Arp 220, may have contributions from other sources of shock excitation, possibly relating to the ongoing merger.

4.5.3 Possible Biases

In any survey of a small sample of objects, with faint emission features, biases in selection, photometry and aperture correction, sensitivity and a large number of other sources may play a significant role. In this subsection we discuss some of the most obvious sources of bias, and try to estimate their role.

One of the largest biases affecting this survey is the size of the sample and the fact that the line detections are preferentially in the most active LINERs; the others are too faint. A significant population of LINERs have featureless infrared spectra and cannot be addressed by the infrared diagnostics. For most quantities discussed, there is a relatively smooth transition from LINER-like spectral properties to Seyfert-like. An important consideration is that the least active LINERs, which have no line information, are less like Seyfert's in their emission mechanism than those discussed in detail, and many of the correlations may not hold for these LINERs. We have tried, in a limited fashion, to address this problem by also using the optical [OI](6300Å) line, which is well correlated with the infrared lines for all LINERs, in examining the excitation mechanisms. Since this line must be detected for a galaxy to be classified as a LINER according to the original definition, it does not suffer from the same selection bias. However, it is possible that the [OI] emission does not arise from the same regions as the infrared lines.

Another bias is the lack of hydrogen recombination line detections. Since we are applying optical extinction estimates to extrapolate the intrinsic strengths of the near infrared features, we may be subject to large uncertainties if the extinctions to the optical and IR emitting regions are significantly different. If the extinction to

the infrared lines were higher than predicted from Hα and Hβ, then the estimated infrared recombination lines would be too low, and the corresponding ratios with [FeII] and H_2 too high. Since the line ratios correlate with the [OI] line, it is not likely that the recombination strengths have been severely underestimated. Also, since the absorption corrected fluxes are typically below the extrapolated line fluxes, it is more likely that the recombination lines are actually biased too high, and that the line ratios are even higher than estimated. A logical next step will be to obtain high signal to noise infrared spectra of several template galaxies for subtraction in order to identify emission lines lost in stellar absorption features.

It is possible that the difference in size between our aperture and those used in the optical plays a role in increasing the observed [FeII] and H_2 ratios. Knop (personal communication 1994) has used a similar small aperture to measure the infrared line ratios in some nearby Seyfert galaxies and has found that many of them have slightly higher [FeII] and H_2 ratios than Seyferts in the literature, but the effect is much too weak to account for the differences seen between the LINERs and the Seyferts. In fact, several of the LINERs that have multi-aperture optical spectra, show stronger low ionization lines in the larger aperture, which implies just the opposite effect.

4.6 Summary and Conclusions

This chapter has described the infrared spectroscopic survey of 12 "classical" LINER galaxies and 4 multiple nuclei galaxies with at least one LINER component. The spectra have concentrated on the [FeII](1.2567μm), Paβ, H_2(2.1218μm) and Brγ infrared lines. The major results are:

1. [FeII] and H_2 are the strongest infrared lines in classical LINERs. Using extrapolated H^+ line strengths from the optical, approximately half of the classical

LINERs have ratios of [FeII]/Paβ and/or H_2/Brγ a factor of two or more higher than typical Seyfert galaxies and a factor of five or more higher than typical starburst galaxies.

2. A natural subdivision between the LINERs occurs at [FeII]/Paβ = 2. The four "strong" [FeII] LINERs exhibit evidence for recent or ongoing star formation. As a group, the [FeII] emission in these LINERs is consistent with shock excitation from compact supernova remnants. The five "weak" [FeII] LINERs have more in common with Seyfert galaxies, including a couple of broad Hα detections, and strong x-ray sources. The lower ratios of "weak" [FeII] LINERs are consistent with hard x-ray heating from a power-law source. Neither excitation mechanism is ruled out for either type of object, however, and it is possible that it is just the relative strengths of the two mechanisms that are different in the two groups.

3. The shallow far infrared spectral slopes of some of the "weak" [FeII] LINERs in comparison to the strengths of H_2 and [OI], appear inconsistent with the correlations observed for starburst and ULIRG galaxies. This argues very strongly that a nonthermal heat source is providing much of the dust heating and line excitation for these objects.

4. LINERs with x-ray detections and Seyferts, particularly Seyfert 1's where extinction probably plays less of a role, have sufficient x-ray luminosity to power the observed infrared lines. Starbursts often have [FeII] and H_2 lines many times stronger than the x-rays luminosity should be able to produce. Again the strong x-ray LINERs do not appear consistent with star formation, but instead behave like mini-Seyferts.

5. For the multiple nuclei objects, only two of the LINER components had detectable emission lines, Arp 220 and IR 17132+5313. These two objects had

infrared line ratios more consistent with Seyfert galaxies than the group of "strong" [FeII] LINERs. All four multiple nuclei objects have steep IRAS α(25:60) index indicating a low ratio of hot to warm dust components. Much of the LINER-like emission lines may be generated in the circumnuclear environments of these galaxies, and may result from cloud-cloud collisions from the ongoing merger events, or from outflowing winds.

6. In most of the LINERs, the estimated amount of Paβ absorption can account for the lack of Paβ in emission. Several of the LINERs have unusually strong Paβ absorption indicative of younger stellar populations. The six galaxies with the strongest absorption all have strong [FeII] lines and supernova remnants from recent star formation are a plausible explanation for their enhanced [FeII] strengths.

7. A strong linear correlation is observed between H_2/Brγ, [FeII]/Paβ and [OI]/Hα for a range of 100 in all ratios and for all of the observed galaxy types. However, the "strong" [FeII] LINERs are stronger in [FeII] than the correlation with [OI] predicts. The general correlation suggests a related excitation mechanism for all of the low ionization lines regardless of the overall environment.

8. Both the H_2/Brγ and to a lesser degree the [FeII]/Paβ ratio, appear to separate the three galaxy classes: LINERs, Seyferts and starbursts. Only six objects have been observed to have H_2/Brγ higher than 3, and all are LINERs. In conjunction with the [OIII]/Hβ ratio, the class distinctions are even clearer.

It will be important in the future to observe other transitions of [FeII] and H_2 now that these lines are known to be strong in many LINERs. With multiple transitions, the level populations can be determined and excitation temperatures measured. This

information can be used to better distinguish between shock and X-ray excitation. Unfortunately, the lines observed in the sample are the strongest available, and it may be difficult to measure more than one or two other lines with reasonable signal to noise.

Since the emission regions of LINERs are so small, and are dwarfed by the surrounding stellar light, further observations with very high resolution will be very important. A high resolution VLA study of LINERs might show weak jets as in Seyferts. Also Hubble Space Telescope narrow band imaging (Hα in particular) may show evidence for winds, nuclear jets or cones. Adaptive optics systems will greatly improve future studies of LINERs in all optical and infrared studies.

Improvements can also be made in future infrared surveys of weak line galaxies in several areas. First, due to the unanticipated strength of Paβ absorption, template galaxies should be observed to help reveal weak emission lines through subtraction. A study of the Paβ and Brγ line strengths in various stellar types would also be invaluable in constraining stellar populations based on absorption line strengths. Additional observations concentrating on the atomic absorption lines are also needed. It may be possible to relate these features to the stellar types and metallicities present in the galaxies and determine the role of star formation as was done with the Ca II triplet in Terlevich et al. (1990).

Infrared spectroscopy has extended the range of spectral diagnostics available for the study of LINERs and other active galaxies. Clearly the sample sizes for all galaxy types need to be dramatically increased. With current and future generations of infrared spectrographs, the number of objects studied should continue to increase steadily.

4.7 References

Aaronson, M., 1977, Ph.D. Thesis, Harvard University.

Blietz, M., Cameron, M., Drapatz, S., Genzel, R., Krabbe, A., Van Der Werf, P., Sternberg, A., & Ward, M., 1994, Ap.J., 421, 92.

Cardelli, J. A., Clayton, G. C., & Mathis, J. S., 1989, Ap.J., 345, 245.

De Grijp, M. H. K., Keel, W. C., Miley, G. K., Goudfrooij, P., & Lub, J., 1992, A.&A.Supp., 96, 389.

Fabbiano, G., Fassnacht, C., & Trinchieri, G., 1994, Ap.J., 434, 67.

Filippenko, A. V., & Sargent, W. L. W. 1985, Ap.J.Supp., 57, 503.

Ford, H. C., Dahari, O., Jacoby, G. H., Crane, P. C., & Ciardullo, R., 1986, Ap.J., 311, L7.

Graham, J. R., Wright, G. S., & Longmore, A. J., 1987, Ap.J., 313, 847.

Graham, J. R., Wright, G. S., & Longmore, A. J., 1990, Ap.J., 352, 172.

Graham, J. R., Wright, G. S., Hester, J. J., & Longmore, A. J., 1991, A.J., 101, 175.

Hall, D. N. B., 1973, Kitt Peak National Observatory: An Atlas of Infrared Spectra of the Solar Photosphere and of Sunspot Umbrae.

Halpern, J. P., & Grindlay, J. E., 1980, Ap.J., 242, 1041.

Heckman, T. M., 1980, A&A, 87 152.

Heckman, T. M., Balick, B., & Crane, P. C., 1980, A&A, 40, 295.

Ho, L. C., Filippenko, A. V., & Sargent, W. L. W., 1993, Ap.J., 417, 63.

Hoffleit, D., 1964, Catalogue of Bright Stars, Yale University Observatory, Third Revised Edition.

Keel, W. C., 1983, Ap.J., 269, 466.

Kleinmann, S. G., & Hall, D. N. B., 1986, Ap.J.S., 62, 501.

Lepp, S. & McCray, R., 1983, Ap.J., 269, 560.

Larkin, J. E., Knop, R. A., Lin, S., Matthews, K., & Soifer, B. T., in preparation.

Maoz, D., Filippenko, A. V., Ho, L. C., Rix, H. W., Bahcall, J. N., Schneider, D. P., & Macchetto, F. D., 1995, Ap.J., 440, 91.

Mollenhoff, C., & Bender, R., 1989, A&A, 214, 61.

Moorwood, A. F. M., & Oliva, E., 1988, A&A, 203, 278.

Mouri, H., Kawara, K., Taniguchi, Y., 1993, Ap.J., 406, 52.

Mouri, H., Taniguchi, Y., 1992, Ap.J., 386, 68.

Miyoshi, M., Moran, J., Herrnstein, J., Greenhill, L., Nakai, N., Diamond, P., & Inoue, M., Nature, 373, 127.

Nakai, N., Inoue, M., & Miyoshi, M., 1993, Nature, 361, 45.

Neugebauer, G., Elias, J., Matthews, K., McGill, J., Scoville, N., & Soifer, B. T., 1987, A.J., 93, 1057.

Oliva, E., Moorwood, A. F. M., 1989, A&A, 193, 327.

Oliva, E., Moorwood, A. F. M., & Danziger, I. J., 1989, A&A, 214, 307.

Oliva, E., & Origlia, L., 1992, A&A, 254, 466.

Osterbrock, D. E., 1989, *Astrophysics of Gaseous Nebulae and Active Galactic Nuclei,* University Science Books.

Rieke, G. H., & Lebofsky, M. J., 1985, Ap.J., 288, 618.

Seab, C. G., & Shull, J. M., 1983, Ap.J., 275, 652.

Serlemitsos, P., 1995, conference proceedings, *The Physics of LINERs in View of Recent Observations* , in preparation.

Terlevich, E., 1995, conference proceedings, *The Physics of LINERs in View of Recent Observations* , in preparation.

Terlevich, E., Diaz, A. I., & Terlevich, R., 1990, M.N.R.A.S., 242, 271.

Willner, S. P., Elvis, M., Gabbiano, G., Lawrence, A., & Ward, M. J., 1985, Ap.J., 299, 443.

Appendix: G Star Equivalent Widths

Infrared spectra of main sequence G stars were taken close in time and airmass to the galaxies presented in chapter 4 in order to remove telluric absorption from the galaxy spectra and serve as flat fields. The stars represent a good approximation to an ideal blackbody at these wavelengths except for weak hydrogen absorption lines. In order to properly correct the galactic spectra, these lines must first be removed from the stellar spectra. Subsection 4.2.1 describes the line removal process. As a byproduct, a frame is produced that is unity everywhere except on the absorption line where the values are the fraction of the light absorbed by the star. This frame, shown in panel e of figure 4.2, can then be used to determine the equivalent width of the absorption line to reasonably good precision (~10%). Table A.5 lists these equivalent widths of Paβ and Brγ for the 19 G stars and one F star used in correcting the spectra in chapter 4, and for the one A star observed for comparison. As expected, the absorption features are strongest in the A star, being a factor of 2-3 stronger in Paβ and 4-5 times stronger in Brγ than a typical G star. The weakest Paβ lines are seen in the latest stars bs 4550, and bs 8631, which are both of type G8. The strongest lines are in bs 5972 (the A star), bs 4767, the F star and bs 3538 (G3V). In the case of bs 3538, the lines are unusually strong compared to the other G3 stars,

and it is possible that this object has been misidentified, or more likely, that a nearby, earlier type star was observed in error. This last possibility is supported by the very different values of Brγ equivalent widths (3.4 and 5.1 respectively) measured on two different dates.

Table A.5
G Star Hydrogen Equivalent Widths

Object (1)	Stellar Type (2)	Paβ EqW (Å) (3)	Brγ EqW (Å) (4)	$\frac{Br\gamma}{Pa\beta}$ (5)
bs 5	G5V	1.4	1.5	1.06
bs 720	G0V	2.1		
bs 3538	G3V	2.1	3.4,5.1[a]	2.02
bs 3881	G0.5Va	1.7	2.2	2.29
bs 4277	G0V	1.5	2.2	1.47
bs 4486	G0V	1.7	2.4	1.40
bs 4550	G8Vp	0.72	1.5	2.08
bs 4767	F8	1.7	3.5	2.06
bs 4767	G0V	1.5	2.2	1.49
bs 4785	G0V	1.6	2.8	1.75
bs 4845	G0V	1.5	1.7	1.13
bs 4983	G0V	1.8		
bs 5070	G6V	1.4	2.4	1.71
bs 5972	A3V	3.9	8.9	2.31
bs 6060	G2Va	1.4	1.3,1.9[a]	1.14
bs 6847	G2V	2.2	2.4	1.09
bs 6981	G2V	1.7		
bs 7260	G5V	1.6	2.0	1.25
bs 7783	G3V	1.6,1.7[a]	2.1	1.31
bs 8631	G8V[b]	1.1	2.3	2.05
bs 8737	G2V[c]	1.4,1.5[a]	2.1	1.36

[a] If star was observed multiple times, the range of values is listed.
[b] Could be the G3V member of this double system.
[c] Could be the G4V member of this double system.

Table A.5: Table of the equivalent widths of hydrogen absorption lines in G star spectra. (1) Object: Name of the star as given in the Yale Bright Star Catalog (Hoffleit 1964). (2) Stellar Type: The standard stellar spectral type of the star. (3) Paβ EqW (Å): The equivalent width of Paβ absorption in angstroms. (4) Brγ EqW (Å): The equivalent width of Brγ absorption in angstroms. (5) $\frac{Br\gamma}{Pa\beta}$: The ratio of Brγ to Paβ equivalent widths.